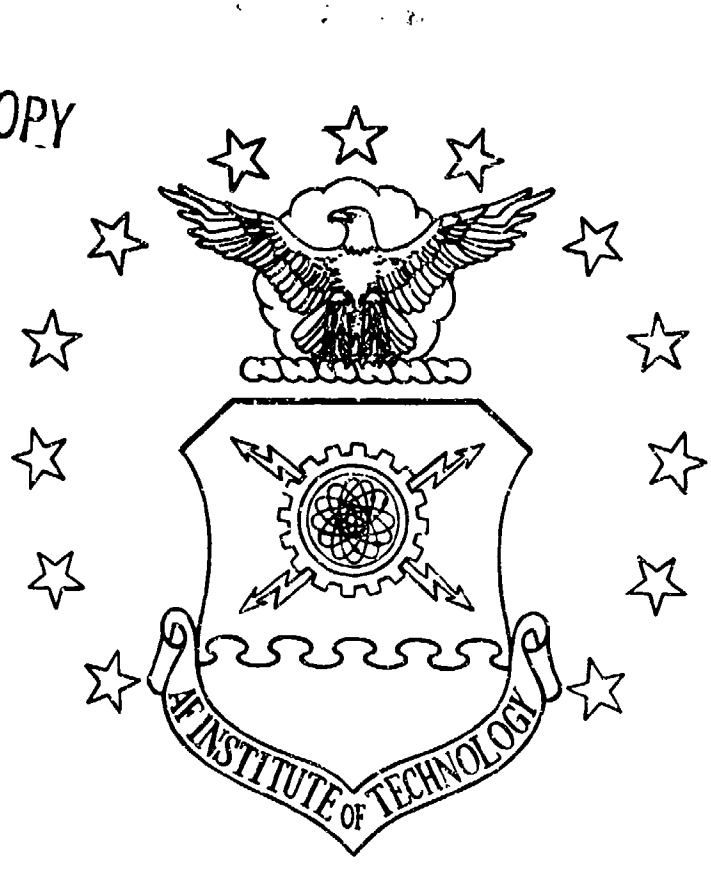

ELECTROMAGNETIC SCATTERING FROM IMPEDANCE STRIPS AND IMPEDANCE-LOADED CONDUCTING STRIPS

THESIS

Mark C. Heaton, First Lieutenant, USAF

AFIT/GE/ENG/90D-26

DEPARTMENT OF THE AIR FORCE
AIR UNIVERSITY
AIR FORCE INSTITUTE OF TECHNOLOGY

Wright-Patterson Air Force Base, Ohio

AFIT/GE/ENG/90D-26

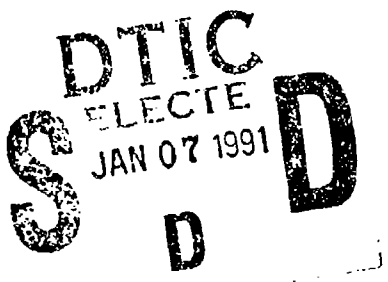

ELECTROMAGNETIC SCATTERING FROM IMPEDANCE STRIPS AND IMPEDANCE-LOADED CONDUCTING STRIPS

THESIS

Mark C. Heaton, First Lieutenant, USAF

AFIT/GE/ENG/90D-26

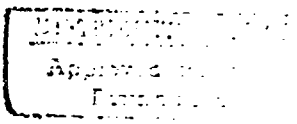

Approved for public release; distribution unlimited

AFIT/GE/ENG/90D-26

ELECTROMAGNETIC SCATTERING FROM IMPEDANCE STRIPS AND IMPEDANCE-LOADED CONDUCTING STRIPS

THESIS

Presented to the Faculty of the School of Engineering
of the Air Force Institute of Technology
Air University
In Partial Fulfillment of the
Requirement for the Degree of
Master of Science in Electrical Engineering

Mark C. Heaton, B.S.
First Lieutenant, USAF

December 1990

Acknowledgements

I would like to express my appreciation to my advisor, Captain Philip Joseph, for his help and guidance throughout this effort. I would also like to thank the members of my thesis committee, Major Harry Barksdale and Dr. Andrew Terzouli, for their help and comments on this project.

There are many others who have helped me during my time at AFIT. I would like to thank Mr. Bob Lindsay and Captain Dan Mullinix for their indispensable help in making RCS and waveguide measurements. Mr. Al Reggiani from Emerson and Cuming also provided much needed assistance in providing impedance materials for this effort. I would also like to thank my fellow low observables students, who were an excellent source of encouragement and support while at AFIT.

I would like to thank my wife, June, for her patience and support during the course of this work. My son, Justin, who happened to be born during my term at AFIT, was also a source of happiness and pleasant distraction during my schooling. I would also like to thank my parents for giving me a strong sense of motivation and for conveying to me the value of education.

Finally, I would like to thank the United States Air Force for giving me this opportunity to further my education.

Table of Contents

List of Figures

Abstract

This paper investigates the scattering from impedance strips and impedance-loaded conducting strips. The UTD diffraction coefficient for an edge in a conductor is heuristically modified for impedance edges and junctions. Essentially, this is done by scaling the UTD diffraction coefficients according to changes in the geometrical optics field. The new diffraction coefficients are then used to investigate the scattering from impedance strips and impedance-loaded conducting strips. Both uniform and tapered impedances are considered. Results are compared to moment method and physical optics predictions and to measured data. The scattering pattern of a uniform impedance strip was seen to behave as that for a conducting strip, but at a lower level. However, tapering the impedance was seen to significantly decrease the sidelobe levels relative to the main lobe. Also, applying an impedance load to a conducting strip reduced the sidelobe levels. This was most pronounced for loads of tapered impedance. The modified UTD approach accurately predicted the sidelobe levels and locations for the simple impedance strips, and worked fairly well for the impedance-loaded conducting strips. The predictions for all geometries were better near broadside incidence than near edge-on.

ELECTROMAGNETIC SCATTERING FROM IMPEDANCE STRIPS

AND IMPEDANCE-LOADED CONDUCTING STRIPS

I. Introduction

Electromagnetic Scattering

The field of electromagnetics affects many facets of today's society. Applications include items from telephones to satellites, and from radio to microwave ovens. One common application is that of radar. Radar is used, among other things, to monitor aircraft, to observe weather conditions, and even to write speeding tickets.

Radar operates by emitting energy in the form of an electromagnetic wave. When it strikes an object, this energy scatters, with some of the scattered energy returning to the radar. This returned energy indicates to the radar the presence of the object, and can also provide information about the object, such as velocity and position.

Scattering occurs because the incident field excites electrical currents in the target. These currents in turn cause a new electromagnetic wave to emanate from the target. This is the scattered field. Monostatic scattering, or backscatter, refers to the energy scattered back in the direction of the incident field. Bistatic scattering refers to energy scattered in other directions.

There are many ways to predict scattering. These include high frequency techniques such as geometrical optics (GO), physical optics (PO), and the uniform theory of diffraction (UTD). GO considers incident, reflected, and refracted fields. PO approximates the currents

induced on the scatterer by the incident magnetic field, then determines the field that these currents reradiate. UTD considers the GO field plus the various possible diffractions from edges, corners, surface curvature, electrical discontinuities and so on. Integral equation methods are a low frequency approach. An integral equation is written relating the currents induced on the scatterer to the incident field. Numerical methods, such as the method of moments, are then used to determine the currents. As with PO, the scattered field is then found from the induced currents. Integral equation methods are highly accurate; however, solving the integral equation typically requires large amounts of computer time. UTD is also very accurate in the high frequency realm and is computationally efficient. However, its application to non-conducting materials is a relatively new topic. Some work has been accomplished in the past several years, (2, 13), while much more remains to be done.

Background

Radar Cross Section. The amount of energy scattered by a target in a given direction determines its radar cross section (RCS). An object's RCS is dependent on many things; these include the object's size, shape, and composition. RCS also depends on the incident wave's frequency and polarization, as well as the relative orientation of the object and the radar. RCS is given by the formula

$$\sigma = \lim_{R\to\infty} 4\pi R^2 \left|\frac{E_s}{E_i}\right|^2 \qquad (1.1)$$

where R is the distance between the radar and the target, E_s is the scattered field, and E_i is the incident field at the target.

When the scatterer is defined in only two dimensions, such as an infinitely long strip, it is characterized by a two-dimensional radar echo length, also called the scattering width. This is written as

$$\sigma_{2D} = \lim_{R\to\infty} 2\pi R \left|\frac{E_s}{E_i}\right|^2 \qquad (1.2)$$

RCS Reduction. Reducing an object's RCS decreases the electromagnetic energy that it scatters towards the radar receiver, thus reducing the chance that the radar detects the object. This provides the object a greater chance of survival in a hostile environment. There are three methods used to reduce an objects RCS: shaping, use of radar absorbing material or structure (RAM or RAS), and impedance loading (9:190-192).

Shaping reduces an object's RCS by causing the incident wave to scatter in directions where it will not cause a threat to detection. Typically, scattering back into the forward sector is undesirable and vehicles are designed to scatter radar energy to the side or rear when illuminated from the forward sector. Another shaping objective is to eliminate geometries that have a large RCS, such as dihedral and trihedral corners. Disadvantages of shaping are that the shape needed for low RCS might not be consistent with the object's mission. For instance, shaping might impede the aerodynamics of an aircraft. Also, desired shapes might be difficult to manufacture.

RAM and RAS reduce the scattered energy by converting some of the incident wave into heat, or by creating multiple echos that cancel one another. RAM is usually applied to an existing structure, while RAS refers to a structure itself that has been designed as an absorber. Disadvantages of RAM are that most types are heavy or bulky, and are often frequency sensitive. RAM and RAS are also expensive.

Impedance loading, or passive cancellation, involves the application of an impedance load to an object to alter its scattering characteristics (4; 5). This may be done to reduce the sidelobes of an antenna, or to create nulls in a scattering pattern. Impedance loading alters the frequency response of an object, since the loads create new scattering sources which cause destructive interference at certain frequencies but not at others. A disadvantage of loading is that its effects are typically frequency dependent.

In practice, a combination of these three methods may be needed to control radar scattering. Shaping and the application of RAM and RAS have been rigorously investigated and research is continuing in these areas. Applications of loading have not been as thoroughly explored, since its effects are frequency sensitive. This is not a desired trait for RCS reduction, but it is in antenna design and other areas. With these applications in mind this study will investigate the use of impedance loading on conducting strips.

Impedance Loading. Previous work on impedance loading has shown it to be significant in altering scattered fields (4,5,14). Haupt and Liepa (5:57) calculated a 15 dB decrease in the edge-on scattering of a conducting strip by applying a parabolically tapered resistive load.

They also developed synthesis techniques for applying tapered loads to conducting strips to generate low sidelobes and nulls at specific angles in the scattering patterns (5:57–79). Harrington investigated the introduction of a resonant current mode in an object due to the presence of a reactive load (4). If no other current modes are near resonance, the resonant current mode of the load becomes dominant. The scattering is then nearly identical to that from this mode alone.

The integral equation method, also called the method of moments or simply moment method, has been used to predict the scattering from impedance strips (12,15,16) and impedance loaded conducting strips (5). Moment methods, however, can only be easily applied to small objects (9:57). When the object is larger than several wavelengths moment methods become inefficient and high frequency techniques, such as UTD, are more desirable.

Uniform Theory of Diffraction. UTD is a very accurate high frequency method. It is a ray method, and it determines the scattered field as a combination of the GO field and various diffracted fields. Keller (8) first introduced the edge diffracted field in his GTD, which gave a simple geometric interpretation to the edge diffracted field. However, his solution became singular in certain regions in space. Kouyoumjian and Pathak (10), using asymptotic methods and the exact eigenfunction solutions for a conducting wedge, developed a uniform geometrical theory of diffraction within the context of Keller's solution.

The UTD is applied to an object with an edge by using a diffraction coefficient that was rigorously derived for an edge in the

canonical shape of a wedge. The UTD is very accurate when the necessary diffraction coefficients are available. Diffractions can arise from geometrical discontinuities such as edges and corners, from discontinuities in electrical parameters, from curved surfaces and so on. Most of the work to date has dealt with perfect conductors.

Burnside and Burgener (2) developed an approximate diffraction coefficient for an edge in a thin lossless dielectric slab. Their approach scaled the perfect electrical conductor diffraction coefficients in accordance with changes in the GO field. Rojas (13) has rigorously developed complicated expressions for the diffraction of an arbitrarily-polarized plane wave obliquely incident on a planar surface with an impedance discontinuity and on an impedance half-plane.

Problem Statement

Predicting the scattering from complex objects, such as an airplane, is a very difficult problem. Simpler geometries must be investigated first to reveal some scattering characteristics. This study will investigate the scattering behavior of impedance strips and impedance loaded conducting strips.

The goals of this thesis are to:

1. Develop a UTD based computer code to calculate the scattering from impedance strips and impedance loaded conducting strips.
2. Verify the UTD methods and the developed code through comparisons of UTD predictions to RCS measurements and moment method predictions.
3. Investigate the scattering from impedance strips and impedance loaded conducting strips.

Approach

Development of the UTD methods used to predict scattering from impedance edges and junctions are contained in chapter 2. First the UTD formulation for diffraction from an edge in a perfect conductor is presented, and is used to determine the multiply diffracted fields for a perfectly conducting strip. Scaling terms based on the GO field are then presented which modify the UTD diffraction coefficients for the cases of impedance edges and junctions.

The methods developed in chapter 2 are applied to scattering from strips in chapter 3. Simplifications that can be used to make scattering width predictions are discussed. The methods used to predict the scattering width of impedance strips and impedance loaded conducting strips are developed. The use of UTD to predict scattering from an impedance taper is also examined. Methods used for comparison with the UTD predictions are also presented.

Scattering predictions are presented in chapter 4. Diffraction sources and the effects that different loads have on them are discussed. Then the UTD predictions are compared to moment method predictions to determine the accuracy of the UTD method.

RCS measurements made on impedance strips and impedance loaded conducting strips are presented in chapter 5. The measurements are compared to UTD and moment method predictions. Target mounting methods and impedance measurement techniques are also discussed.

Finally, chapter 6 summarizes the information presented in this thesis. Conclusions on the effects of impedance loading and on the accuracy of the UTD method are drawn, based on the information contained

herein. Potential applications of this work and areas where further research can be conducted are also presented.

II. Theory

Formulae that will be used to predict scattering from impedance strips and impedance-loaded conducting strips are developed herein. First, the Uniform Theory of Diffraction (UTD) is reviewed. Its application to the first-order scattering from the edge of a conducting semi-infinite half-plane and from a finite conducting strip is discussed. The multiply-diffracted fields for the finite conducting strip are also discussed and determined. Next, the GO field for an impedance plane is found, and the reflection and transmission coefficients are noted. Finally, a heuristically modified UTD formulation is presented which incorporates these coefficients to predict the scattering from impedance edges and junctions.

Uniform Theory of Diffraction

The electromagnetic scattering from a conducting object in the high-frequency regime can be decomposed into GO and diffracted fields. The GO field consists of an incident field from the source and the reflection of this field by the object. Expressions for these fields may be found in (1:782; 11:8-18), they will not be discussed here. If the scattering object is a half-plane, then the reflected and incident fields create shadow boundaries as shown in figure 2.1. The angles ϕ, ϕ' and distances ρ, ρ' are defined in this figure. Note that the source is located by the polar coordinates (ρ', ϕ') and the observer is located by the polar coordinates (ρ, ϕ). The reflection shadow boundary (RSB) is located at $\phi = \pi - \phi'$, while the incident shadow boundary (ISB) is

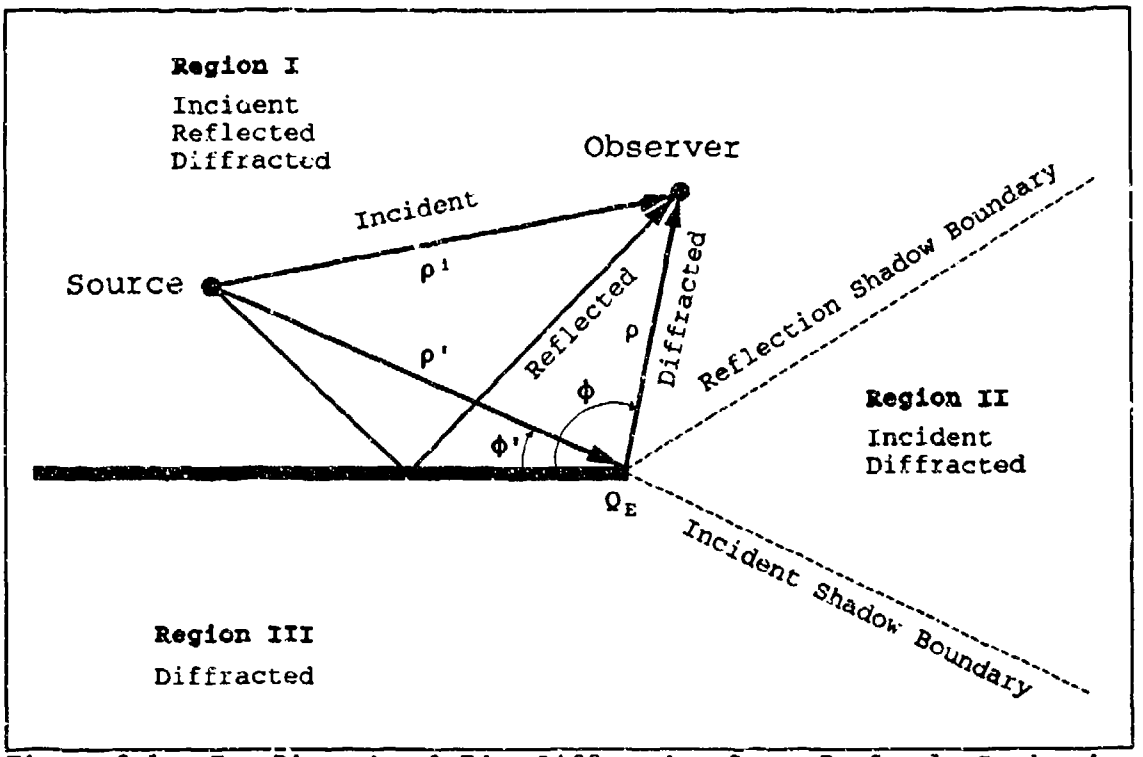

Figure 2.1. Two Dimensional Edge Diffraction for a Perfectly-Conducting Half-Plane

located at $\phi = \pi + \phi'$.

Since the reflected field stops abruptly at the RSB, and the incident field stops abruptly at the ISB, the GO field is discontinuous across both shadow boundaries. UTD eliminates these discontinuities by adding the diffracted field to the GO solution.

Diffraction from an Edge in a Conductor. The diffracted field from the edge of a conducting half-plane is (10:1452):

$$u^d = u^i(Q_E) D_{s,h} \frac{e^{-jk\rho}}{\sqrt{\rho}} \tag{2.1}$$

where $u^i(Q_E)$ is the field incident at the edge (Q_E), k is the free space wave number $2\pi/\lambda$, and $D_{s,h}$ is the diffraction coefficient. The

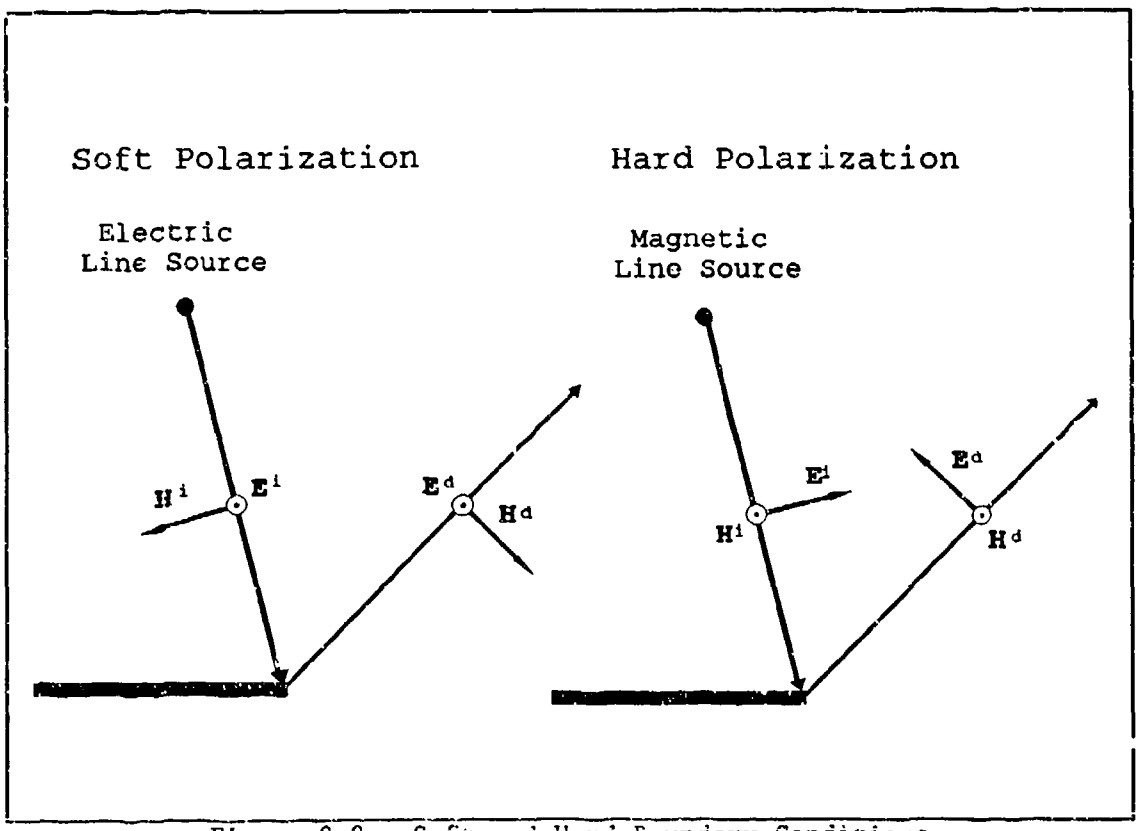

Figure 2.2. Soft and Hard Boundary Conditions

subscripts s and h denote soft or hard boundary conditions (transverse electric (TE or E) or transverse magnetic (TM or H) polarization) respectively, as shown in figure 2.2. For the soft case, u represents E; for the hard case, u represents H. Thus, either polarization is treated as a scalar problem.

The diffraction coefficient is given by (10:1456):

$$D_{s,h}(\phi',\phi,L) = \frac{-\exp[-j(\pi/4)]}{2\sqrt{2\pi k}} \cdot \left\{ \frac{F[kLa(\phi-\phi')]}{\cos[(\phi-\phi')/2]} \mp \frac{F[kLa(\phi+\phi')]}{\cos[(\phi+\phi')/2]} \right\} \tag{2.2}$$

where

$$L = \frac{\rho\rho'}{\rho+\rho'} \tag{2.3}$$

$$a(x) = 2\cos^2(x/2) \tag{2.4}$$

$$F(x) = 2j\sqrt{x}e^{jx}\int_{\sqrt{x}}^{\infty} e^{-j\tau^2}d\tau \tag{2.5}$$

The transition function F(x), as introduced by Kouyoumjian and Pathak, contains a Fresnel integral which is easily evaluated using a computer algorithm contained in (1:850).

The diffraction coefficient may be expressed as:

$$D_{s,h}(\phi',\phi,L) = D(\phi-\phi') \mp D(\phi+\phi') \tag{2.6}$$

where

$$D(\phi\pm\phi') = \frac{-\exp(-j\pi/4)}{2\sqrt{2\pi k}} \frac{F[kLa(\phi\pm\phi')]}{\cos[(\phi\pm\phi')/2]} \tag{2.7}$$

The $D(\phi - \phi')$ term is discontinuous at the ISB, while the $D(\phi + \phi')$ term is discontinuous at the RSB. These discontinuities compensate for those in the GO field, yielding a smooth and continuous total field. This is expected, since the diffracted field was found in a rigorous manner.

Scattering from a finite strip can be calculated using UTD edge diffractions. Since high frequency edge diffraction is a local phenomenon, the diffracted field formulation for either edge of a finite strip is identical to that for the edge of a half-plane. Scattering from the strip then consists of the GO field and the diffracted fields from the two edges. In contrast to the half-plane, the strip has two RSBs and two ISBs. As shown in figure 2.3, the reflected field exists

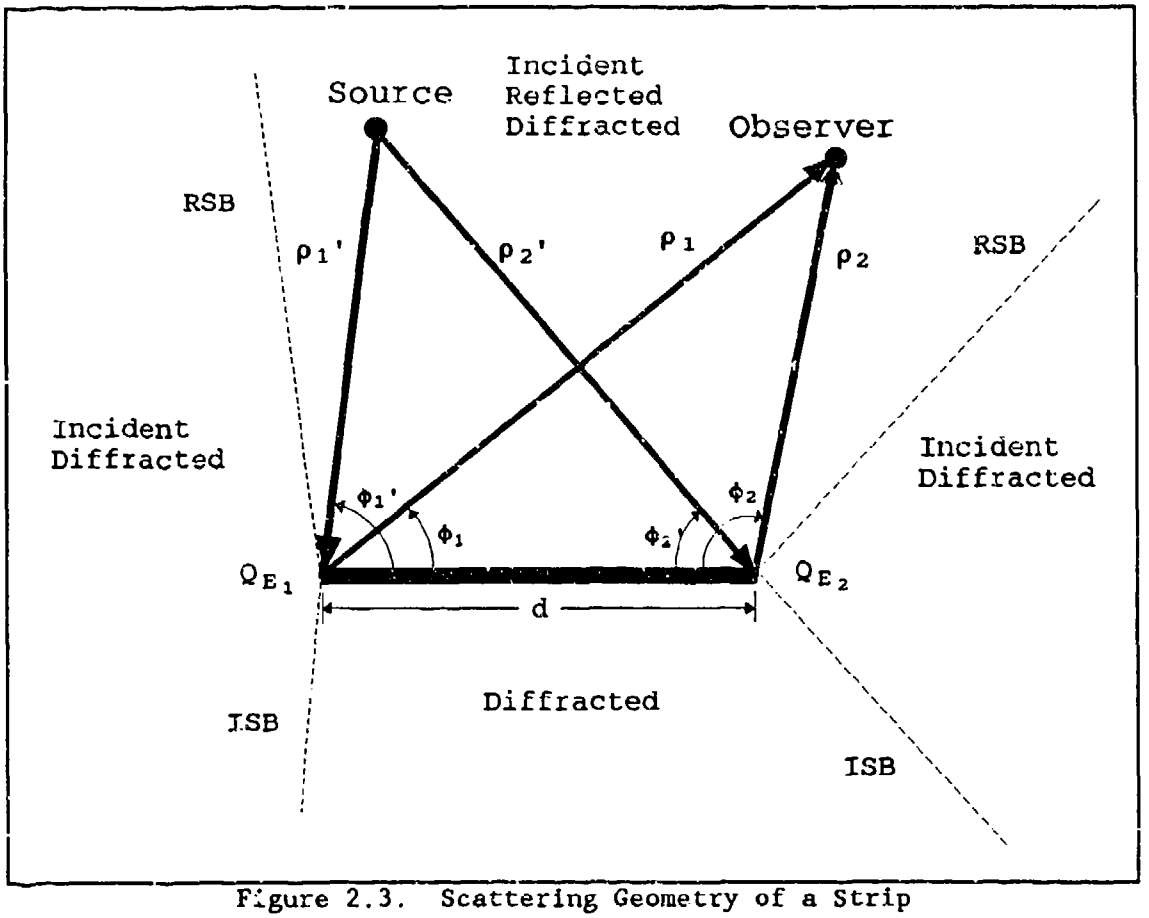

Figure 2.3. Scattering Geometry of a Strip

only between the RSBs and the incident field is present everywhere except between the ISBs.

Multiple Diffractions. Double diffractions are fields that diffract from one edge, travel along the surface of the strip, and then diffract from the opposite edge. This is illustrated in figure 2.4. The doubly diffracted rays that travel again along the surface back to the original edge produce triple diffractions, and so on to infinity. These are all considered multiple diffractions.

All multiple diffractions may be accounted for in closed form. The analysis begins by noting that all multiply diffracted fields

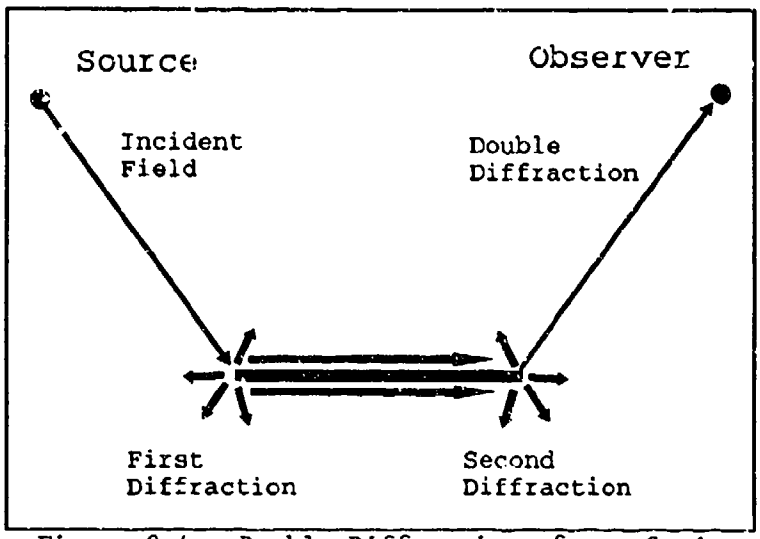

Figure 2.4. Double Diffractions for a Strip

traveling above (or below) the strip from one edge to the other can be expressed as a single composite field above (or below) the strip. The total field diffracted from each edge is due to these composite fields and the incident field diffracting from that edge.

At this point, we wish to find expressions for the total diffracted fields emanating from points Q_{E_1} and Q_{E_2}. Recall that equations (2.1) through (2.5) describe any one diffraction, where (ρ', ϕ') locate the source relative to the point of diffraction (Q_E), and (ρ, ϕ) locate the field point (observer) relative to Q_E. This was illustrated in figure 2.1. When one considers a finite strip and singly-diffracted fields only, it is natural to introduce the notation Q_{E_1}, Q_{E_2}, ρ_1', ρ_1, ϕ_1', ϕ_1, ρ_2', ρ_2, ϕ_2', ϕ_2; as shown in figure 2.3. (Where ρ' normally denotes distance from the source to the edge diffraction point Q_E, ρ_1' now denotes the distance from the source to Q_{E_1}, and so on.) However, when one considers multiply-diffracted fields, the edges become additional source points, and the problem

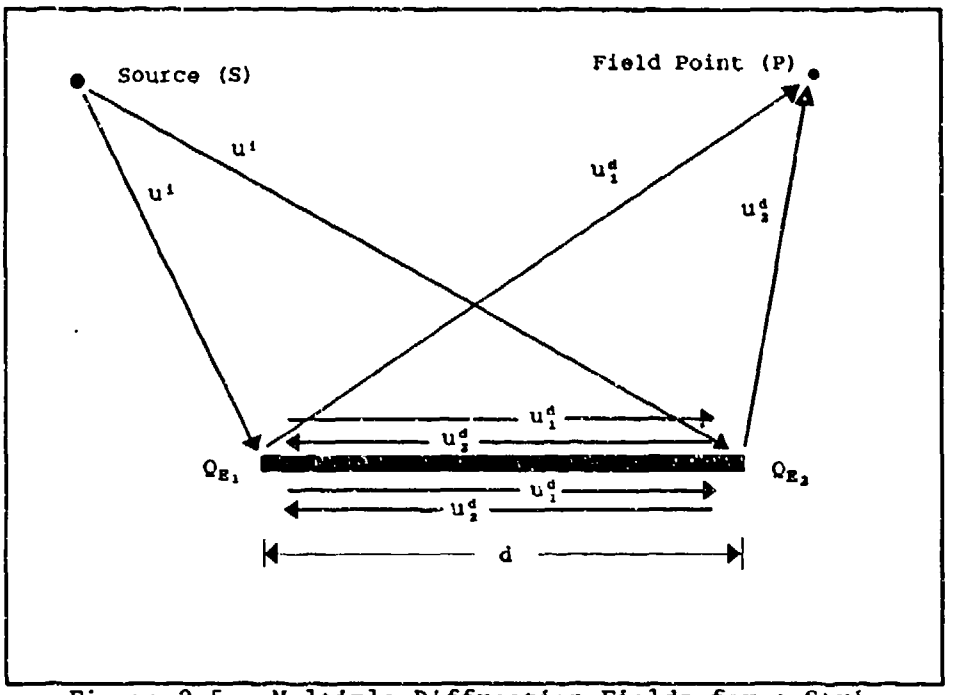

Figure 2.5. Multiple Diffraction Fields for a Strip

solution involves writing field expressions which treat the edges as observation points also. The notation can quickly become very cumbersome; certain choices will avoid this. Here, we will reserve the variables (ρ_1', ϕ_1'), (ρ_1, ϕ_1), (ρ_2', ϕ_2'), (ρ_2, ϕ_2) to locate the source point (S) and field point (P) relative to the two edges, as shown in figure 2.3. The incident field is denoted u^i, the total diffracted field from Q_{E_1} is denoted u_1^d, and the total diffracted field from Q_{E_2} is denoted u_2^d. These fields are illustrated in figure 2.5. (We refer to u_1^d and u_2^d as "total" diffracted fields since they are the result of the incident field and an infinite number of multiply-diffracted fields illuminating Q_{E_1} and Q_{E_2}, respectively. Also, note that our solution will necessarily involve the ray of u_1^d that propagates to Q_{E_2} via paths both above and below the strip; thus, these ray paths are shown in

figure 2.5 along with the ray that propagates to P. A similar remark holds for u_2^d.)

The total diffracted fields u_1^d and u_2^d at the field point P are given by

$$u_1^d(P) = \left[u^i(Q_{E_1})\, D_{s,h}(\phi_1', \phi_1, L_1) + \tfrac{1}{2} u_2^d(Q_{E_1}^T)\, D_{s,h}(0, \phi_1, L_3) + \tfrac{1}{2} u_2^d(Q_{E_1}^B)\, D_{s,h}(2\pi, \phi_1, L_3)\right] \frac{e^{-jk\rho_1}}{\sqrt{\rho_1}} \tag{2.8.a}$$

$$u_2^d(P) = \left[u^i(Q_{E_2})\, D_{s,h}(\phi_2', \phi_2, L_2) + \tfrac{1}{2} u_1^d(Q_{E_2}^T)\, D_{s,h}(0, \phi_2, L_4) + \tfrac{1}{2} u_1^d(Q_{E_2}^B)\, D_{s,h}(2\pi, \phi_2, L_4)\right] \frac{e^{-jk\rho_2}}{\sqrt{\rho_2}} \tag{2.8.b}$$

where the factors of ½ account for grazing incidence (10), the superscripts T and B refer to rays that travel to an edge point Q_E via a path along the top or bottom of the strip, and the distance parameters are given by

$$L_1 = \frac{\rho_1 \rho_1'}{\rho_1 + \rho_1'} \tag{2.9.a}$$

$$L_2 = \frac{\rho_2 \rho_2'}{\rho_2 + \rho_2'} \tag{2.9.b}$$

$$L_3 = \frac{\rho_1 d}{\rho_1 + d} \tag{2.9.c}$$

$$L_4 = \frac{\rho_2 d}{\rho_2 + d} \tag{2.9.d}$$

To solve for $u_1^d(P)$ and $u_2^d(P)$, we begin by writing the following expressions from eq (2.8)

$$u_1^d(Q_{E_2}^T) = \left[u^i(Q_{E_1}) D_{s,h}(\phi_1', 0, L_5) + \tfrac{1}{2} u_2^d(Q_{E_1}^T) D_{s,h}(0, 0, L_6) + \tfrac{1}{2} u_2^d(Q_{E_1}^B) D_{s,h}(2\pi, 0, L_6)\right] \frac{e^{-jkd}}{\sqrt{d}} \tag{2.10.a}$$

$$u_1^d(Q_{E_2}^B) = \left[u^i(Q_{E_1}) D_{s,h}(\phi_1', 2\pi, L_5) + \tfrac{1}{2} u_2^d(Q_{E_1}^T) D_{s,h}(0, 2\pi, L_6) + \tfrac{1}{2} u_2^d(Q_{E_1}^B) D_{s,h}(2\pi, 2\pi, L_6)\right] \frac{e^{-jkd}}{\sqrt{d}} \tag{2.10.b}$$

$$u_2^d(Q_{E_1}^T) = \left[u^i(Q_{E_2}) D_{s,h}(\phi_2', 0, L_7) + \tfrac{1}{2} u_1^d(Q_{E_2}^T) D_{s,h}(0, 0, L_6) + \tfrac{1}{2} u_1^d(Q_{E_2}^B) D_{s,h}(2\pi, 0, L_6)\right] \frac{e^{-jkd}}{\sqrt{d}} \tag{2.10.c}$$

$$u_2^d(Q_{E_1}^B) = \left[u^i(Q_{E_2}) D_{s,h}(\phi_2', 2\pi, L_7) + \tfrac{1}{2} u_1^d(Q_{E_2}^T) D_{s,h}(0, 2\pi, L_6) + \tfrac{1}{2} u_1^d(Q_{E_2}^B) D_{s,h}(2\pi, 2\pi, L_6)\right] \frac{e^{-jkd}}{\sqrt{d}} \tag{2.10.d}$$

where

$$L_5 = \frac{\rho_1' d}{\rho_1' + d} \tag{2.11.a}$$

$$L_6 = d/2 \tag{2.11.b}$$

$$L_7 = \frac{\rho_2' d}{\rho_2' + d} \tag{2.11.c}$$

Let A, B, and C be (known) complex quantities defined as

$$A = D_{s,h}(\phi_1', 0, L_5) \frac{e^{-jkd}}{\sqrt{d}} = -D_{s,h}(\phi_1', 2\pi, L_5) \frac{e^{-jkd}}{\sqrt{d}} \tag{2.12.a}$$

$$B = \tfrac{1}{2}D_{s,h}(0,0,L_6)\frac{e^{-jkd}}{\sqrt{d}} = -\tfrac{1}{2}D_{s,h}(2\pi,0,L_6)\frac{e^{-jkd}}{\sqrt{d}}$$
$$= -\tfrac{1}{2}D_{s,h}(0,2\pi,L_6)\frac{e^{-jkd}}{\sqrt{d}} = \tfrac{1}{2}D_{s,h}(2\pi,2\pi,L_6)\frac{e^{-jkd}}{\sqrt{d}} \qquad (2.12.b)$$

$$C = D_{s,h}(\phi_2',0,L_7)\frac{e^{-jkd}}{\sqrt{d}} = -D_{s,h}(\phi_2',2\pi,'L_7)\frac{e^{-jkd}}{\sqrt{d}} \qquad (2.12.c)$$

where we have used the fact that a 2π change in either of the first two arguments of $D_{s,h}$ produces a sign change in $D_{s,h}$. Eqs (2.10) may then be rewritten as:

$$u_1^d(Q_{E_2}^T) = Au^i(Q_{E_1}) + B[u_2^d(Q_{E_1}^T) - u_2^d(Q_{E_1}^B)] \qquad (2.13.a)$$

$$u_1^d(Q_{E_2}^B) = -u_1^d(Q_{E_2}^T) \qquad (2.13.b)$$

$$u_2^d(Q_{E_1}^T) = Cu^i(Q_{E_2}) + B[u_1^d(Q_{E_2}^T) - u_1^d(Q_{E_2}^B)] \qquad (2.13.c)$$

$$u_2^d(Q_{E_1}^B) = -u_2^d(Q_{E_1}^T) \qquad (2.13.d)$$

Finally, using eq (2.13.d) in (2.13.a) and eq (2.13.b) in (2.13.c) yields

$$u_1^d(Q_{E_2}^T) = Au^i(Q_{E_1}) + 2Bu_2^d(Q_{E_1}^T) \qquad (2.14.a)$$

$$u_2^d(Q_{E_1}^T) = Cu^i(Q_{E_2}) + 2Bu_1^d(Q_{E_2}^T) \qquad (2.14.b)$$

These two equations can be solved for $u_1^d(Q_{E_2}^T)$ and $u_2^d(Q_{E_1}^T)$, which results in

$$u_1^d(Q_{E_2}^T) = \frac{Au^i(Q_{E_1}) + 2BCu^i(Q_{E_2})}{1 - 4B^2} \qquad (2.15.a)$$

$$u_2^d(Q_{E_1}^T) = \frac{Cu^i(Q_{E_2}) + 2ABu^i(Q_{E_1})}{1 - 4B^2} \qquad (2.15.b)$$

Substituting equations (2.13.b, d) into (2.8), and again noting that a 2π change in the first argument of $D_{s,h}$ produces a sign change in $D_{s,h}$, the final form for the total diffracted fields emanating from Q_E and Q_{E_2} is found to be

$$u_1^d(P) = [u^i(Q_{E_1}) D_{s,h}(\phi_1', \phi_1, L_1) + u_2^d(Q_{E_1}^T) D_{s,h}(0, \phi_1, L_3)] \frac{e^{-jk\rho_1}}{\sqrt{\rho_1}} \qquad (2.16.a)$$

$$u_2^d(P) = [u^i(Q_{E_2}) D_{s,h}(\phi_2', \phi_2, L_2) + u_1^d(Q_{E_2}^T) D_{s,h}(0, \phi_2, L_4)] \frac{e^{-jk\rho_2}}{\sqrt{\rho_2}} \qquad (2.16.b)$$

where eqs (2.9) define $L_{1,2,3,4}$ and eqs (2.15), (2.12), and (2.11) are used to determine $u_1^d(Q_{E_2}^T)$ and $u_2^d(Q_{E_1}^T)$.

Diffractions from Impedance Edges and Junctions

The diffracted field from a perfect conductor smooths out the discontinuities in the GO field at the shadow boundaries. Consider now the case of a half-plane or strip with a finite impedance. The discontinuities in the GO field are different than those for a perfect conductor; this difference depends on the magnitudes of the reflected and transmitted fields. Of course, the diffracted field must again smooth these new discontinuities.

A planar sheet of finite impedance has a reflection coefficient (R) and transmission coefficient (T) that are dependent on the sheet impedance and on the incoming plane wave's angle of incidence. In contrast, R and T for a perfect conductor are fixed at ± 1 and 0 ,

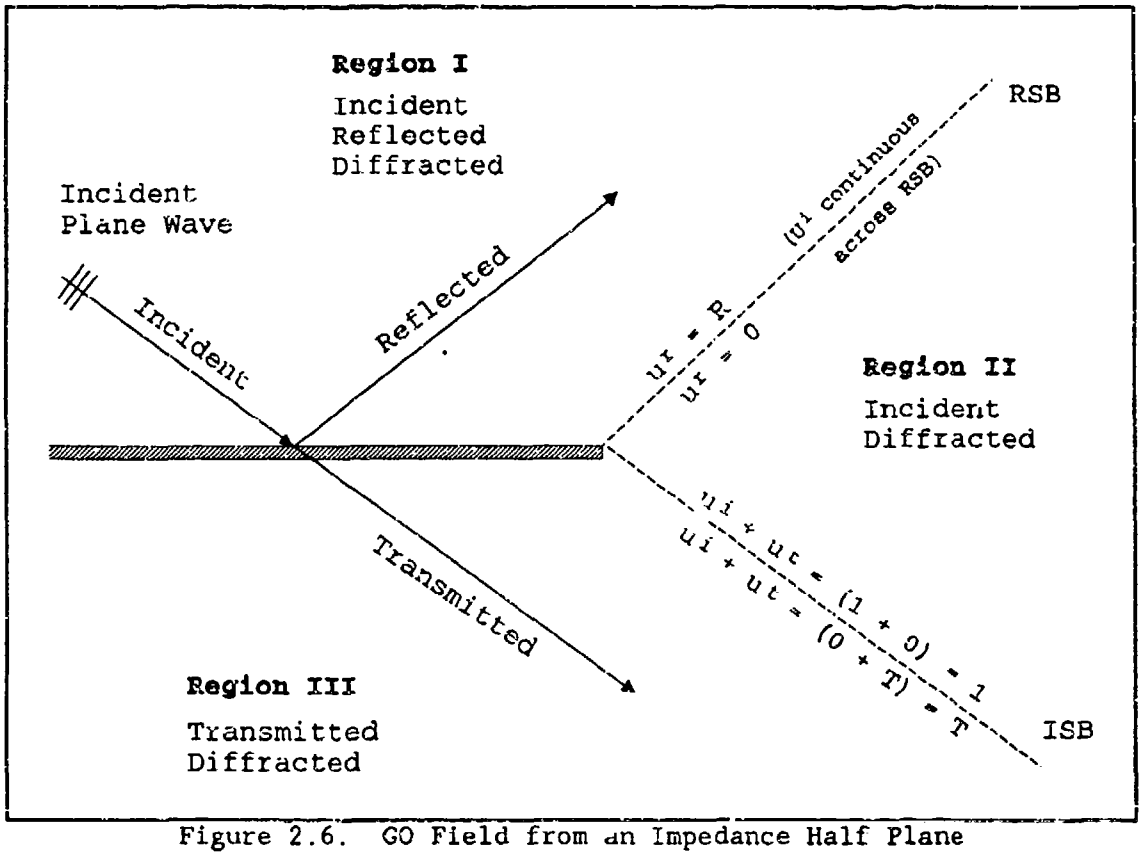

Figure 2.6. GO Field from an Impedance Half Plane

respectively (where +1 is for H polarization and -1 for E polarization). For either material the GO discontinuity across the RSB is R and that across the ISB is 1 - T. (This assumes that the incident field's magnitude is equal to one.) These discontinuities are indicated in figure 2.6.

Since the GO discontinuities associated with the impedance half-plane are scaled relative to those for the perfectly-conducting half-plane, the diffracted field at the shadow boundaries must be scaled in the same manner. An approximate way to determine the diffracted field in all space is to assume that the scale factors found at the shadow boundaries apply to all space. This was the approach used by Burnside

and Burgener (2) for a dielectric half-plane. Thus, the diffraction coefficient is written as

$$D_{s,h} = (1 - T_{s,h}) D(\phi - \phi') + R_{s,h} D(\phi + \phi') \qquad (2.17)$$

In (2), it was shown that this approach gave good agreement with moment method calculations for a finite dielectric strip. The approach of (2) has been applied to impedance strips (7); this method will be used here.

Geometrical Optics Field from a Plane of Finite Impedance. The GO field from an impedance plane consists of an incident, reflected, and transmitted field. These are found for both polarizations assuming the incident field is a plane wave.

Soft (TE) Boundary Conditions. The GO fields for soft boundary conditions are:

$$\boldsymbol{E}^i = \hat{z} E_o \exp[jk(-x\sin\theta^i + y\cos\theta^i)] \qquad (2.18.a)$$

$$\boldsymbol{H}^i = (-\hat{x}\cos\theta^i - \hat{y}\sin\theta^i) \frac{E_o}{Z_o} \exp[jk(-x\sin\theta^i + y\cos\theta^i)] \qquad (2.18.b)$$

$$\boldsymbol{E}^r = \hat{z} R_s E_o \exp[jk(-x\sin\theta^i - y\cos\theta^i)] \qquad (2.18.c)$$

$$\boldsymbol{H}^r = (\hat{x}\cos\theta^i - \hat{y}\sin\theta^i) R_s \frac{E_o}{Z_o} \exp[jk(-x\sin\theta^i - y\cos\theta^i)] \qquad (2.18.d)$$

$$\boldsymbol{E}^t = \hat{z} T_s E_o \exp[jk(-x\sin\theta^i + y\cos\theta^i)] \qquad (2.18.e)$$

$$\boldsymbol{H}^t = (-\hat{x}\cos\theta^i - \hat{y}\sin\theta^i) T_s \frac{E_o}{Z_o} \exp[jk(-x\sin\theta^i + y\cos\theta^i)] \qquad (2.18.f)$$

where $\mathbf{E}^i$, $\mathbf{H}^i$ are the incident electric, magnetic fields, $\mathbf{E}^r$, $\mathbf{H}^r$ are the reflected electric, magnetic fields, and $\mathbf{E}^t$, $\mathbf{H}^t$ are the transmitted

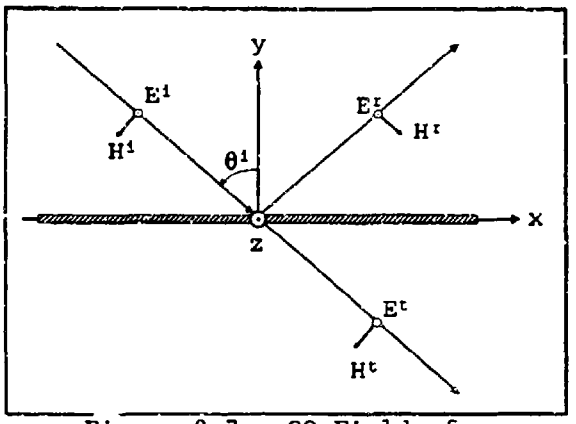

Figure 2.7. GO Fields for Soft Polarization

electric, magnetic fields. E_o is the magnitude of the incident electric field, Z_o is free space impedance (377Ω), R_s and T_s are the reflection and transmission coefficients for soft boundary conditions, and θ^i is the plane wave's incident angle, measured counterclockwise from the plane's normal as shown in figure 2.7. The source is assumed to be in the y>0 half space, mandating the condition $-\pi/2 < \theta^i < \pi/2$.

R_s and T_s are found by applying the appropriate boundary conditions. The tangential components of the electric field must be continuous across the impedance plane:

$$E_z^t = E_z^i + E_z^r \qquad |_{y=0} \tag{2.19}$$

This leads to:

$$T_s = 1 + R_s \tag{2.20}$$

The tangential component of the magnetic field is discontinuous across the impedance plane by the strip current density:

$$\boldsymbol{J} = \hat{y} \times [(\boldsymbol{H}^i + \boldsymbol{H}^r) - \boldsymbol{H}^t] \qquad |_{y=0} \tag{2.21}$$

Entering the magnetic field expressions and using eq (2.20), this can be solved to obtain:

$$J = -\hat{z}\,2R_s\cos\theta^i \frac{E_o}{Z_o} e^{-jkx\sin\theta^i} \qquad (2.22)$$

The strip current density is equal to the total tangential electric field divided by the strip impedance:

$$J_z = \frac{E_z^i + E_z^r}{Z} \Big|_{y=0} \qquad (2.23)$$

This is solved for R_s using eqs (2.22), (2.18.a), and (2.18.c):

$$R_s = \frac{-1}{1 + 2\eta\cos\theta^i} \qquad (2.24)$$

where η is the normalized impedance, Z/Z_o.

Results for R_s and T_s are plotted in figure 2.8 as functions of strip resistance and incident angle. Notice that R_s is -1 and T_s is 0 when η is 0, as they should be for a perfect conductor. The GO fields are now determined by using the expressions for R_s and T_s in eqs (2.24) and (2.20) in eqs (2.18).

Hard (TM) Boundary Conditions. The GO fields for hard boundary conditions are:

$$E^i = E_o(\hat{x}\cos\theta^i + \hat{y}\sin\theta^i)\exp[jk(-x\sin\theta^i + y\cos\theta^i)] \qquad (2.25.a)$$

$$H^i = \hat{z}\frac{E_o}{Z_o}\exp[jk(-x\sin\theta^i + y\cos\theta^i)] \qquad (2.25.b)$$

$$E^r = R_h E_o(-\hat{x}\cos\theta^i + \hat{y}\sin\theta^i)\exp[jk(-x\sin\theta^i - y\cos\theta^i)] \qquad (2.25.c)$$

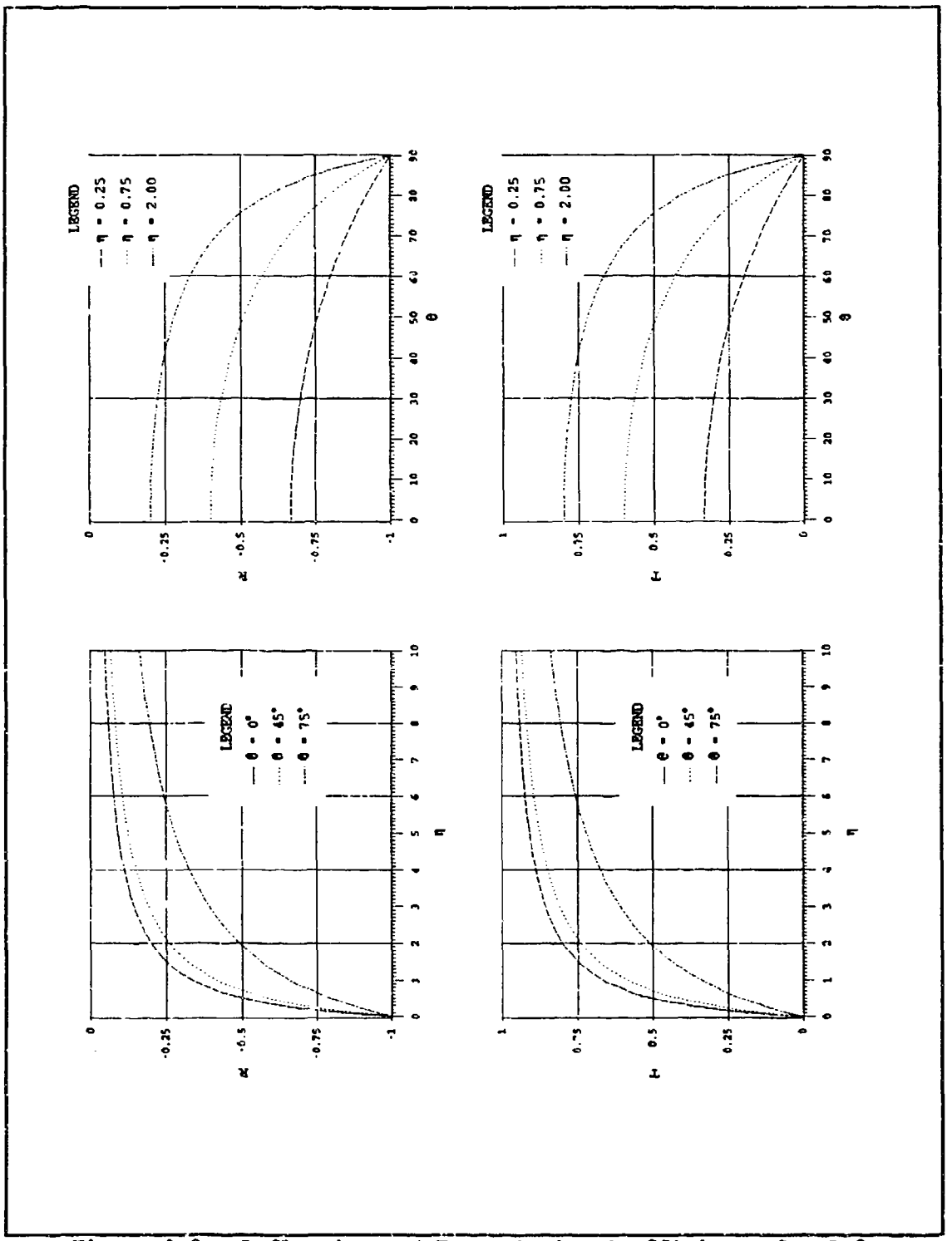

Figure 2.8. Reflection and Transmission Coefficients for Soft Polarization

$$\mathbf{H}^r = 2R_h \frac{E_o}{Z_o} \exp[jk(-x\sin\theta^i - y\cos\theta^i)] \qquad (2.25.d)$$

$$\mathbf{E}^t = T_h E_o (\hat{x}\cos\theta^i + \hat{y}\sin\theta^i) \exp[jk(-x\sin\theta^i + y\cos\theta^i)] \qquad (2.25.e)$$

$$\mathbf{H}^t = 2T_h \frac{E_o}{Z_o} \exp[jk(-x\sin\theta^i + y\cos\theta^i)] \qquad (2.25.f)$$

where R_h and T_h are the reflection and transmission coefficients for hard boundary conditions. The fields are displayed in figure 2.9. Once

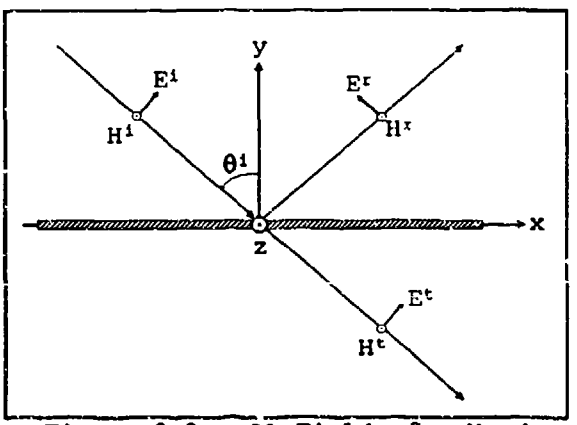

Figure 2.9. GO Fields for Hard Polarization

again, boundary conditions are applied to obtain solutions for R_h, T_h, and J. The electric field must be continuous across the impedance plane:

$$E_x^t = E_x^i + E_x^r \qquad |_{y=0} \qquad (2.26)$$

This results in:

$$T_h = 1 - R_h \tag{2.27}$$

The tangential component of the magnetic field is discontinuous across the impedance plane by the strip current density:

$$\boldsymbol{J} = \hat{\boldsymbol{y}} \times [(\boldsymbol{H}^i + \boldsymbol{H}^r) - \boldsymbol{H}^t] \quad |_{y=0} \tag{2.28}$$

This yields the strip current density:

$$\boldsymbol{J} = \hat{\boldsymbol{x}} 2 R_h \frac{E_o}{Z_o} e^{-jkx\sin\theta^i} \tag{2.29}$$

Finally, the strip current density is equal to the total tangential electric field divided by the strip impedance:

$$J_x = \frac{E_x^i + E_x^r}{Z} \quad |_{y=0} \tag{2.30}$$

This is solved to obtain an expression for R_h:

$$R_h = -\frac{\cos\theta^i}{2\eta + \cos\theta^i} \tag{2.31}$$

R_h and T_h are plotted as functions of η and θ in figure 2.10. Notice that R_h is 1 and T_h is 0 when η is 0, as they should be for a perfect conductor. The GO fields can be found by using the expressions for R_h and T_h in (2.31) and (2.27) into eqs (2.25).

A Modified Diffraction Coefficient for Impedance Edges. A formulation for the edge diffraction of an impedance half-plane was developed by Joseph (7), this will now be presented. The reflection and transmission coefficients from the previous section were used to scale the diffraction coefficient for the perfect conductor, as shown:

$$D_{s,h}^{(1)}(\phi',\phi,L,Z) = (1 - T_{s,h}) D(\phi - \phi') + R_{s,h} D(\phi + \phi') \tag{2.32}$$

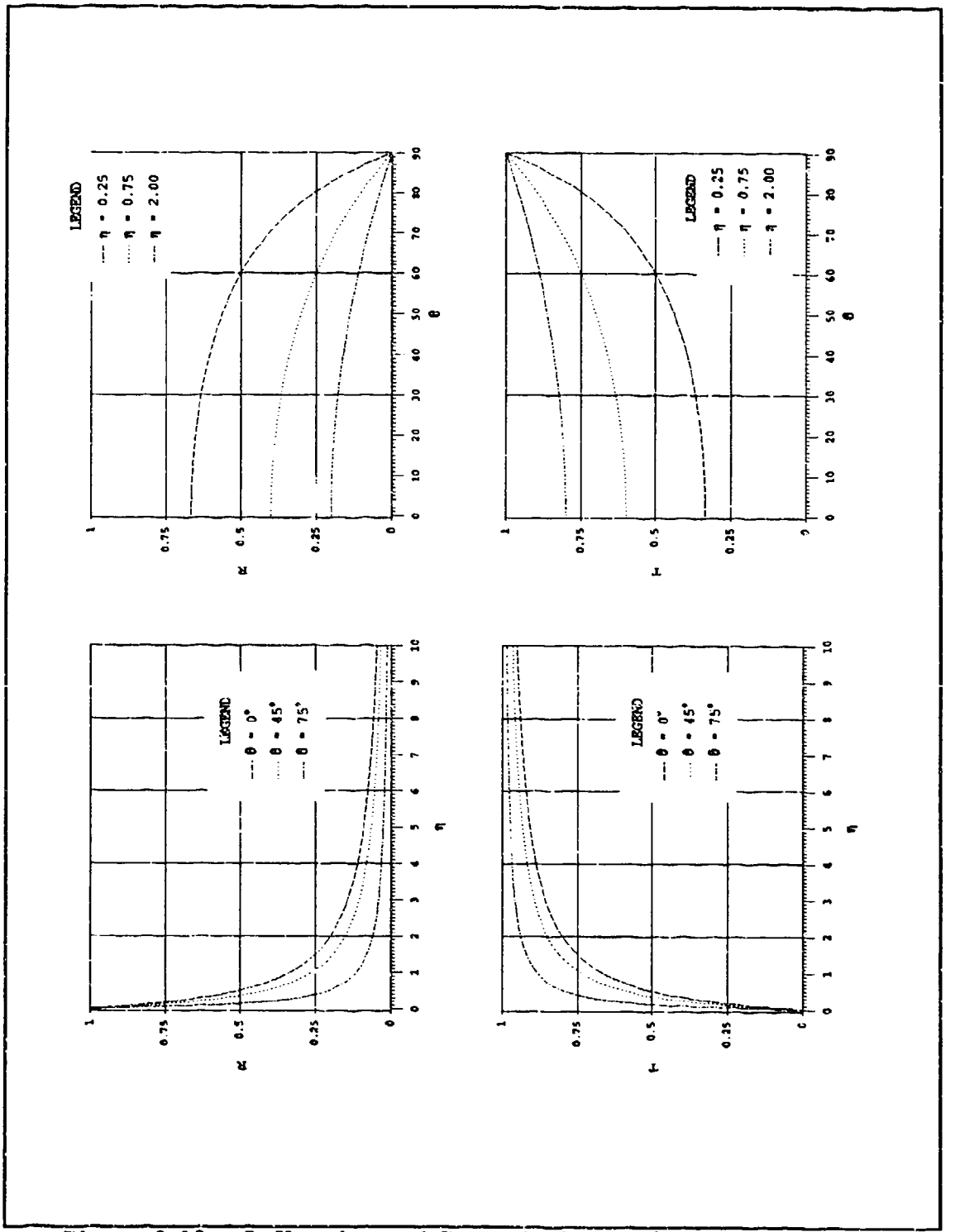

Figure 2.10. Reflection and Transmission Coefficients for Hard Polarization

This expression reduces to the correct form for a perfectly conducting edge, where $R_{s,h} = \mp 1$ and $T_{s,h} = 0$.

There are two problems with the above formulation, both of which deal with the reflection and transmission coefficients. The first problem applies only to soft boundary conditions. When $\theta^i = 90°$, R_s and T_s are -1 and 0, respectively, the same as for a perfect conductor. Thus, the edge-on scattering prediction for the impedance half-plane will be identical to that for the perfectly-conducting half-plane. This is counter to what one would expect, due to the nature of the impedance half-plane as opposed to the conducting half-plane. Comparisons of predictions using the modified UTD solution with measurements and with an eigenfunction solution have indeed illustrated this problem. To overcome this, R_s and T_s are determined using $\theta^i = 0°$ over all incidence angles. Since R_s and T_s depend on the cosine of θ^i, where $\theta^i = 0$ at normal incidence, this will solve the near edge-on problem without markedly changing the predictions elsewhere.

The other problem is that the above diffraction coefficient does not satisfy reciprocity. $R_{s,h}$ and $T_{s,h}$ are functions of the incident angle θ^i, and not the scattered angle θ^s. Therefore, if ϕ and ϕ' are interchanged, the diffracted field prediction will also change. However, as the observer approaches a shadow boundary (where the diffracted field is most significant), the solution becomes reciprocal. Two ways were considered to overcome this problem. The first uses a constant incidence angle to determine $R_{s,h}$ and $T_{s,h}$. This method was already chosen to determine R_s and T_s in order to overcome the edge-on scattering problems. For hard boundary conditions, the incident angle

θ^i is taken as the average of θ^i and θ^s, which forces the solution to satisfy reciprocity. Naturally, the assumption is being made that this will improve the approximate solution.

The reflection and transmission coefficients are now given by:

$$R_{s,h} = \begin{Bmatrix} \frac{-1}{1 + 2\eta} \\ \frac{\cos\theta}{2\eta + \cos\theta} \end{Bmatrix} \tag{2.33.a}$$

$$T_{s,h} = 1 \pm R_{s,h} \tag{2.33.b}$$

where

$$\theta = \frac{\theta^i + \theta^s}{2} \tag{2.34}$$

where $0 \leq \theta^i \leq \pi/2$ and θ^s is measured either clockwise or counterclockwise from the nearest surface normal, so that $0 \leq \theta^s \leq \pi/2$, as seen in figure 2.11.

A Modified Diffraction Coefficient for Impedance Junctions. A formulaton for the diffraction at an impedance junction was developed by Joseph (7), in a manner similar to that for the impedance half-plane. Although the development is similar, unique problems arise. The discontinuity across the RSB is now $R^A_{s,h} - R^B_{s,h}$, and the discontinuity across the ISB is $T^B_{s,h} - T^A_{s,h}$, as seen in figure 2.11. This discontinuity corresponds to the decrease in the field while moving in the positive ϕ direction. When these discontinuities are used to scale the diffraction coefficient, the result is:

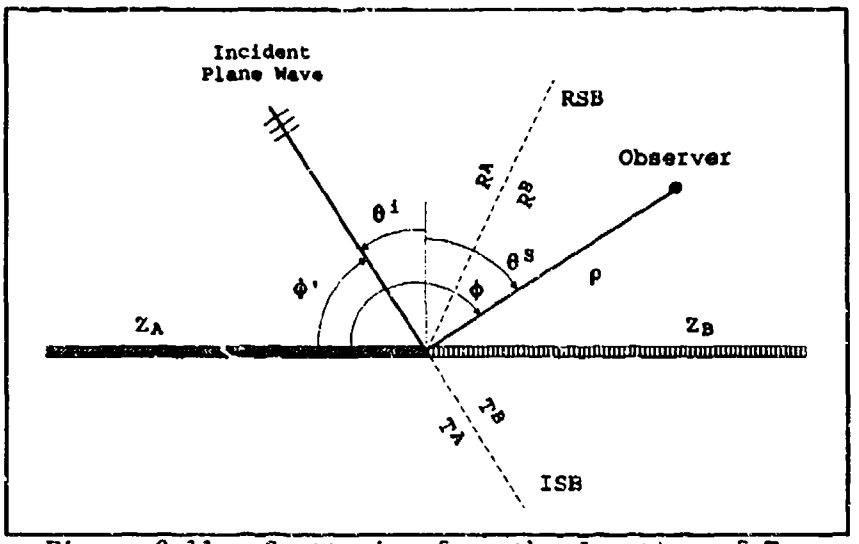

Figure 2.11. Scattering from the Junction of Two Impedance Half Planes

$$D^{(2)}_{s,h}(\phi', \phi, L, Z_A, Z_B) = (T^B_{s,h} - T^A_{s,h})\, D(\phi - \phi') + (R^A_{s,h} - R^B_{s,h})\, D(\phi + \phi') \qquad (2.35)$$

where both ϕ and ϕ' are measured from material A. The problems discussed for the case of edge diffraction are also present here, and are also overcome using $R_{s,h}$ and $T_{s,h}$ from eqs (2.33.a) and (2.33.b). However, an additional problem exists. Different solutions are obtained depending on which material is chosen as A or B (7). This is illustrated as follows. Number the materials as one and two, as shown in figure 2.12. First material 1 is selected as A and material 2 as B; then A and B are reversed. Recall that ϕ, ϕ' are measured from A; thus they are measured as shown in figure 2.12, where we rename them as ψ, ψ' for the second case in 2.12.b. One can show:

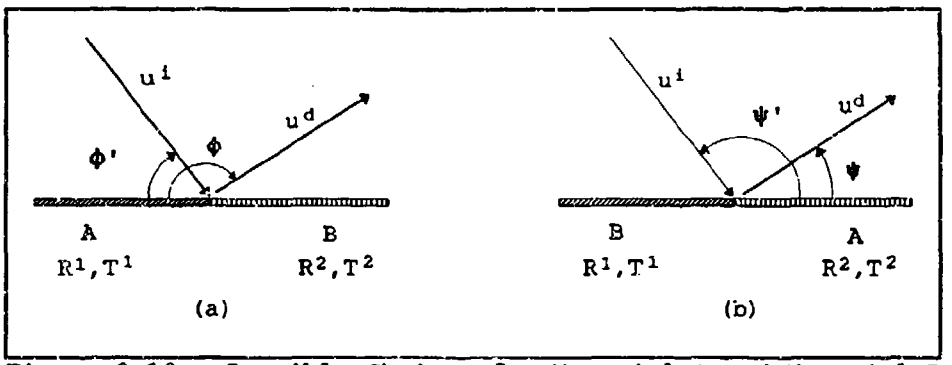

Figure 2.12. Possible Choices for Material A and Material B

$$\psi = \begin{cases} \pi - \phi & 0 < \phi < \pi \\ 3\pi - \phi & \pi < \phi < 2\pi \end{cases} \tag{2.36.a}$$

and

$$\psi' = \begin{cases} \pi - \phi' & 0 < \phi' < \pi \\ 3\pi - \phi' & \pi < \phi' < 2\pi \end{cases} \tag{2.36.b}$$

Consider the first term in eq (2.35), which smooths the ISB. Evaluating this term for the case of figure 2.12a:

$$(T^B_{s,h} - T^A_{s,h})\, D(\phi - \phi') = (T^2_{s,h} - T^1_{s,h})\, D(\phi - \phi') \tag{2.37}$$

Evaluating this term for the case of figure 2.12b:

$$(T^B_{s,h} - T^A_{s,h})\, D(\psi - \psi') = (T^1_{s,h} - T^2_{s,h}) \cdot \begin{cases} D(\phi' - \phi) & 0 < \phi, \phi' < \pi \\ D(\phi' - \phi) & \pi < \phi, \phi' < 2\pi \\ D(\phi' - \phi - 2\pi) & 0 < \phi < \pi < \phi' < 2\pi \\ D(\phi' - \phi + 2\pi) & 0 < \phi' < \pi < \phi < 2\pi \end{cases} \tag{2.38}$$

which reduces to:

$$(T^B_{s,h} - T^A_{s,h})\, D(\psi - \psi') = (T^2_{s,h} - T^1_{s,h}) \cdot \begin{cases} -D(\phi - \phi') & \begin{cases} 0<\phi,\phi'<\pi \text{ or} \\ \pi<\phi,\phi'<2\pi \end{cases} \\ D(\phi - \phi') & \begin{cases} 0<\phi<\pi<\phi'<2\pi \text{ or} \\ 0<\phi'<\pi<\phi<2\pi \end{cases} \end{cases} \tag{2.39}$$

Consider the second term in eq (2.35) which smooths the RSB. Evaluating this term for the case of figure 2.12a:

$$(R^A_{s,h} - R^B_{s,h})\, D(\phi + \phi') = (R^1_{s,h} - R^2_{s,h})\, D(\phi + \phi') \tag{2.40}$$

Evaluating this term for the case of figure 2.12b:

$$(R^A_{s,h} - R^B_{s,h})\, D(\psi + \psi') = (R^2_{s,h} - R^1_{s,h}) \cdot \begin{cases} D(2\pi - \phi - \phi') & 0<\phi,\phi'<\pi \\ D(6\pi - \phi - \phi') & \pi<\phi,\phi'<2\pi \\ D(4\pi - \phi - \phi') & 0<\phi<\pi<\phi'<2\pi \\ D(4\pi - \phi - \phi') & 0<\phi'<\pi<\phi<2\pi \end{cases} \tag{2.41}$$

This reduces to:

$$(R^A_{s,h} - R^B_{s,h})\, D(\psi + \psi') = (R^1_{s,h} - R^2_{s,h}) \cdot \begin{cases} D(\phi + \phi') & \begin{cases} 0<\phi,\phi'<\pi \text{ or} \\ \pi<\phi,\phi'<2\pi \end{cases} \\ -D(\phi + \phi') & \begin{cases} 0<\phi<\pi<\phi'<2\pi \text{ or} \\ 0<\phi'<\pi<\phi<2\pi \end{cases} \end{cases} \tag{2.42}$$

Thus, the choice of material A and B affects the solution. However, when the source and observer are in the same half-space, where the RSB term is more significant, the two RSB terms agree. This is seen when comparing eq (2.40) to (2.42). Likewise, when the source and observer are on opposite sides of the plane, where the ISB term is more significant, the two ISB terms agree. This is seen when comparing eq (2.37) to (2.39). This suggests a solution that incorporates only the more significant term of eq 2.35 (7):

$$D^{(2)}_{s,h}(\phi',\phi,L) = \begin{cases} (R^A_{s,h} - R^B_{s,h})\, D(\phi+\phi') & \begin{cases} 0<\phi,\phi'<\pi \\ \pi<\phi,\phi'<2\pi \end{cases} \\ (T^B_{s,h} - T^A_{s,h})\, D(\phi-\phi') & \begin{cases} 0<\phi<\pi<\phi'<2\pi \\ 0<\phi'<\pi<\phi<2\pi \end{cases} \end{cases} \qquad (2.43)$$

where $R^{A,B}_{s,h}$ and $T^{A,B}_{s,h}$ are determined from eqs (2.33).

Although eq (2.43) omits one of the diffraction terms, the result is still very similar to that when both terms are present. This can be seen in figure 2.13. The diffraction from the junction of two impedance half planes is plotted, where the reflection and transmission coefficients for material 1 are R = -0.75 and T = 0.25 and for material 2 are R = -0.25 and T = 0.75. The figures display the cosine terms (scaled by the reflection or transmission coefficients) of the far field diffractions only. Figure 2.13.a gives the bistatic prediction for θ^i = 0°, and figure 2.13.b gives the bistatic prediction for θ^i = 60°. The figures show the results of the equivalent term only and the results when both terms are incorporated, with either material 1 or material 2 chosen as A.

The equivalent term is seen to be an average of the other two curves. This is because the non-equivalent terms differ in sign, and will cancel each other when averaged. The results of all three methods are nearly identical near the shadow boundaries, and are still very similar elsewhere. It should be noted that in figure 2.13.b, where θ^i = 60°, there is more disagreement between the three curves. This can be explained because each term is most significant near its shadow boundary. When the shadow boundaries are close together the omitted, non-equivalent, term is still large, producing a larger disagreement between the three diffraction patterns.

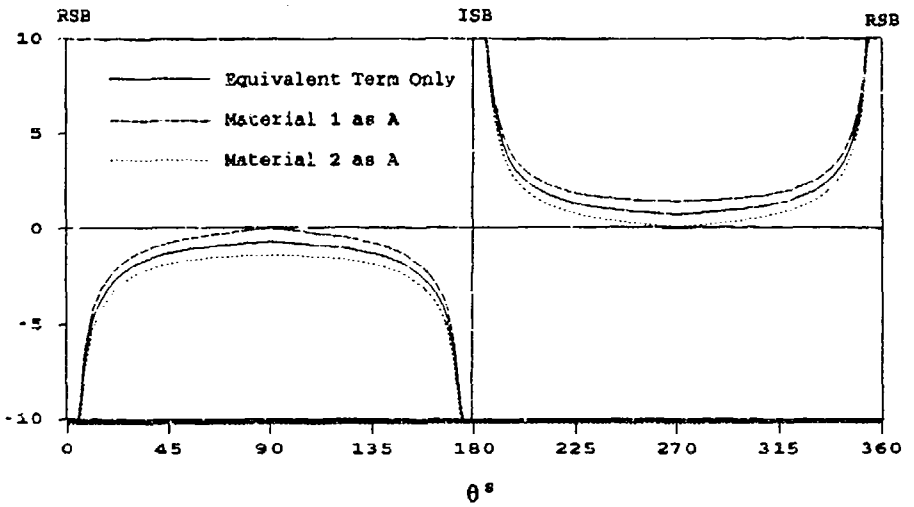

a. $\theta^i = 0°$

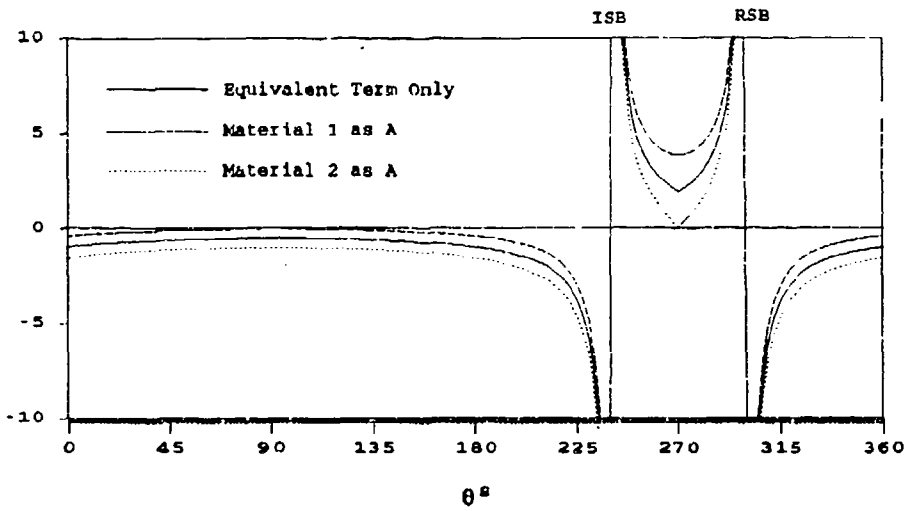

b. $\theta^i = 60°$

Figure 2.13. Bistatic Diffractions from an Impedance Junction

III. Scattering Width Predictions of Impedance Strips and Impedance-Loaded Conducting Strips

The formulae developed in the previous chapter are applied herein to predict the scattering width of impedance strips and impedance loaded conducting strips. First, scattering width simplifications are incorporated into these formulae. Then, they are used to create Fortran programs that predict scattering from impedance strips and impedance loaded conducting strips. The method used to model a tapered impedance in these programs is also discussed. Finally, integral equation and physical optics methods that are used to evaluate the UTD method's accuracy are briefly discussed.

Simplifications

Scattering width is the two-dimensional RCS. Scattering width is defined in eq 1.2:

$$\sigma_{2D} = \lim_{R\to\infty} 2\pi R \left|\frac{\bar{E}^r}{\bar{E}^i}\right|^2 \tag{3.1}$$

$R \to \infty$ indicates that the diffracted field variables ρ, $\rho' \to \infty$ also. This allows the incident field to be modeled as a uniform plane wave, and causes the two ISBs and the two RSBs from each edge of the strip to be parallel. The area between the RSBs, where the reflected field exists, subtends nearly zero angle when viewed from far away. The area between the ISBs, where the incident field is absent, also subtends nearly zero angle for large ρ. This can be seen in figure 3.1; as $\rho\to\infty$, α (the angular region in which the GO reflected field exists) and β (the

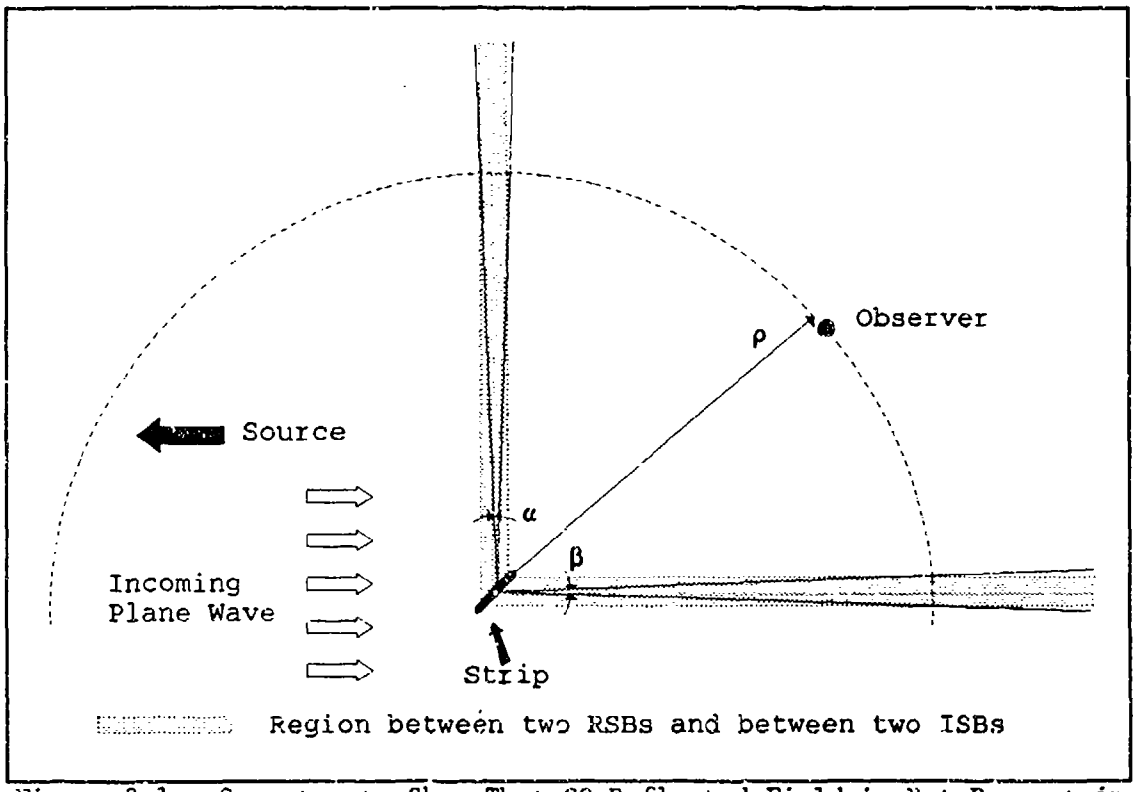

Figure 3.1. Geometry to Show That GO Reflected Field is Not Present in Far Zone Scattering ($\rho \to \infty$) of Strip, Plane Wave Illumination

angular region where the incident field is shadowed by the strip), approach 0. Therefore the GO reflected field is not present in the far zone (except precisely along the RSB, where it is of no use since this is a caustic).

A simplification that can be used when determining scattering width occurs because L approaches infinity when both ρ and ρ' approach infinity. This causes $F[kLa(\phi \pm \phi')] \approx 1$ (10:1453), except on the shadow boundaries where $a(\phi \pm \phi') = 0$ and the argument of F becomes indeterminate. $F[kLa(\phi \pm \phi')]$ can therefore be replaced with one when determining scattering width (single diffraction component only) except directly on the shadow boundaries. However, the observer can be placed

infinitely close to the shadow boundary, and scattering patterns can be calculated using $F[kLa(\phi \pm \phi')] = 1$. That is, instead of attempting to determine the scattered fields directly on one of the shadow boundaries, one can determine the field slightly to either side of it. Accurate results are obtained since the scattered field is continuous. This eliminates the need to calculate $F(kLa(\phi \pm \phi'))$.

In the scattering width predictions the center of the strip is used as phase reference for the incident field, E^i. Since scattering width is independent of $|E^i|$, this magnitude is set equal to one at the center of the strip. Because the incident field is a uniform plane wave, it also has a magnitude of one at the strip's edges. Figure 3.2 illustrates the far field scattering variables for a strip. R' is the

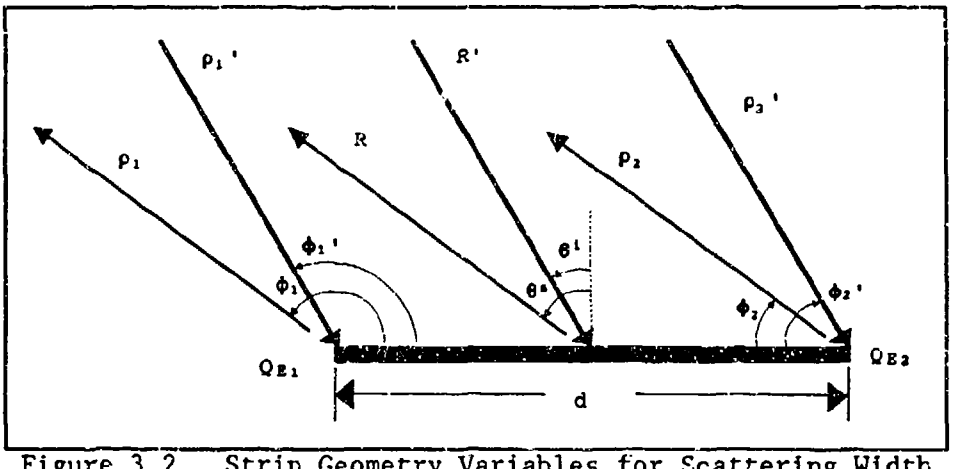

Figure 3.2. Strip Geometry Variables for Scattering Width Determinations

distance from the source to the strip's center and R is the distance from the strip's center to the observer; both R, R' → ∞. θ^i and θ^s are the incident and scattered angles as discussed in chapter 2. The diffraction variables are determined from R, R', θ^i, and θ^s as follows

$$\rho'_{1,2} = R' \mp \frac{d}{2}\sin\theta^i \qquad (3.2.a)$$

$$\rho_{1,2} = R \mp \frac{d}{2}\sin\theta^s \qquad (3.2.b)$$

$$\phi'_{1,2} = \pi/2 \pm \theta^i \qquad (3.3.a)$$

$$\phi_{1,2} = \pi/2 \pm \theta^s \qquad (3.3.b)$$

The scattering width is independent of phase, only the relative phase between scattering sources is important. The relative phase distances, referenced to the strip's center, are given by

$$a'_{1,2} = \rho'_{1,2} - R' = \mp\frac{d}{2}\sin\theta^i \qquad (3.4.a)$$

$$a_{1,2} = \rho_{1,2} - R = \mp\frac{d}{2}\sin\theta^s \qquad (3.4.b)$$

In addition, since the distance $a_{1,2}$ is very small compared to $\rho_{1,2}$, R can replace $\rho_{1,2}$ for magnitude determinations.

Constant Impedance Strips

To predict the scattering width of a constant impedance strip, the effects of multiple diffractions are incorporated. Eqs 2.16 account for all multiple diffractions in predicting the scattered field. These are repeated here with the value for L given for scattering width determinations:

$$u_1^d(P) = \left[u^i(Q_{E_1})\, D_{s,h}^{(1)}(\phi'_1, \phi_1, L\to\infty) + u_2^d(Q_{E_1}^T)\, D_{s,h}^{(1)}(0, \phi_1, d)\right]\frac{e^{-jka_1}}{\sqrt{R}} \qquad (3.5.a)$$

$$u_2^d(P) = \left[u^i(Q_{E_2})\, D_{s,h}^{(1)}(\phi_2', \phi_2, L\to\infty) + u_1^d(Q_{E_2}^T)\, D_{s,h}^{(1)}(0, \phi_2, d)\right] \frac{e^{-jka_2}}{\sqrt{R}} \tag{3.5.b}$$

$D_{s,h}^{(1)}$ is given in eq 2.32. The composite multiple diffraction fields, $u_1^d(Q_{E1}^T)$ and $u_2^d(Q_{E2}^T)$ are given in eqs 2.15 and are repeated here:

$$u_1^d(Q_{E_2}^T) = \frac{Au^i(Q_{E_1}) + 2BCu^i(Q_{E_2})}{1 - 4B^2} \tag{3.6.a}$$

$$u_2^d(Q_{E_1}^T) = \frac{Cu^i(Q_{E_2}) + 2BAu^i(Q_{E_1})}{1 - 4B^2} \tag{3.6.b}$$

A, B, and C are given in eqs 2.12. They are repeated here with the distance parameter's (L) value entered for scattering width determinations:

$$A = D_{s,h}^{(1)}(\phi_1', 0, d)\frac{e^{(-jkd)}}{\sqrt{d}} \tag{3.7.a}$$

$$B = \tfrac{1}{2} D_{s,h}^{(1)}(0, 0, d/2)\frac{e^{(-jkd)}}{\sqrt{d}} \tag{3.7.b}$$

$$C = D_{s,h}^{(1)}(\phi_2', 0, d)\frac{e^{(-jkd)}}{\sqrt{d}} \tag{3.7.c}$$

Using the center of the strip as phase reference, the incident field at the edges of the strip is given by:

$$u^i(Q_{E_{1,2}}) = \exp(\pm jk\tfrac{d}{2}\sin\theta^i) \tag{3.8}$$

These equations are incorporated into three programs to predict the scattering width of a constant impedance strip from $\theta^s = 0.5°$ to 89.5°. Two programs calculate the monostatic scattering width for E-Polarization and for H-Polarization. The third calculates the bistatic

scattering width for H-Polarization. In these programs the strip's width (in wavelengths) and normalized impedance are entered. The incident angle is also entered in the bistatic program. The scattering width in dBλ is returned.

Impedance Loaded Conducting Strips

Multiple diffractions are not considered for loaded strips, due to their increased complexity and because the heuristic UTD modifications are not accurate near edge-on incidence or scattering, which is the case for these multiple diffractions. Only single diffractions are considered. Diffractions from the junctions of the conducting strip and the load are determined using $D_{s,h}^{(2)}$ from eq 2.43. Diffractions from the outer edges of the loads are determined using $D_{s,h}^{(1)}$ from eq 2.32. The incident field is given in eq (3.8). The term $e^{-jk\rho}/\sqrt{\rho}$ in eq (2.1) is also replaced by $e^{-jka}/\sqrt{R}$.

Two Fortran programs to predict the monostatic scattering width of a loaded strip using single diffractions were written. Each does this for either E or H-Polarization. Scattering is evaluated from $\theta^s = 0.5°$ to 89.5° in dBλ.

Variable Impedance Strips and Conducting Strips with Tapered Loads.

Again only single diffractions are considered for these geometries. Diffractions from the conductor/load junctions and the loads' edges are determined in the same manner as for a strip with a constant load. To predict scattering from tapered loads, they are modeled as a sequence of constant impedance loads (7). The impedance of each load in the sequence is determined at its midpoint as indicated in

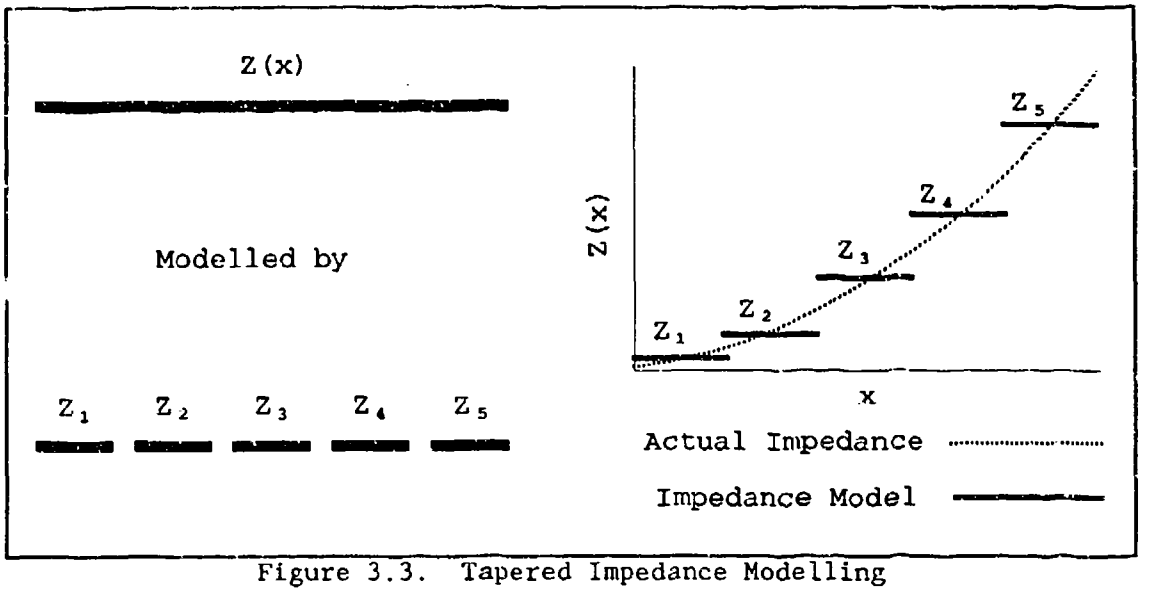

Figure 3.3. Tapered Impedance Modelling

figure 3.3. In all predictions presented herein the model used ten loads per wavelength, the same as the moment method predictions. It was found that as few as five loads per wavelength in the model provided good results, and ten loads per wavelength produced nearly identical results as using fifty. This is shown in figure 3.4 for backscatter from a loaded strip, where the loads have a $4x^2$ taper. Diffractions from the junction of each of these loads are determined using $D_{s,h}^{(2)}$, in eq 2.43. Diffractions from the outer edges of the loads are determined using $D_{s,h}^{(1)}$ from eq 2.32.

Four Fortran programs which predict the scattering width of this geometry using single diffractions were written. Two predict the monostatic scattering width for either E or H-Polarization. The other two programs make bistatic scattering width predictions for the two polarizations. These programs make the predictions for $\theta^s = 0.5°$ to 89.5° in dBλ.

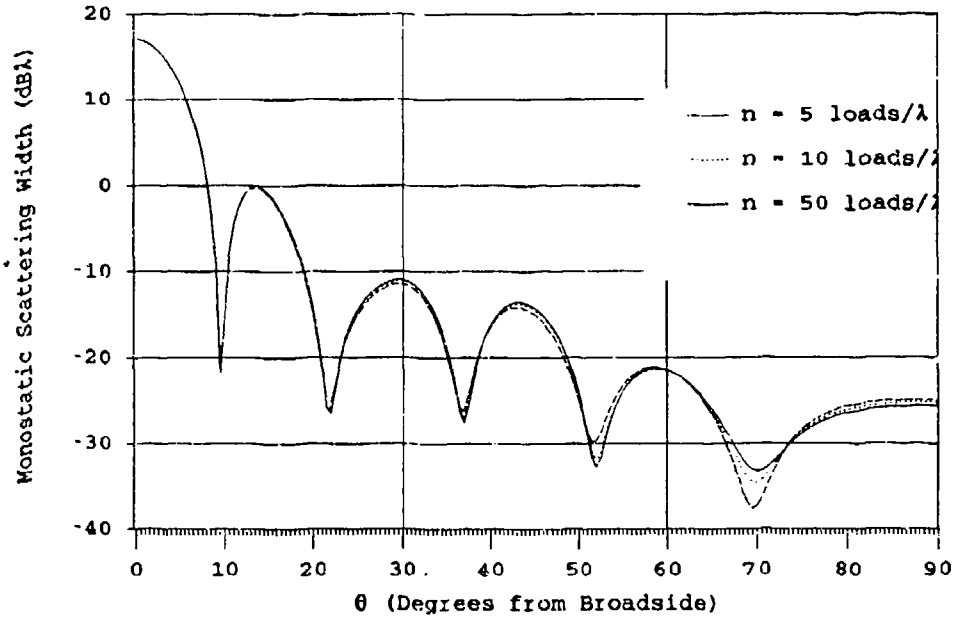

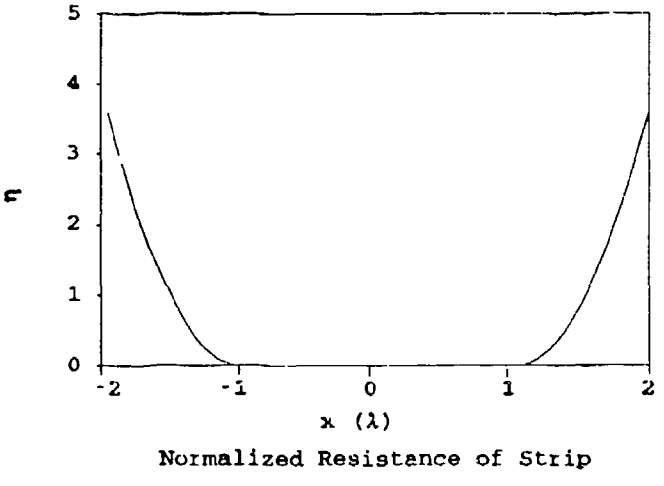

Figure 3.4. Backscatter from a 2λ conducting strip with 1λ, $\eta = 4x^2$ loads: n = 5, 10, 20 models in the load: E-Polarization

These programs could also be used to predict the scattering width of tapered impedance strips, constant impedance strips, or conducting strips with constant loads. The impedance strip calculations are made by entering zero when prompted for the conductor width. The constant loads are simply computed by entering one when prompted for the number of loads in the taper model.

Method of Comparison for Validation of UTD Predictions

Integral Equation Method. In order to verify the accuracy of the UTD scattering predictions, a reliable scattering prediction is required. Haupt (5) investigated scattering from impedance loaded conducting strips and resistive tapers using an integral equation approach. He related the incident field to the surface current that it induces (5:12,13). For TE polarization:

$$H_o e^{jkx\cos\phi_o'} = \eta(x) J_z(x) + \frac{k}{4}\int_{-d}^{d} J_z(x') H_o^{(2)}(k|x-x'|)\,dx' \qquad (3.9.a)$$

and for TM polarization:

$$H_o \sin\phi_o' e^{jkx\cos\phi_o'} = \eta(x) J_x(x) + \frac{k}{4}\int_{-d}^{d} J_x(x') \frac{1}{k|x-x'|} H_1^{(2)}(k|x-x'|)\,dx' \qquad (3.9.b)$$

where the strip lies along the x-axis, centered at x=0. H_o is the magnitude of the incident magnetic field, ϕ_o is the angle of the incident plane wave measured from the positive x-axis, $\eta(x)$ is the normalized surface impedance at x, $J_{z,x}(x)$ is the surface current at x, and $\pm d$ are the positions of the strip's edges on the x-axis.

The method of moments is used to solve these two equations for $J_{z,x}(x)$. Pulse basis functions and a 10 point per wavelength sampling interval are used in the moment method routine (5:16-26). The scattering width is then found from the surface currents (5:40). For TE Polarization:

$$\sigma_{2D} = \frac{k}{4H_o^2}\left|\int_{-d}^{d} J_z(x')\, e^{jkx'\cos\phi_o}\, dx'\right|^2 \qquad (3.10.a)$$

and for TM polarization:

$$\sigma_{2D} = \frac{k}{4H_o^2}\left|\sin\phi_o \int_{-d}^{d} J_x(x')\, e^{jkx'\cos\phi_o}\, dx'\right|^2 \qquad (3.10.b)$$

A program using this method to predict scattering width was obtained (6) to verify the UTD method's accuracy.

Physical Optics Method. In order to determine the utility of the UTD approach its results should be compared to another method of similar complexity. Physical Optics is also a relatively simple way to predict scattering. The PO currents were derived in chapter 2 and are given in eqs (2.22) and (2.29). These currents are then inserted into eqs (3.10) to determine the PO scattering width. For the PO predictions presented herein the integrations in eqs (3.10) are performed using a rectangular pulse integration method with 20 points per wavelength. The PO method was only used to predict the monostatic scattering width since the PO method does not satisfy reciprocity.

All of the predictions were made using an IBM compatible 80386 computer running at 25 MHz. The predictions were made over 179 angles from $\theta^\circ = 0.5^\circ$ to 89.5° at half degree increments. As expected, the

moment method program took the longest to run at 2 minutes. It provided both bistatic and monostatic scattering predictions. The physical optics code took 16 seconds to run. This time could have been halved by using only 10 points per wavelength in the integration routine. The UTD program took from 3 seconds to run for the constant load programs, to 15 seconds for the multiload programs for a tapered strip (calculating 42 diffractions).

IV. Scattering Prediction Results

Scattering predictions for impedance strips and impedance loaded conducting strips are contained herein. First, the diffraction sources from loaded strips are identified. The effect of different impedance loads on them are discussed. Next the results of both UTD and moment method predictions are plotted for various impedance strips and impedance loaded conducting strips. The effects of the different impedance tapers and loads on the scattering patterns are examined. Finally, the accuracy of the UTD predictions, when compared to the moment method results, is discussed.

Diffraction Sources

The diffraction coefficients used to predict scattering from impedance edges and junctions are scaled according to the discontinuities in the GO field. This is an approximation to the scattering solution, and has limited accuracy as either source or observer approaches edge-on. The following discussion is based on the scaled diffraction coefficients; its limited accuracy should be kept in mind.

The diffractions from an impedance loaded conducting strip arise from four locations, the two outer edges of the loads, and the two junctions of the loads with the conducting strip. To observe the effects of the diffraction sources on the loaded strip, the four diffractions are combined into two pairs, those from the outer edges of the strip, and those from the conductor/load junctions. If each

diffraction was viewed independently its effect on the total scattered field would not be readily apparent.

The diffraction coefficients are scaled using the reflection and transmission coefficients of the loads, which are functions of the load impedance. Diffractions from the outer edges of the load are dominant when the load has a low impedance. This is easily seen in figure 4.1; the diffractions from the outer edges of the loads have peaks from six to twelve dB higher than the diffractions from the inner junctions. Since the conductor also has low impedance (zero actually), the impedance discontinuity at the load/conductor interface is smaller than at the loads' outer edges. Similarly, diffractions from the load/conductor junctions are dominant when the load is of high impedance, since the impedance discontinuities at the loads' edges are smaller than at the load/conductor junctions. This is easily seen in figures 4.2 and 4.3; the diffractions from the inner junctions have peaks from six to ten dB higher than the diffractions from the outer junctions.

When the diffraction coefficients for both the inner junctions and the outer edges are scaled by the same amount, they both have an equal influence on the total return. This occurs when $R_{s,h} = \mp 0.5$, which happens for $\eta = 0.5$ for E-Polarization, and $\eta = 0.5 \cos\theta$ for H-Polarization. The diffractions from a conducting strip with $\eta = 0.5$ loads are plotted in figure 4.4. The envelopes of the diffractions from the inner junctions and the outer edges are basically identical. The dominant diffraction sources are also dependent on polarization. Diffractions from the strip's leading edge are dominant for E-

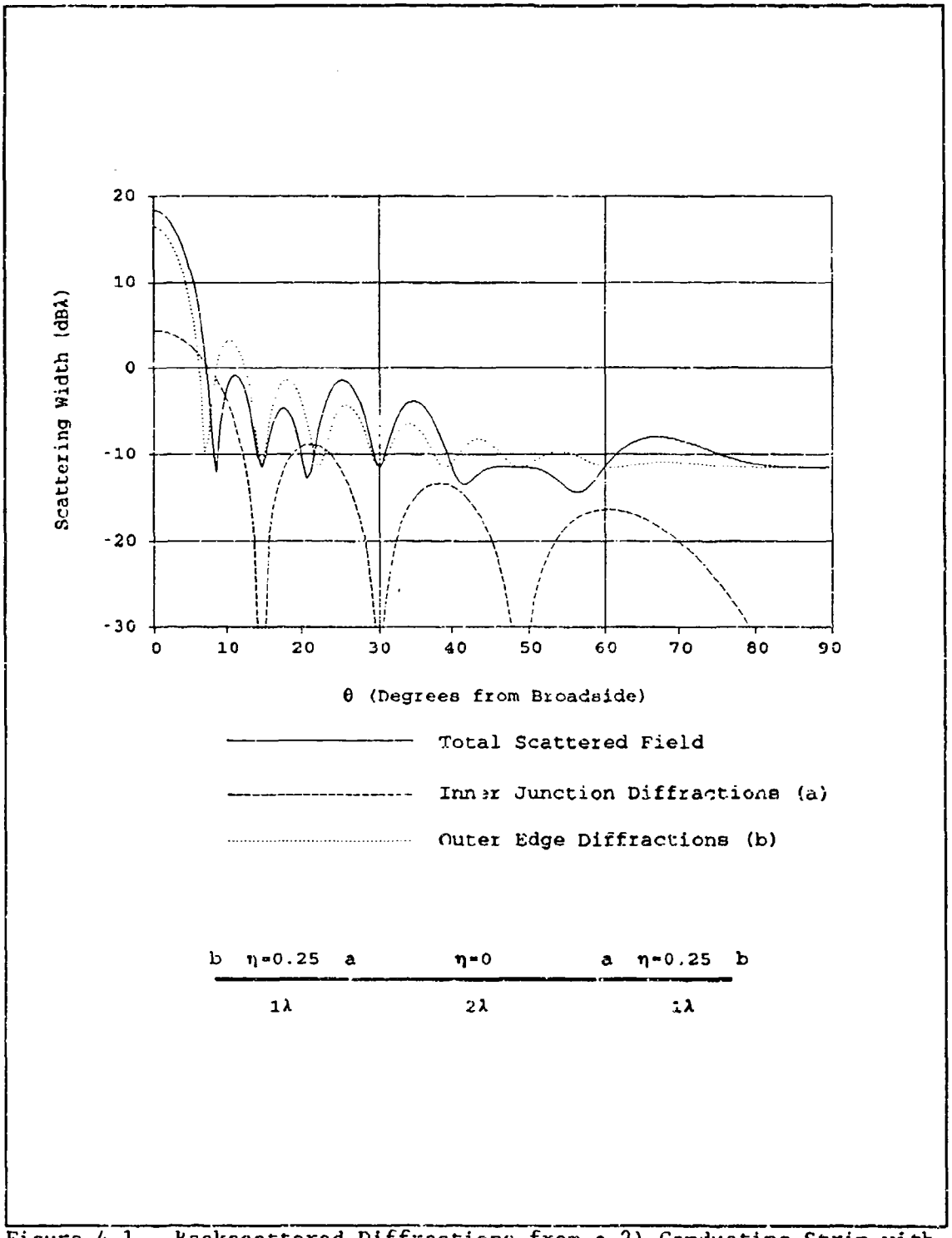

Figure 4.1. Backscattered Diffractions from a 2λ Conducting Strip with 0.25η, 1λ Loads; E-Polarization

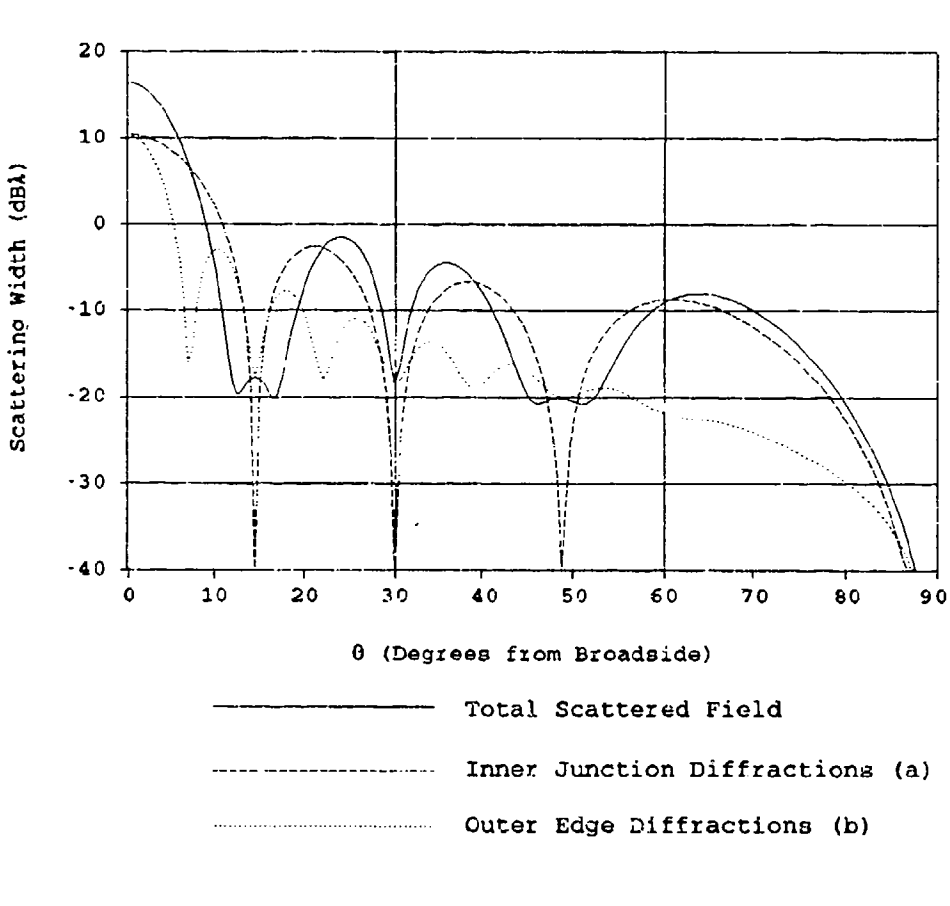

Figure 4.2. Backscattered Diffraction from a 2λ Conducting Strip with 1η, 1λ Loads; H-Polarization

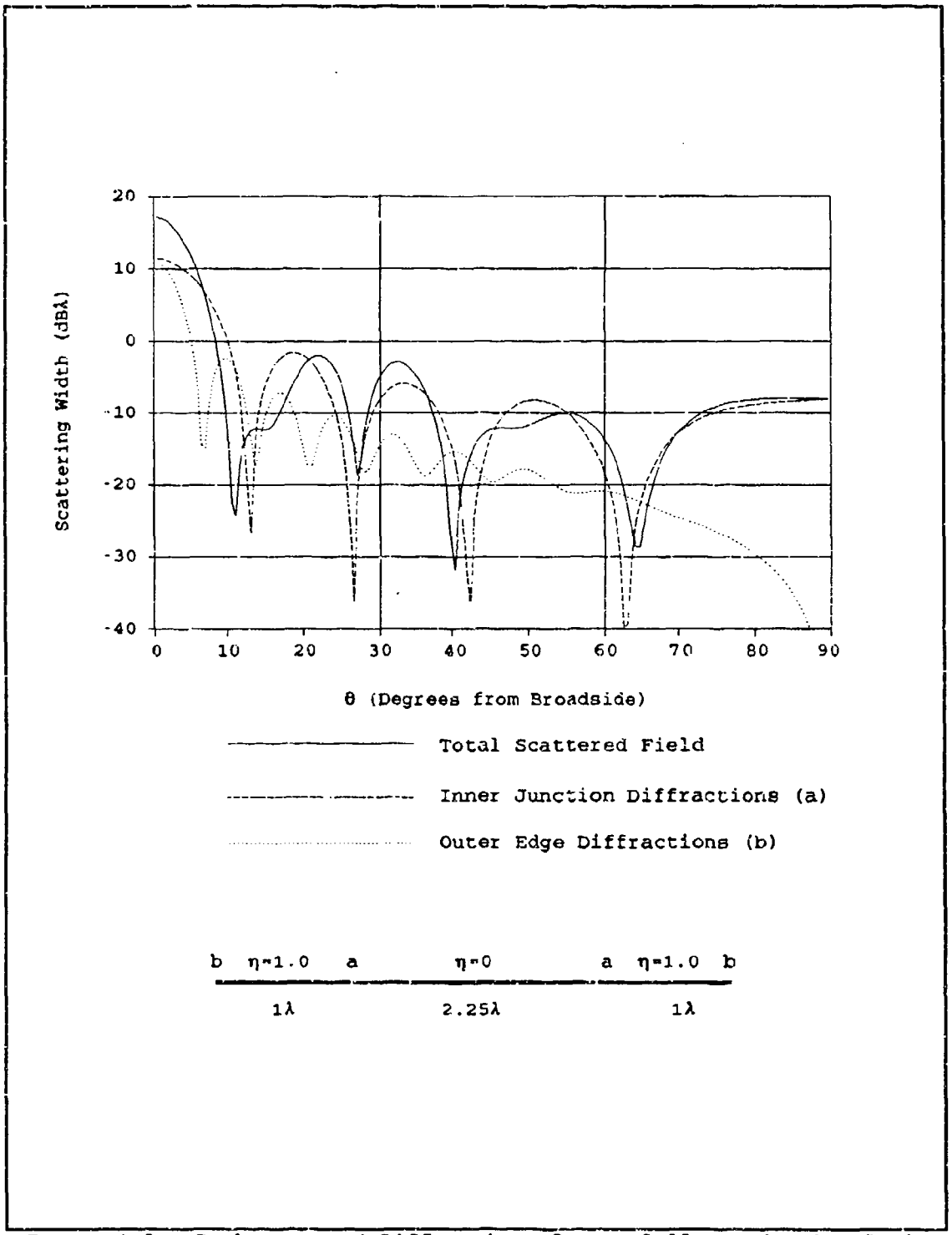

Figure 4.3. Backscattered Diffractions from a 2.25λ Conducting Strip with 1η, 1λ Loads; H-Polarization

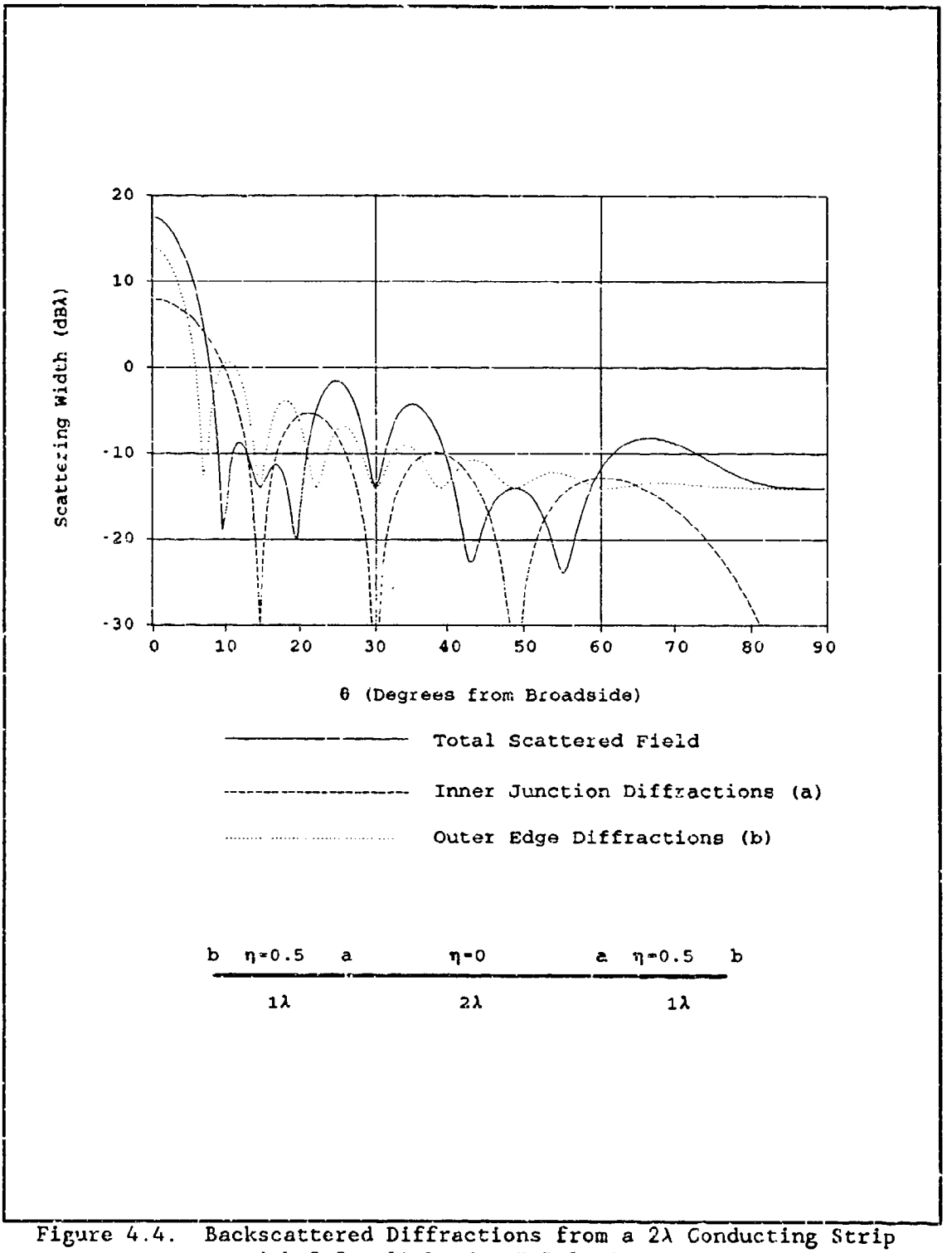

Figure 4.4. Backscattered Diffractions from a 2λ Conducting Strip with 0.5η, 1λ Loads; E-Polarization

Polarization, while diffractions from the strip's trailing edge are dominant for H-Polarization.

When viewing the strip at edge-on incidence, R_h approaches zero and T_h approaches one. When these values are entered into eq 2.32 they drive $D_{s,h}^{(1)}$ to zero, indicating zero diffractions from the edges of an impedance strip for H-Polarization. H-Polarized scattering from a conducting strip also goes to zero for edge-on incidence, but this results from multiple diffractions.

In contrast to the impedance edge diffractions discussed above, H-Polarized diffractions from the load/conductor junction do not approach zero for edge-on incidence. If the conducting strip is an integral number of half-wavelengths wide, however, the diffractions from each side of it will cancel, since they are of equal magnitude but opposite sign. This has a strong impact on the H-Polarization scattering predictions of loaded strips. These effects are seen when viewing scattering from the inner junctions and the outer edges in figures 4.2 and 4.3. The diffractions from the outer edges go to zero, as they do for all H-Polarization cases when $\theta = 90°$. However, diffractions from the load/conductor junctions at $\theta = 90°$ are dependent on the width of the conducting strip.

Scattering Predictions

Impedance Strips. Scattering predictions of strips with constant impedances are presented in figures 4.5 through 4.11. In each figure (a.) displays the impedance of the strip normalized to 377Ω, where x is in wavelengths. Monostatic scattering width predictions using moment method, UTD, and PO methods are plotted in (b.). The bistatic

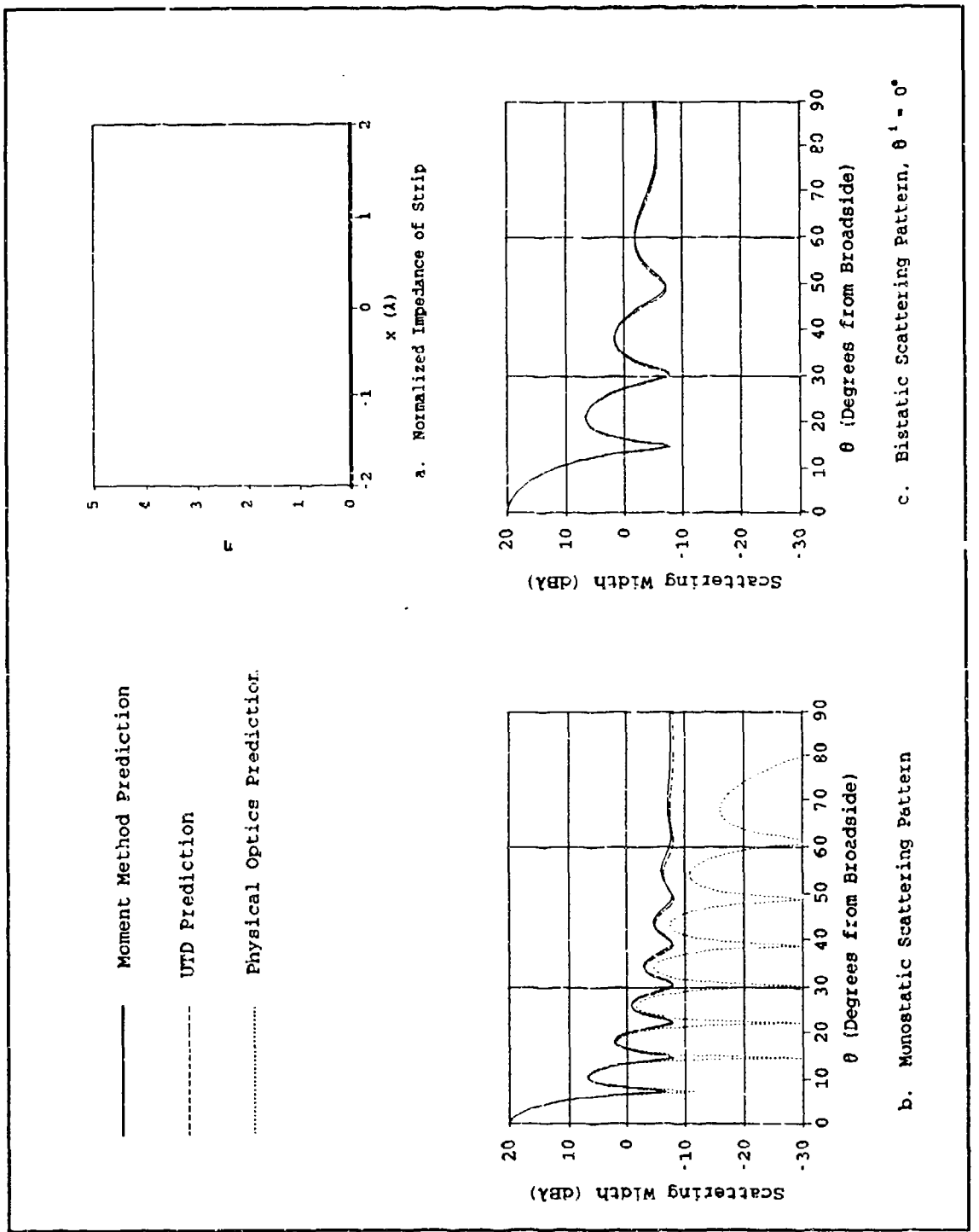

Figure 4.5. Scattering Predictions for a 4λ conducting strip, E-Polarization

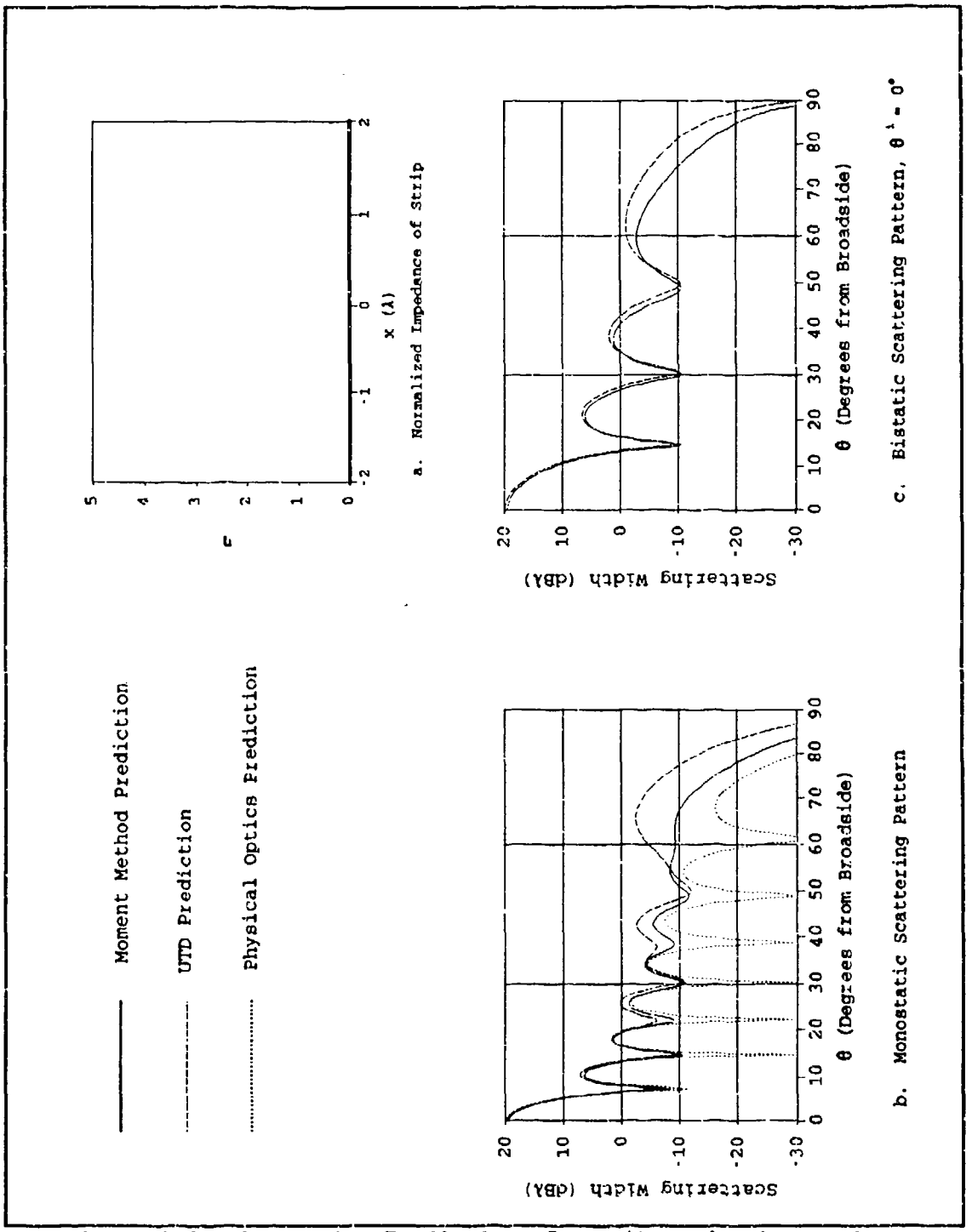

Figure 4.6. Scattering Predictions for a 4λ conducting strip, H-Polarization

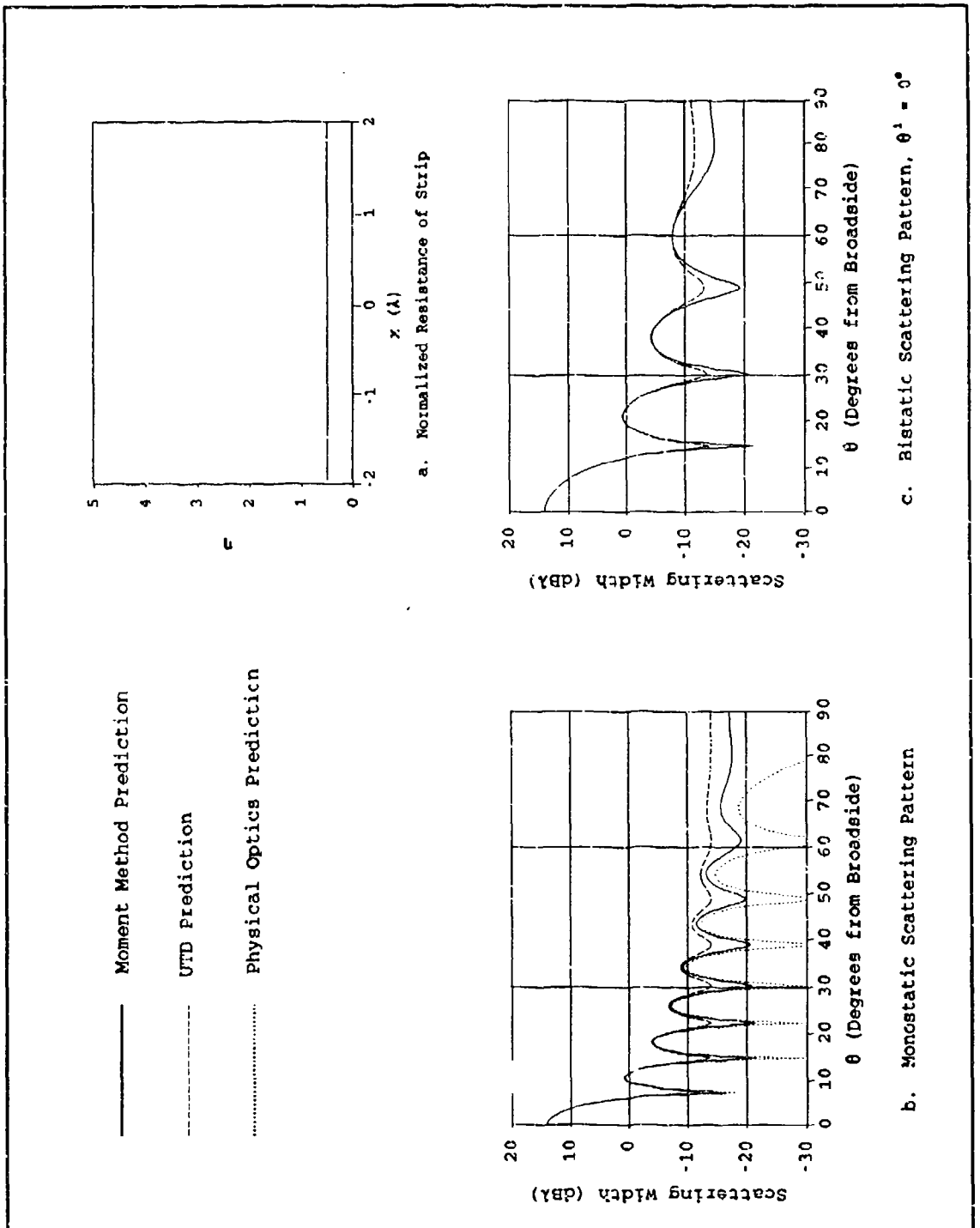

Figure 4.7. Scattering Predictions for a 4λ impedance strip with $\eta = 0.5$, E-Polarization

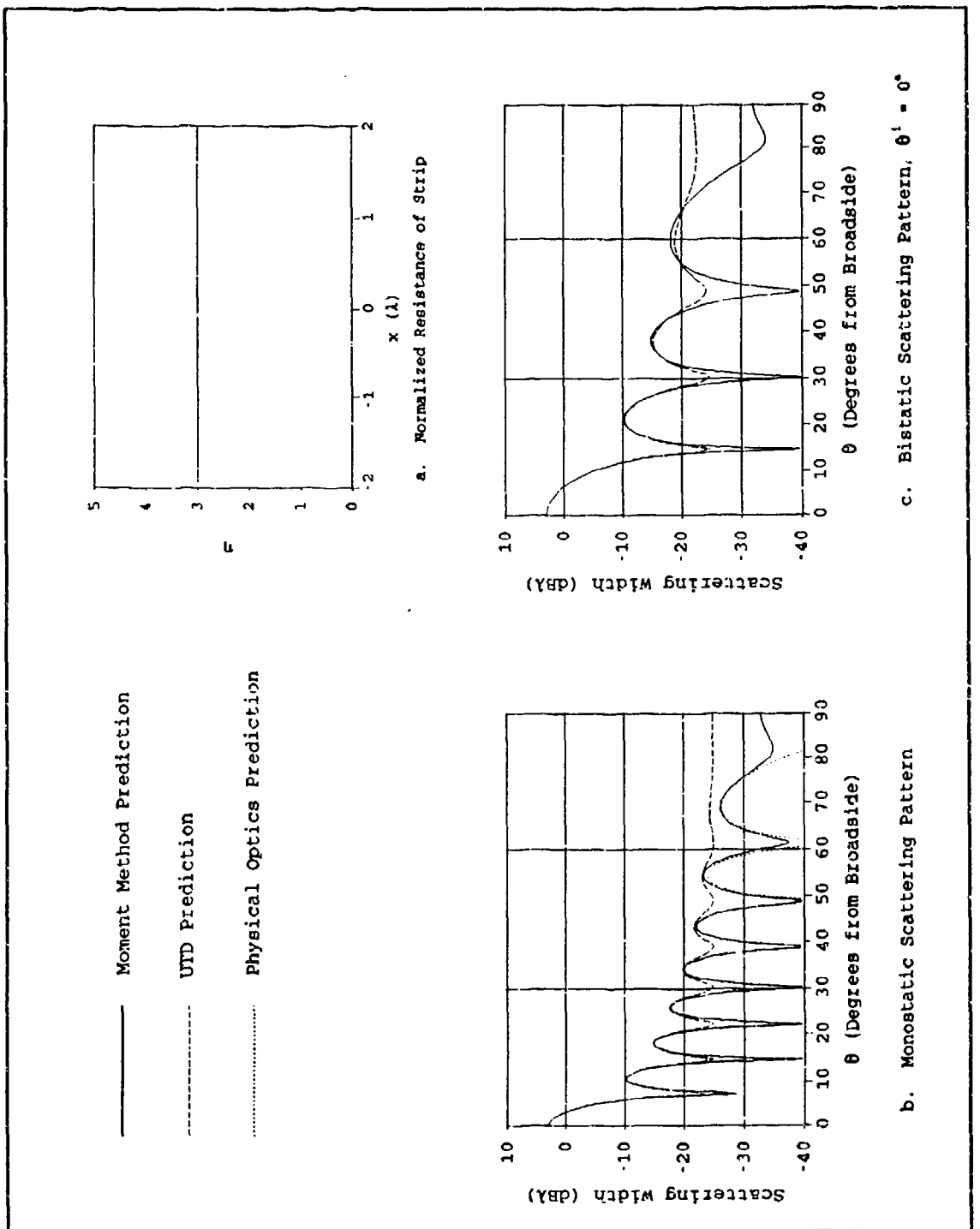

Figure 4.8. Scattering Predictions for a 4λ impedance strip with η = 3.0, E-Polarization

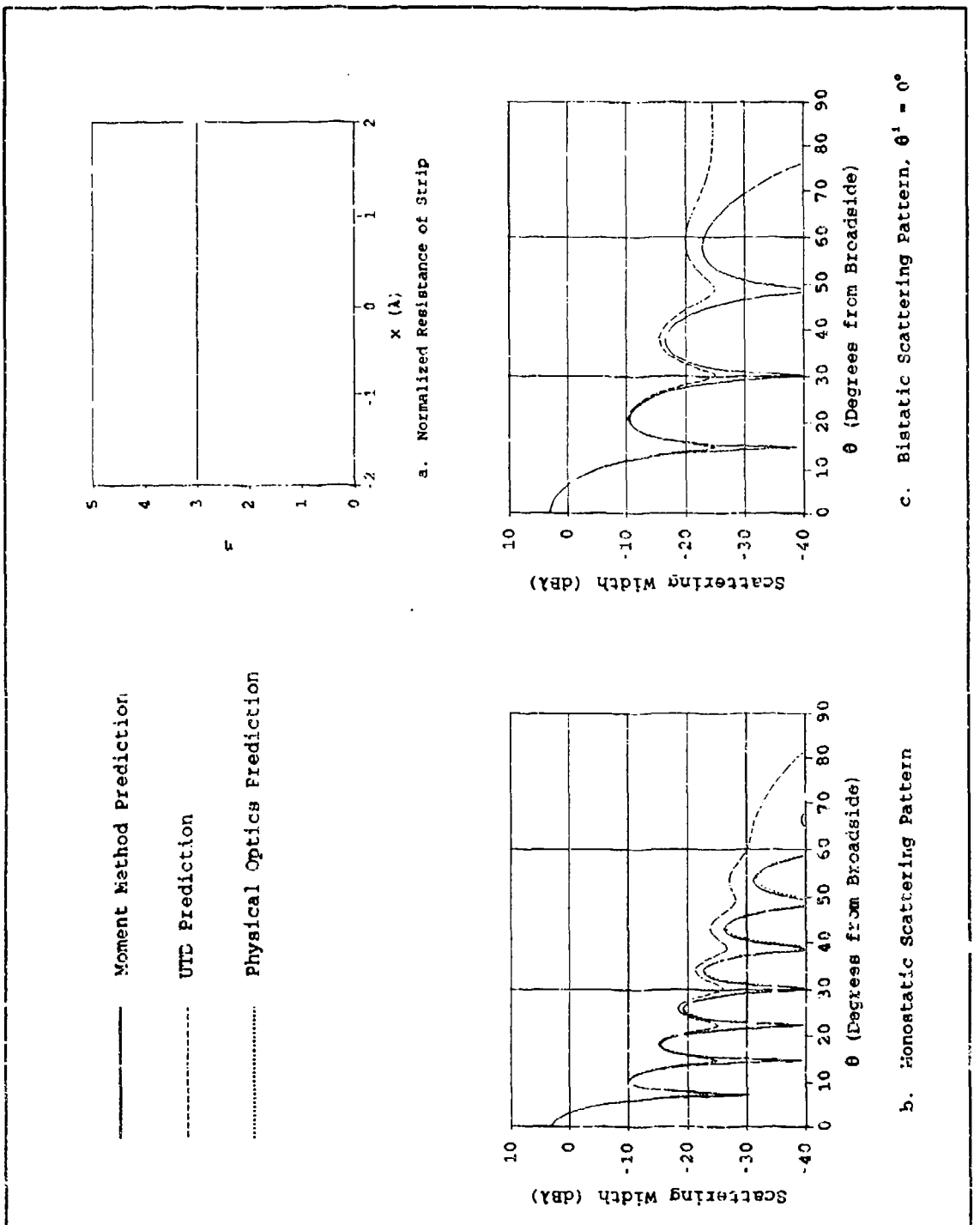

Figure 4.9. Scattering Predictions for a 4λ impedance strip with η = 3.0, H-Polarization

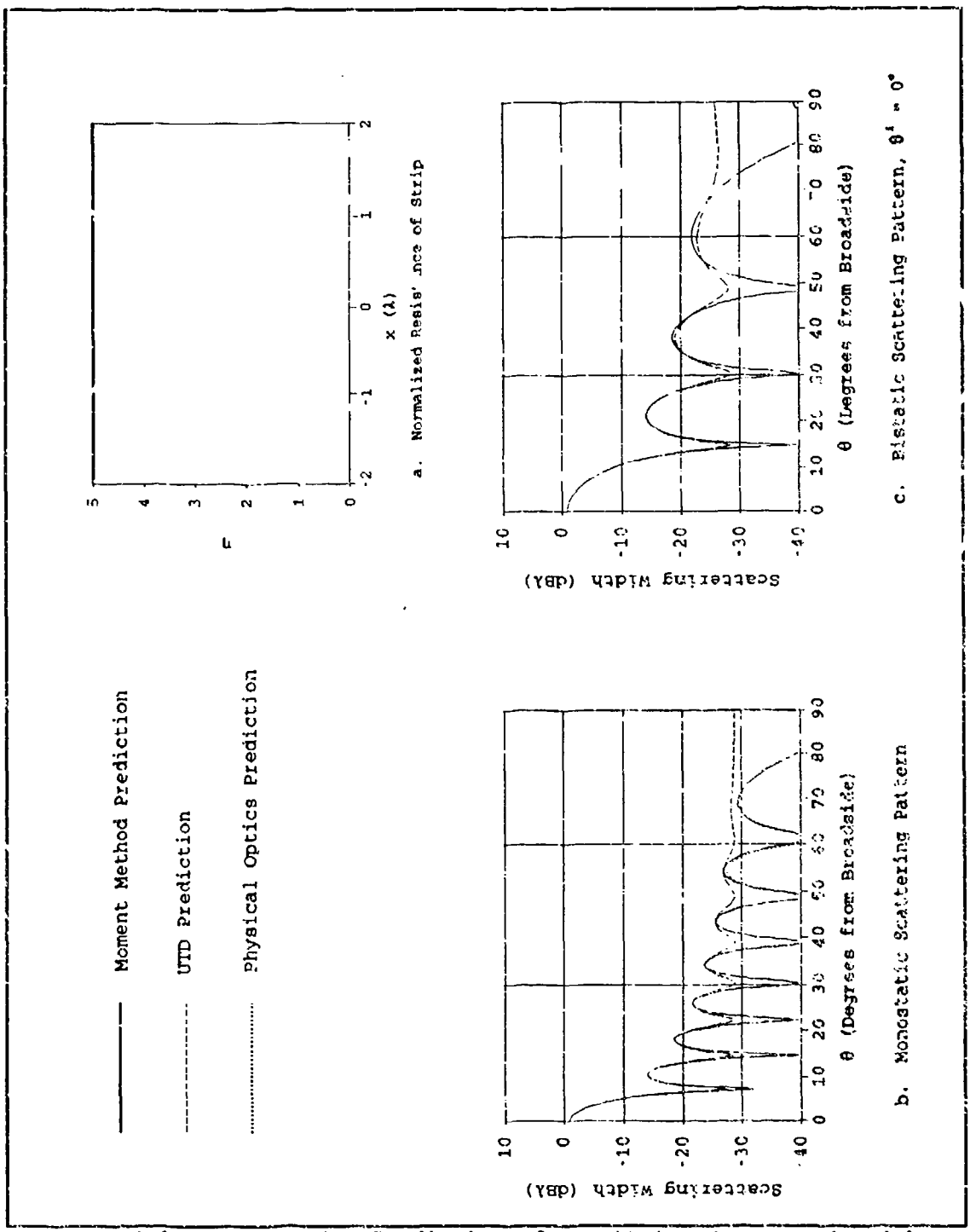

Figure 4.10. Scattering Predictions for a 4λ impedance strip with $\eta = 5.0$, E-Polarization

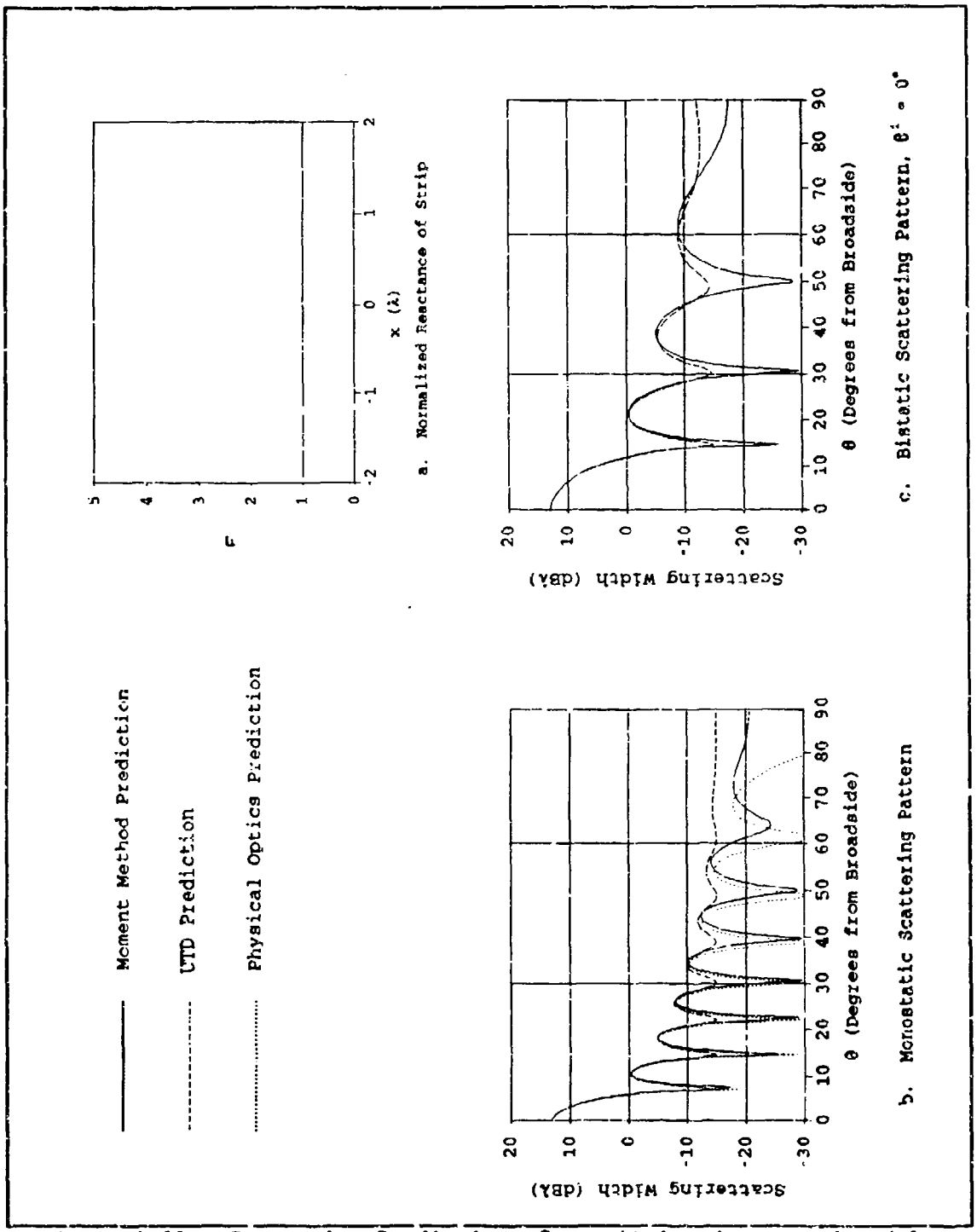

Figure 4.11. Scattering Predictions for a 4λ impedance strip with η = j1.0, E-Polarization

predictions using both moment method and UTD methods are plotted in (c.). The PO solution is not included for bistatic predictions because it does not satisfy reciprocity. This format is also used for the tapered and loaded strips.

Strips with finite, constant impedances have reduced scattering patterns when compared to perfectly conducting strips. The strip's scattering width decreases with increased impedance. In the limit, a strip with infinite impedance has no scattering, since its reflection and transmission coefficients would go to zero and one, the same as free space. However, objects with extremely high impedances are not easily produced. The sidelobes of the constant impedance strips' scattering patterns are not significantly reduced relative to the main lobe. The total scattering pattern is, in essence, scaled by the magnitude of the impedance strip's reflection coefficient. This results in a 6.0 dB reduction for $\eta = 0.5$ (figure 4.7), a 16.9 dB reduction for $\eta = 3.0$ (figures 4.8 and 4.9), a 20.8 dB reduction for $\eta = 5.0$ (figure), and a 7.0 dB reduction for $\eta = j1.0$ (figure 4.11). This reduction corresponds to the reflection coefficient of the impedance material given in eq 2.33.a.

In addition to the overall decrease in the level of the scattering pattern, the nulls are deeper for strips of higher impedance. This is easily seen in figures 4.5 through 4.11. This deepening of the nulls is caused by an increased level of destructive interference between diffractions from the strip's two edges. This implies that the magnitudes of the two diffracted fields are closer for high impedance strips than for conducting strips. This is not seen in the UTD

predictions because both diffractions are scaled by the same value, $R_{s,h}$, so that the same ratio exists between them as for the perfect conductor. In addition, the edge-on scattering for the strips with high impedances is much lower than simple scaling would suggest. This is most easily seen in figures 4.8 and 4.10 where the edge-on scattering is reduced by six and twelve dB in addition to the scale factor R_s.

Another observation is that the sidelobes in the moment method prediction for the reactive strip in figure 4.11 are displaced slightly away from the main beam. The moment method code was not verified for reactive materials, and the similarities in the peaks' positions for the UTD and PO results indicate that the moment method code might not be accurate for reactive materials.

The UTD prediction is practically identical to the integral equation prediction for the E-Polarized, perfectly conducting strip in figure 4.5. The H-Polarization case in figure 4.6 shows quite a bit of disparity between the two predictions, however. The UTD solution is presumed to be right. The moment method prediction doesn't exhibit the travelling wave, which is known to exist for H-Polarization. The travelling wave's position from edge-on incidence is given by (9:149):

$$\theta = 49.35 \sqrt{\lambda/l} \qquad (4.1)$$

where l is the width of the strip (4λ). This yields the location of the travelling wave at 25° from edge-on, which corresponds to the UTD prediction. In addition, the moment method prediction routine uses pulse basis functions, which do not accurately solve the 2-dimensional

integral equation for H-Polarization (3). This implies that the moment method results should be suspect in later H-Polarization predictions.

The UTD method accurately predicts the sidelobes in the scattering patterns of the constant impedance strips, both for monostatic and bistatic scattering. In all E-Polarization cases the UTD sidelobe levels for $\theta < 60°$ are within one dB of the moment method predictions, and are most often within 0.2 dB. The UTD method still accurately predicts the sidelobe level for $\theta > 60°$; the UTD and moment method solution are within two dB of each other. The UTD method does not accurately predict the edge-on scattering levels though, with the differences being greater for higher impedance values. The UTD method also fails to predict the depth of the nulls.

The PO predictions were not very accurate for low impedance values. They accurately predicted the innermost sidelobes, but the accuracy rapidly diminished as θ increased. However for higher impedance values the PO prediction was found to be very accurate. This is easily seen in figure 4.10 where the moment method and PO solutions are nearly identical.

Scattering patterns of strips with tapered impedances are shown in figures 4.12 through 4.16. Only one H-Polarized prediction (figure 4.16) is made because of the problems with the moment method routine and because multiple diffractions could not be incorporated into these UTD predictions. Applying a variable taper to a strip reduces the sidelobes relative to the main lobe when compared to a perfectly conducting strip. It also widens the main lobe. Increasing the impedance taper decreases the sidelobe and edge-on scattering levels. This is seen when comparing

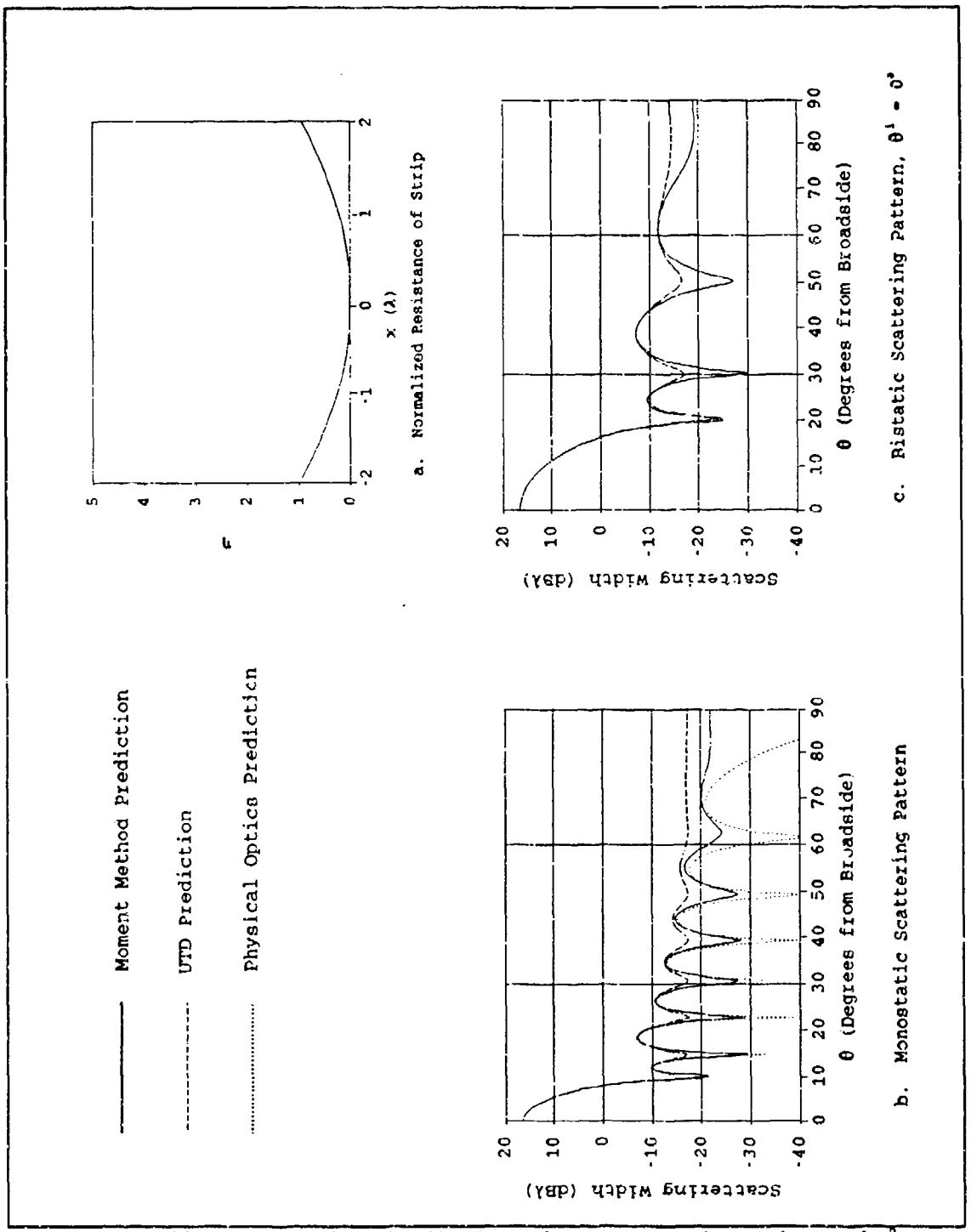

Figure 4.12. Scattering Predictions for a 4λ strip with $\eta = \frac{1}{4}x^2$, E-Polarization

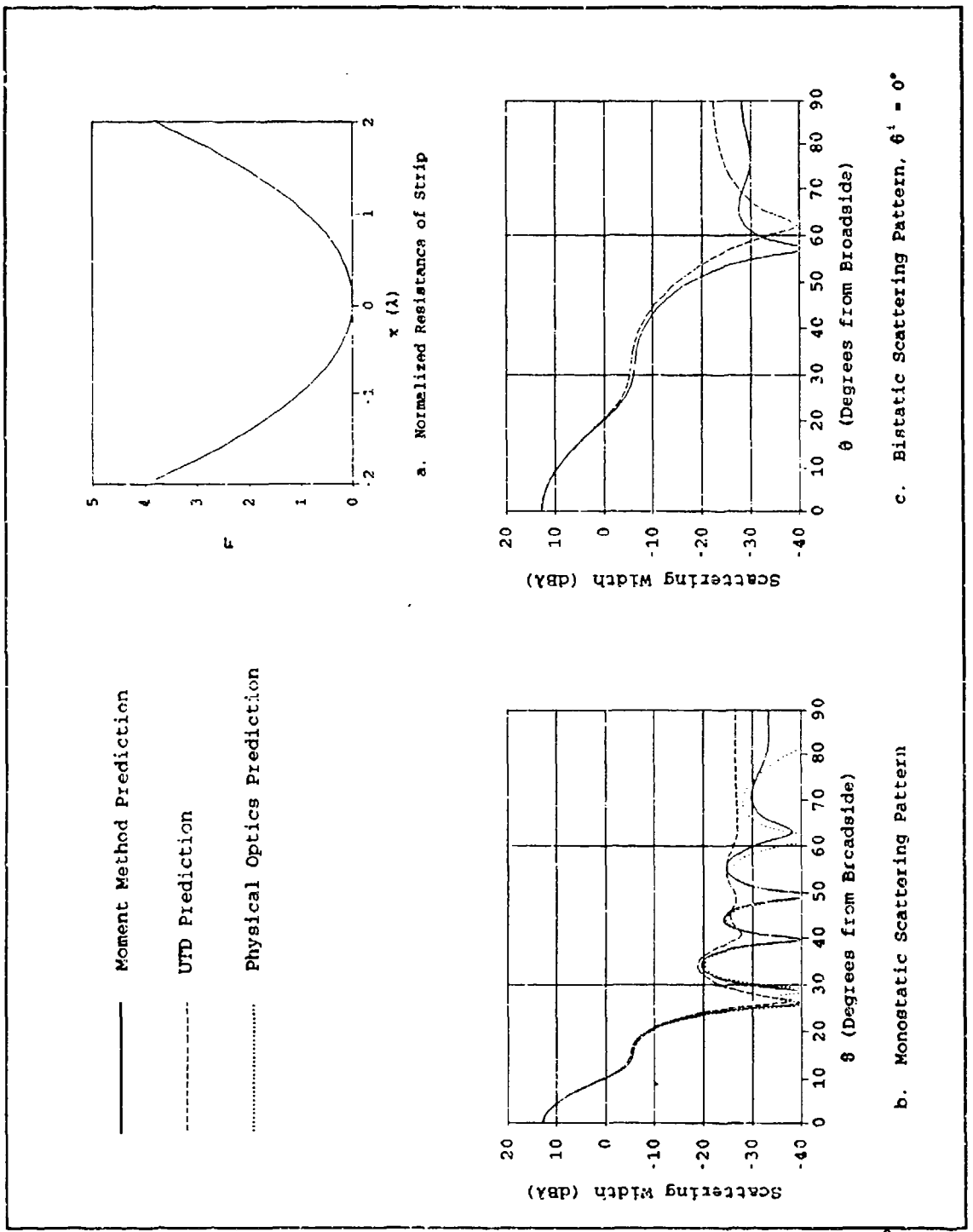

Figure 4.13. Scattering Predictions for a 4λ strip with $\eta = x^2$, E-Polarization

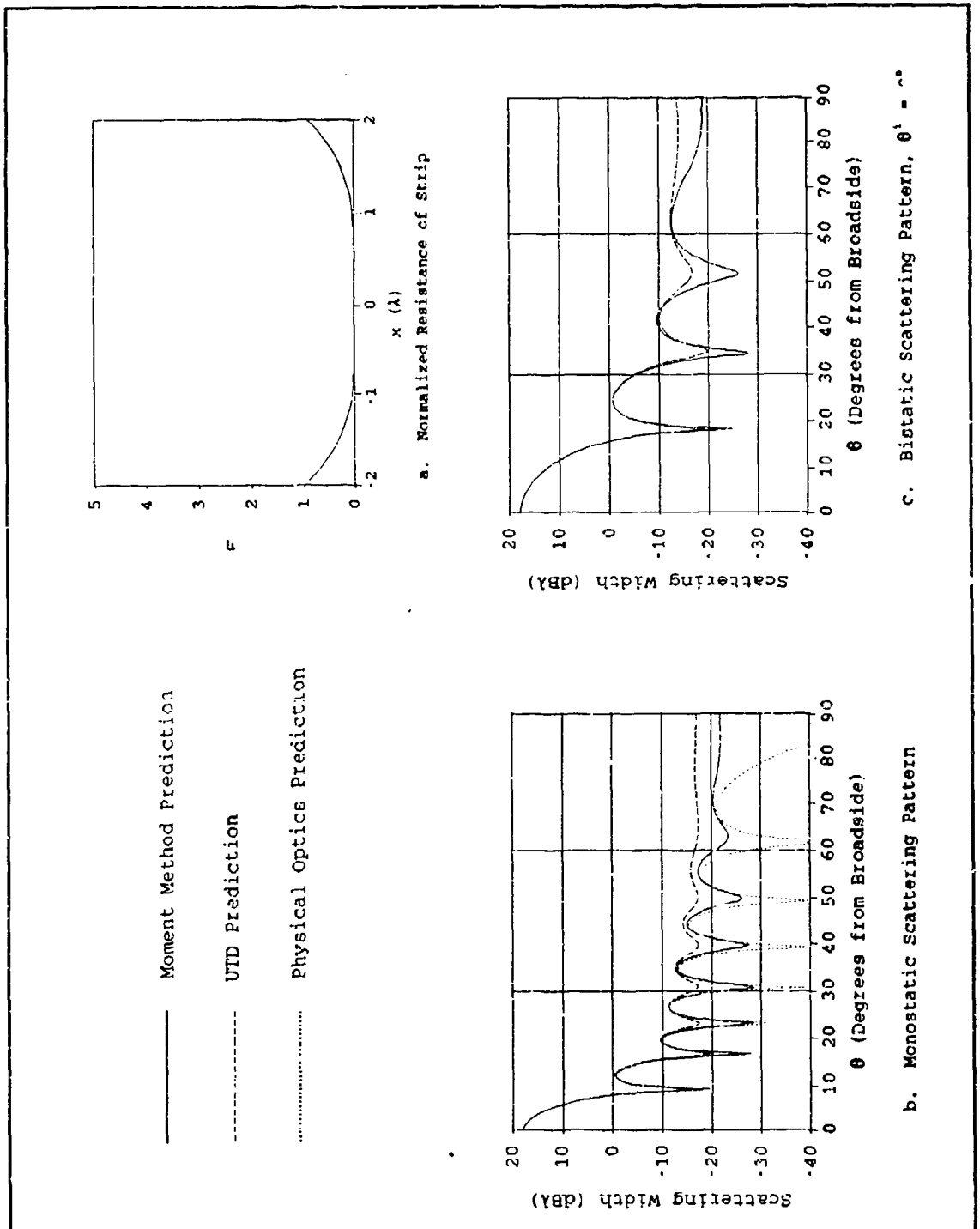

Figure 4.14. Scattering Predictions for a 4λ strip with $\eta = 1/16\ x^4$, E-Polarization

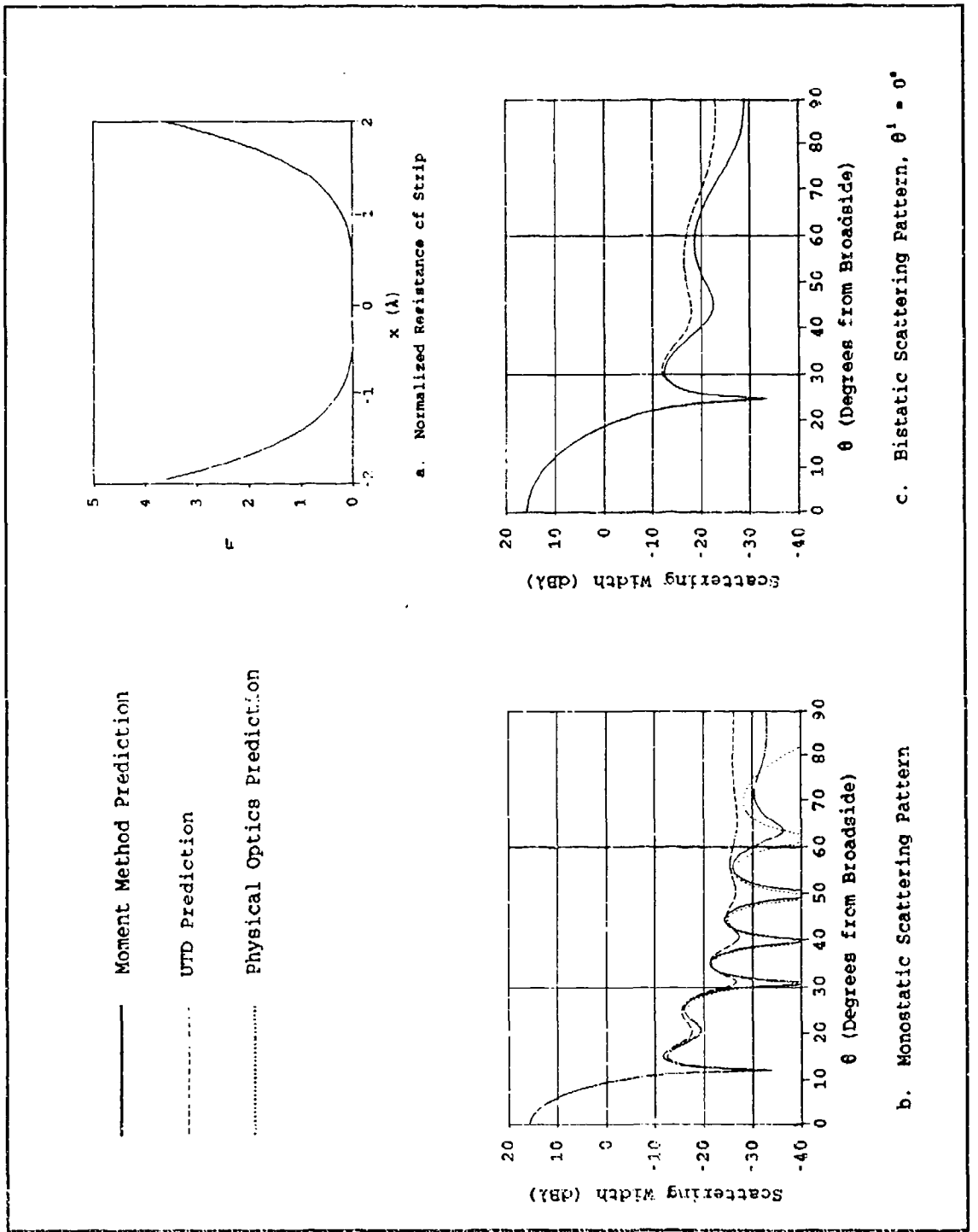

Figure 4.15. Scattering Predictions for a 4λ strip with $\eta = \frac{1}{4}x^4$, E-Polarization

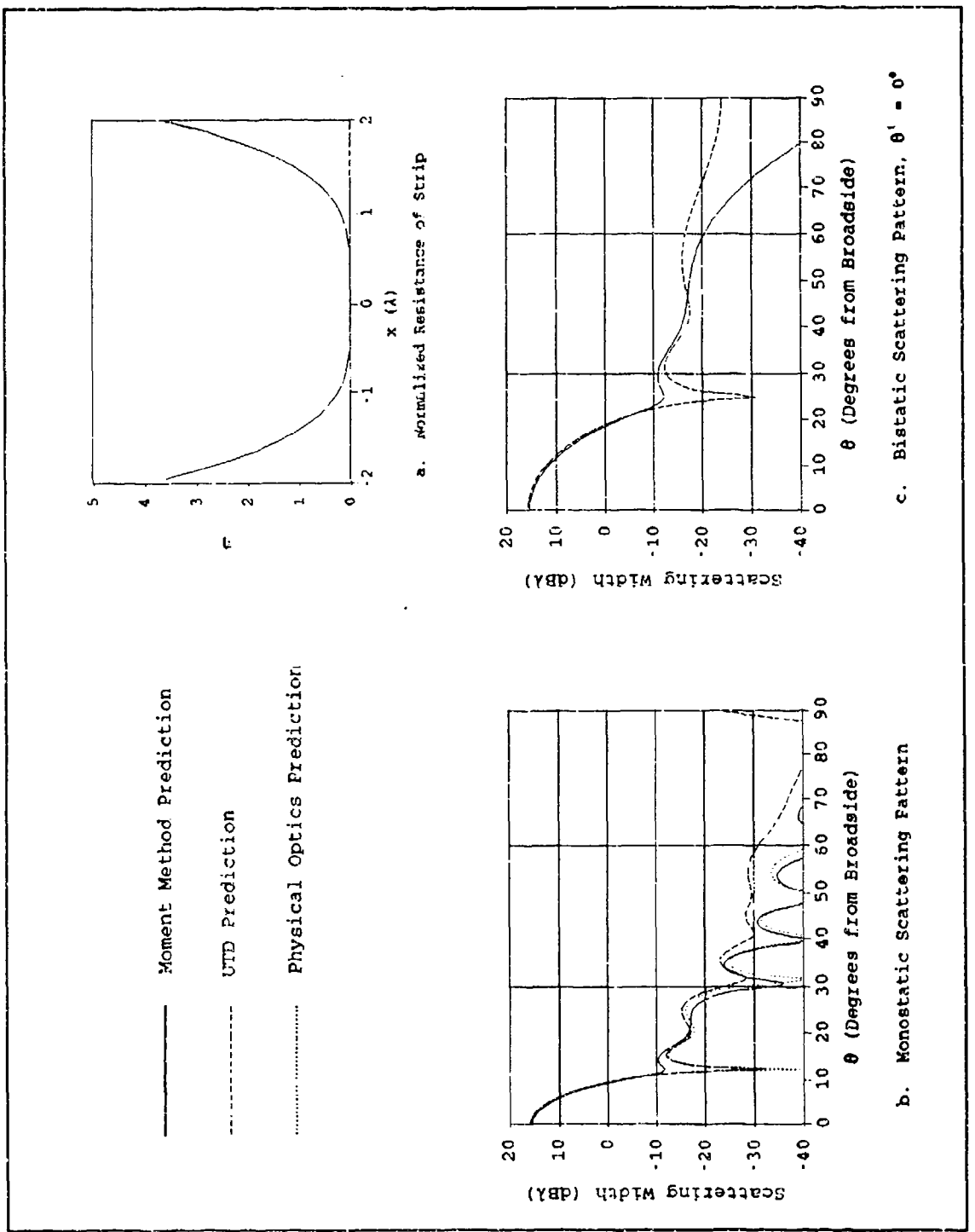

Figure 4.16. Scattering Predictions for a 4λ strip with $\eta = \frac{1}{4}x^4$, H-Polarization

figure 4.12 to figure 4.13 and figure 4.14 to figure 4.15. The sidelobe levels in figure 4.13 are seven to ten dB lower than those in figure 4.12. The edge-on scattering level is also reduced by 11 dB. The main lobe is also wider for the higher taper. Similar results are noted for figures 4.14 and 4.15.

Increasing the impedance taper from the second to the fourth power has practically no impact on the scattering pattern except within 30° of broadside. The differences near broadside are easily noticed when comparing figure 4.13 with figure 4.15. Increasing the taper's power narrows the main lobe and creates two new sidelobes from the main lobe's shoulder. The main lobe's magnitude also increases since the average impedance is lower, causing greater reflection. A similar situation occurs in the bistatic patterns, but the entire scattering patterns are different in figures 4.13.c and 4.15c.

Again, the UTD predictions match the moment method predictions very well near broadside. The UTD predictions are very good at predicting the magnitude and the location of the sidelobes; within 60° of broadside the UTD predictions differ by no more than 2 dB from the moment method results and are usually much closer. The UTD and moment method edge-on scattering levels vary by five to seven dB. As with the constant impedance strips, however, the UTD predictions do not calculate the nulls accurately. The UTD and moment method predictions for the H-Polarization pattern presented in figure 4.16 do not match well, though. This is likely due to the omission of multiple diffractions in the UTD solution and the problems previously discussed with the H-Polarization moment method predictions. The monostatic UTD prediction is also

observed to rise dramatically to −24 dBλ approaching edge-on. This is because the diffractions from the loads used to model the tapered impedance are adding more or less coherently near edge-on. Although R_h approaches 0 for all loads in the model near edge on (which would produce zero diffractions because the GO discontinuity goes to zero), the low impedance values in the model near the strip's center still yield moderate reflection values for near grazing incidence. These can cause significant diffractions. The sudden rise in scattering width is similar to that seen in figure 4.3.

The PO method also predicts the sidelobe levels and positions well, more-so near broadside. As with the constant impedance strips it also does a better job of predicting the scattering for the higher impedance tapers.

Impedance-Loaded Conducting Strips. Scattering predictions for conducting strips with constant impedance loads are presented in figures 4.17 through 4.21. Predictions were made for a 2λ conducting strip with 1λ loads of $\eta = 0.5$ (figures 4.17 and 4.18), $\eta = 2$ (figure 4.19), $\eta = 4$ (figure 4.20), and $\eta = j0.5$ (figure 4.21). In all of these cases the main lobes' magnitudes are reduced when compared to the unloaded conducting strip in figures 4.5 and 4.6. This is because of the diminisned reflection from the loads. The main lobe is also broadened. This is because most of the scattering contribution comes from the conductor, which has a smaller area than the 4λ conducting strip. In addition, the loads cause a reduction in some of the sidelobe levels in figures 4.17 and 4.18. The edge-on monostatic scattering level is also approximately 10 dB lower in figures 4.17.a and 4.21.a than for the

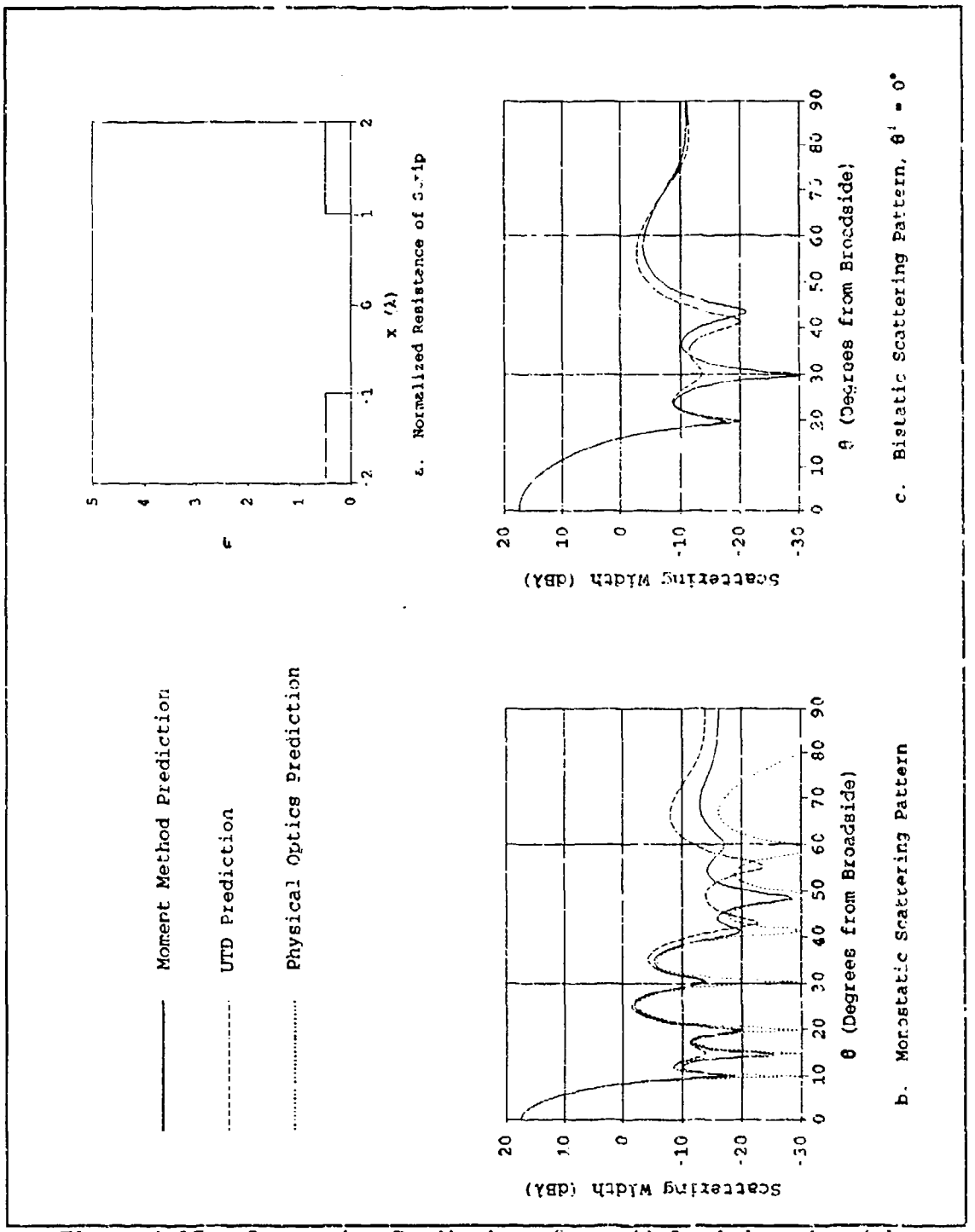

Figure 4.17. Scattering Predictions for a 4λ loaded strip with 0.5η loads, 1λ from the strip's edges, E-Polarization

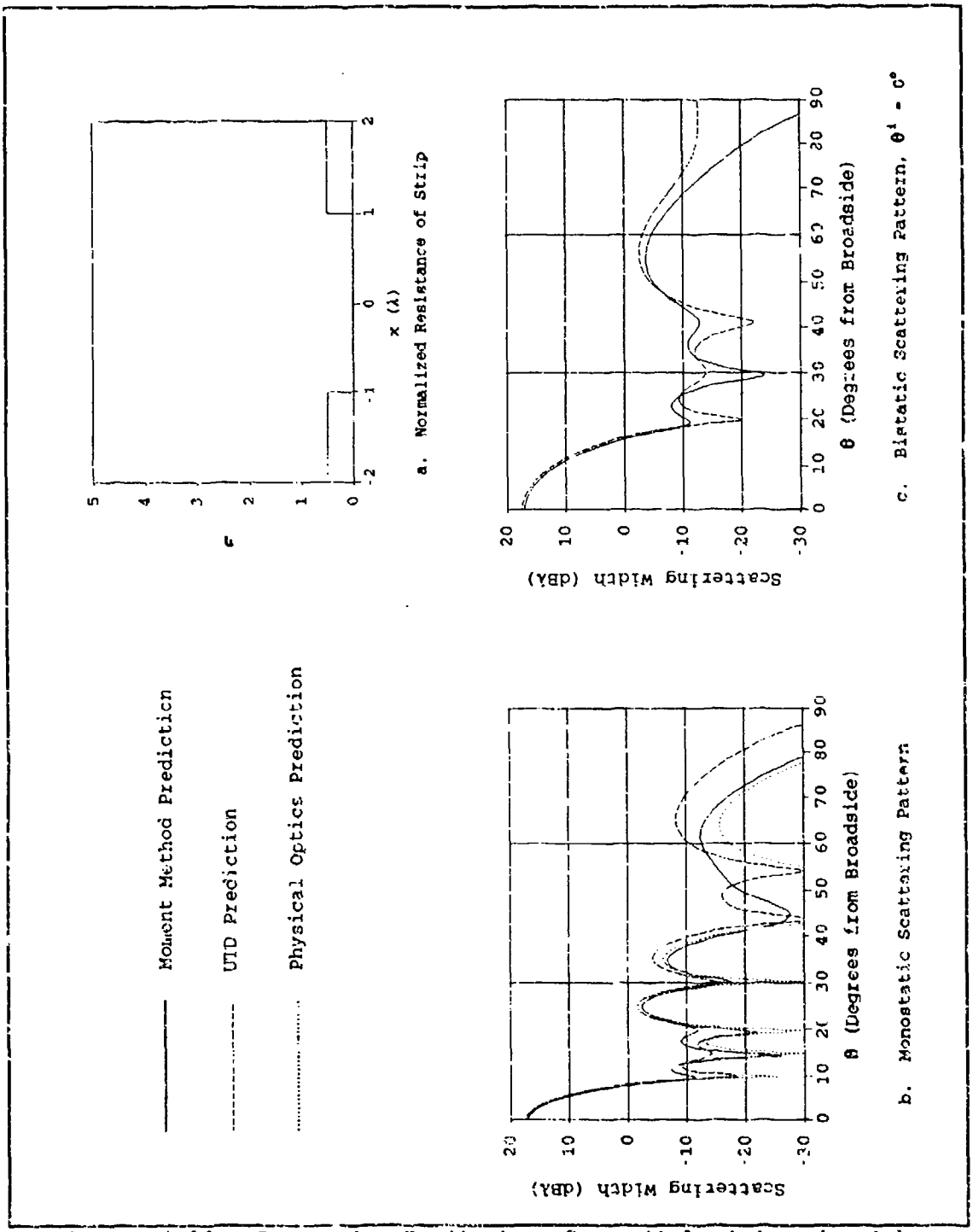

Figure 4.18. Scattering Predictions for a 4λ loaded strip with 0.5η loads, 1λ from the strip's edges, H-Polarization

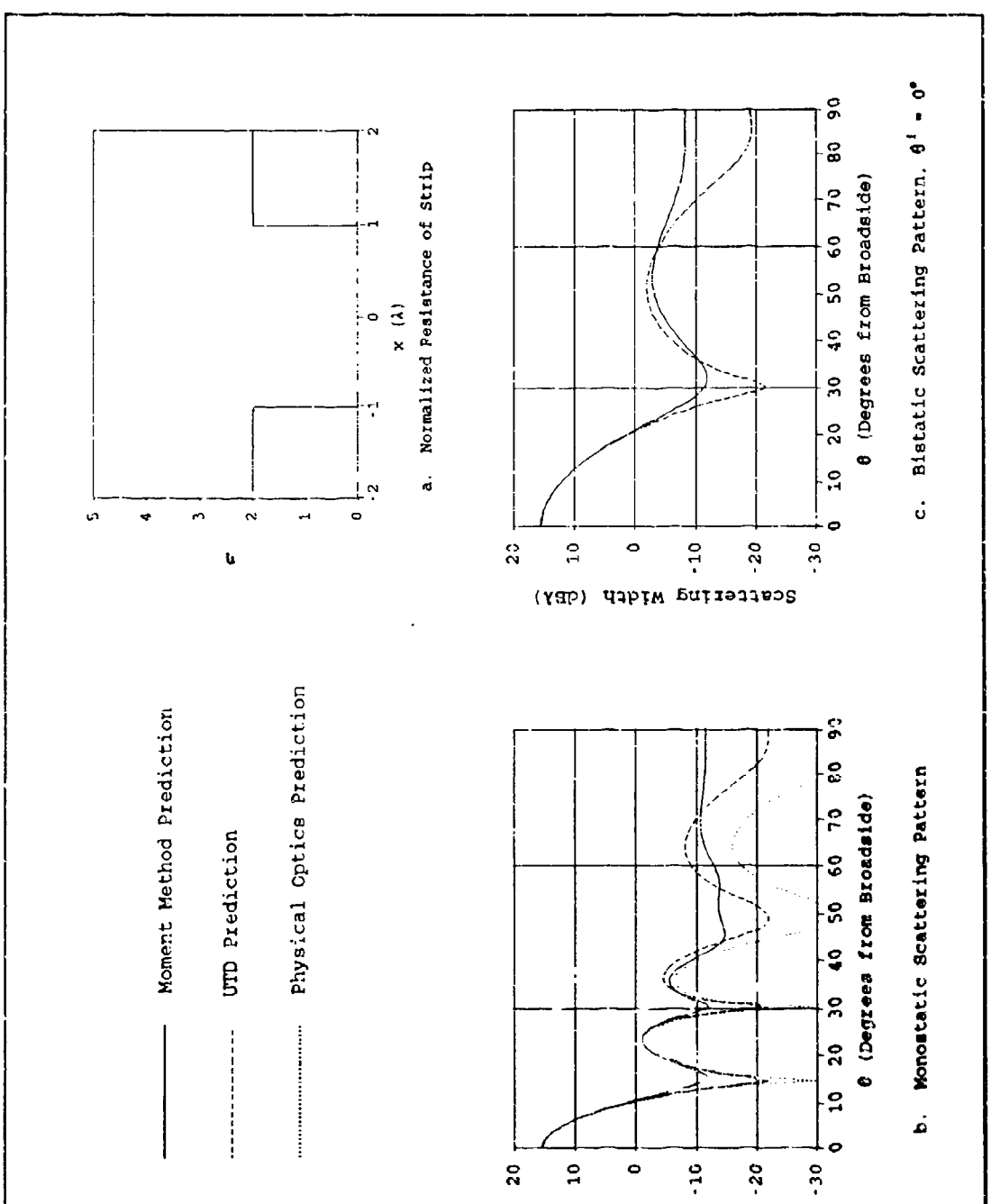

Figure 4.19. Scattering Predictions for a 4λ loaded strip with 2η loads, 1λ from the strip's edges, E-Polarization

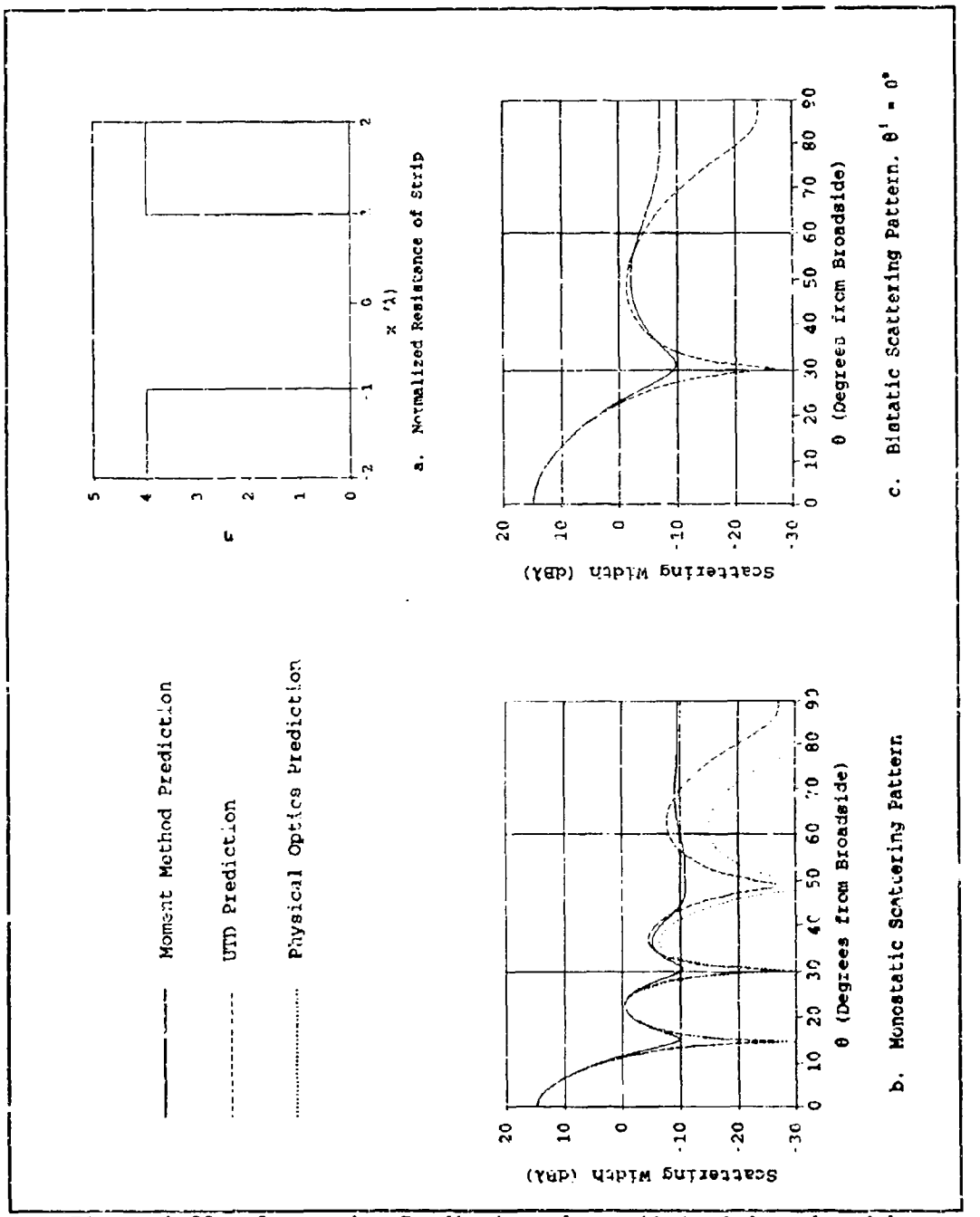

Figure 4.20 Scattering Predictions for a 4λ loaded strip with 4.0η loads, 1λ from the strip's edges, E-Polarization

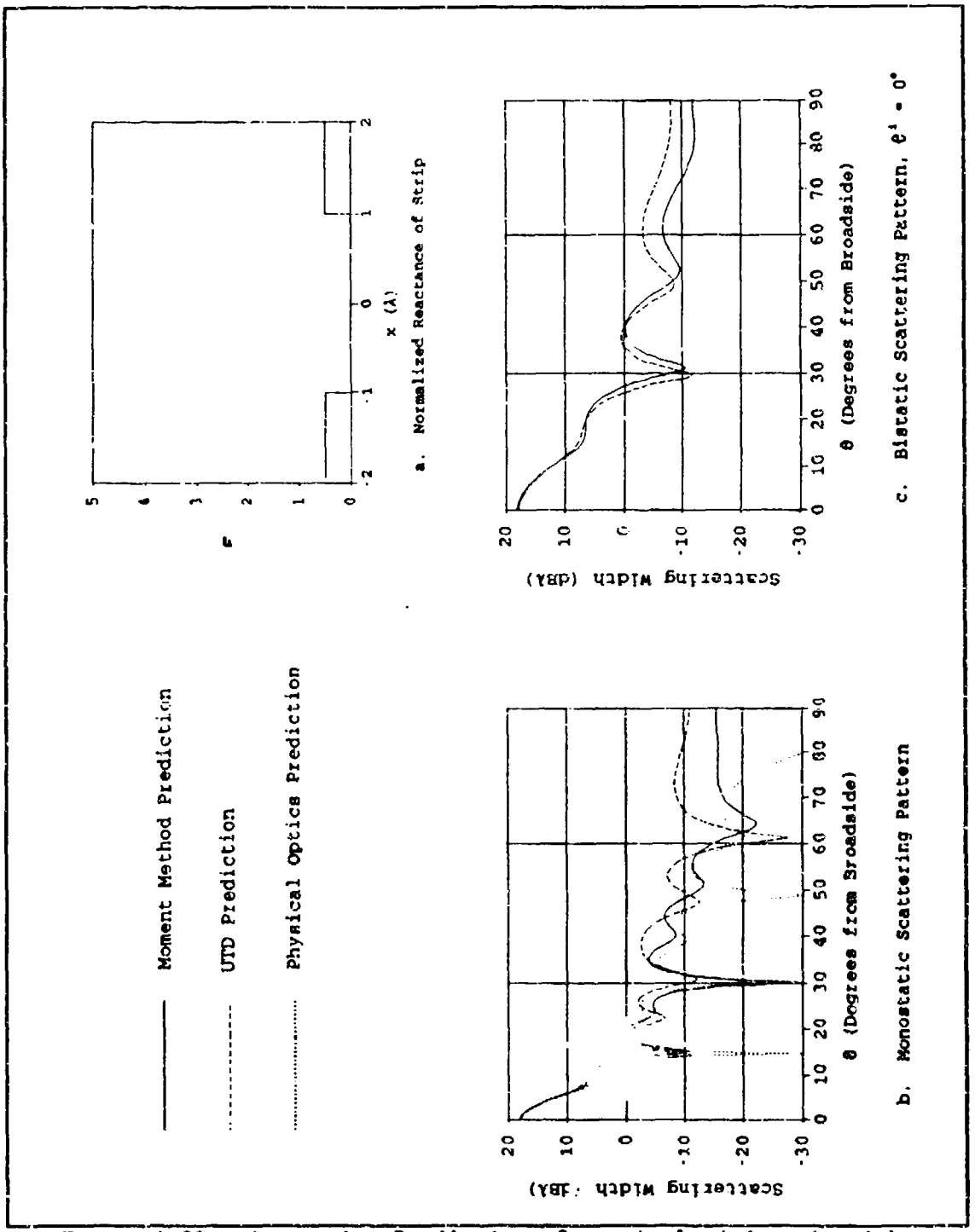

Figure 4.21. Scattering Predictions for a 4λ loaded strip with j0.5η loads, 1λ from the strip's edges, E-Polarization

perfect conductor. This is because these loads reduce the diffractions from the conducting strip's edges, while not causing significant diffractions from their own edges.

The $\eta = 2$ and $\eta = 4$ loads in figures 4.19 and 4.20 are nearly transparent to the incident field. This is because the high impedance values offer a low reflectance and high transmittance, similar to free space. The resultant patterns are very similar to that of a 2λ conducting strip alone. This indicates that diffractions from the loads outer edges are negligible compared to those from the conductor/load junctions.

The UTD predictions correspond well to the moment method predictions for scattering within 40° of broadside in the monostatic predictions and, in general, over the entire bistatic predictions. Peak level differences between the UTD and moment method solutions are less than 2 dB within these regions. In all of the constant load cases the UTD solution failed to predict the lobing structure for $40° < \theta < 60°$. The reason for this is, in part, that the non-equivalent term in the original diffraction coefficient is omitted for impedance junctions. When this term is included (selecting the conducting strip as side A) the behavior of the UTD prediction in the region $40° < \theta < 60°$ more closely resembles the moment method solution. This is illustrated for backscatter from a 2λ conducting strip with 1λ, 0.5η loads (figure 4.22.a) and 1λ, 2.0η loads (figure 4.22.b).

In general, however, including the non-equivalent does not improve the UTD solution, and more typically degrades it, as can be seen in figure 4.22.a's edge-on scattering levels. The only cases where

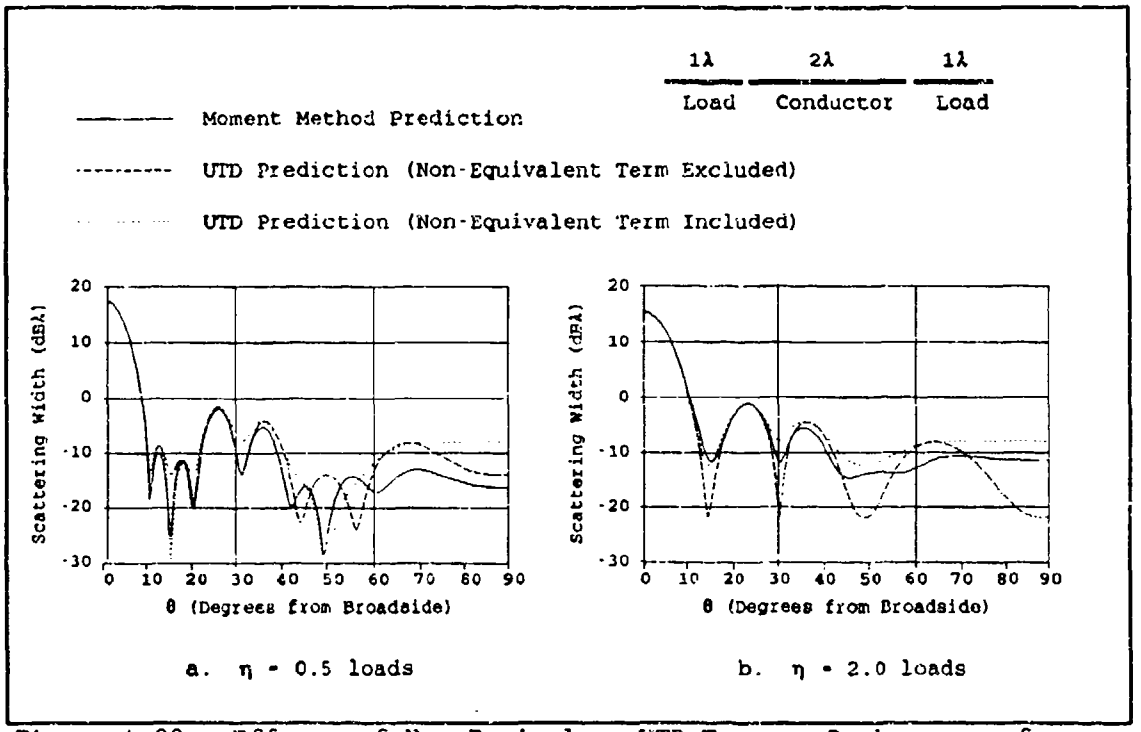

Figure 4.22. Effects of Non-Equivalent UTD Term on Backscatter from an Impedance-Loaded Conducting Strip

including the non-equivalent term improves the solution is for the cases of the constant impedance loads presented here. For other cases they typically have a detrimental effect or no significant effect at all. This is because the large impedance discontinuity between the conductor and the load is similar to the impedance discontinuity between the conductor and free space, where both terms are needed. Including the non-equivalent term may be beneficial when calculating diffractions from a conductor/impedance junction, but this decision should be further investigated first. In general, the PO predictions seem to match the moment method results slightly better than the UTD predictions for the constant impedance load cases presented here.

Scattering predictions for strips with tapered loads are displayed in figures 4.23 through 4.30. The tapered loads create a smoother sidelobe envelope and yield lower sidelobe levels in general than the constant impedance loads. The edge-on scattering levels are also significantly reduced from the constant load cases. Whereas the constant loads yielded monostatic edge-on scattering levels from -10 to -17 dBλ, the tapered loads provided levels from -21 to -32 dBλ.

Increasing the taper of the load had an interesting effect on the scattering patterns. This can be seen when comparing figures 4.24 and 4.26 to figures 4.25 and 4.27. The loads with the higher tapers in figures 4.25 and 4.27 have only six lobes in the backscatter patterns. This is a characteristic of a 3λ wide strip, not 4λ strips. This result is likely due to the higher impedance levels at the outer edges of the loads not contributing significantly to the scattering patterns, causing the strip to appear only 3λ wide.

Of the tapered impedance loads $\eta = 4x^2$ in figure 4.25 produces the lowest overall monostatic scattering pattern. Although the first sidelobe is relatively high at 18dB below the main lobe, no other lobe is within 30dB of the main lobe, and the edge on scattering is 49 dB below the main lobe's level, at -32dBλ. This can be compared to a 4λ conducting strip which has an edge-on scattering level only 28 dB below its main beam. The exponentially loaded strips in figure 4.28 and 4.30 also have low sidelobes which are comparable to or lower than the sidelobe levels in figure 4.25 but edge-on scattering is six to seven dB higher. An important observation in this comparison though, is that the

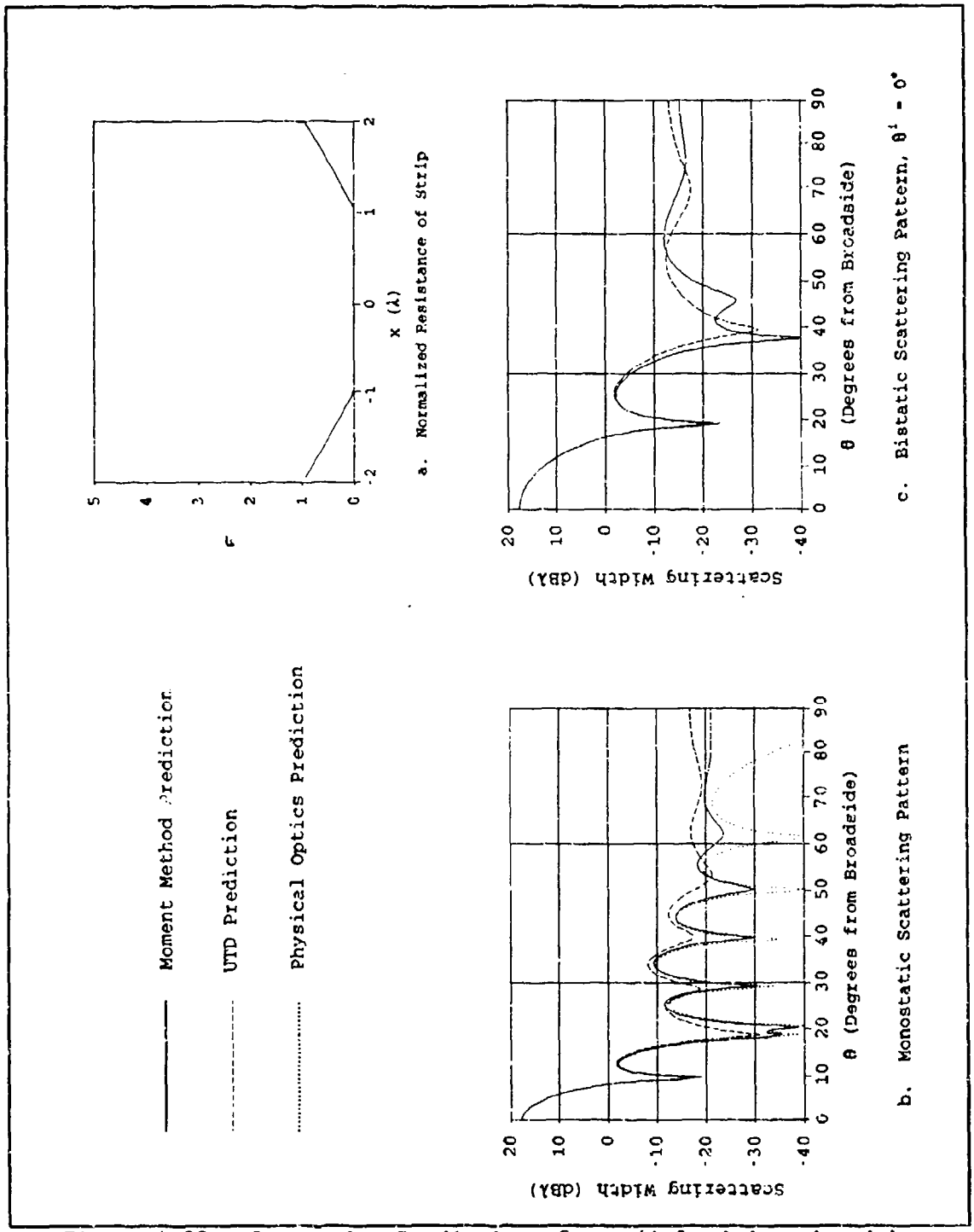

Figure 4.23. Scattering Predictions for a 4λ loaded strip with $\eta = x$ loads 1λ from the strip's edges, E-Polerization

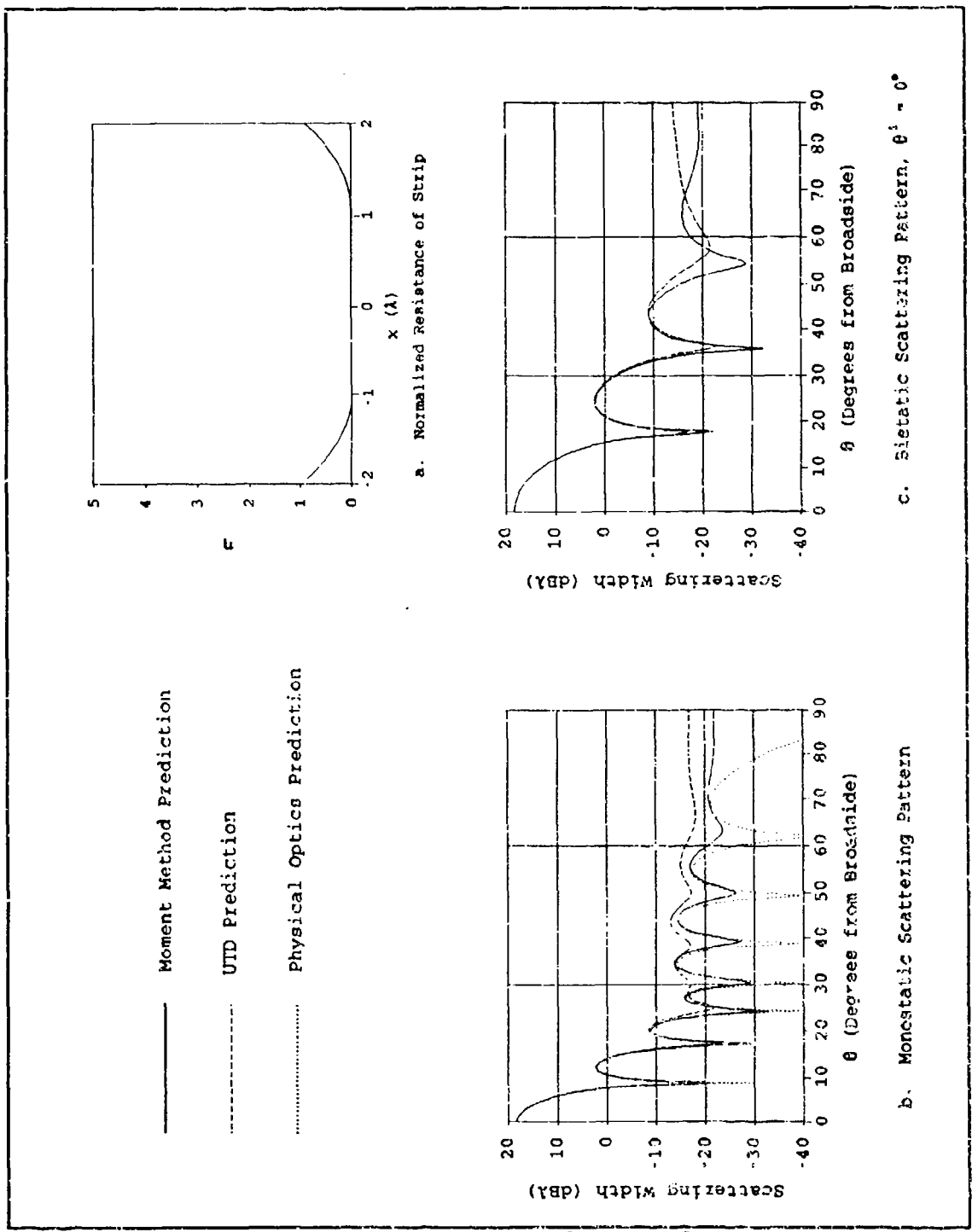

Figure 4.24. Scattering Predictions for a 4λ loaded strip with $\eta = x^2$ loads 1λ from the strip's edges, E-Polarization

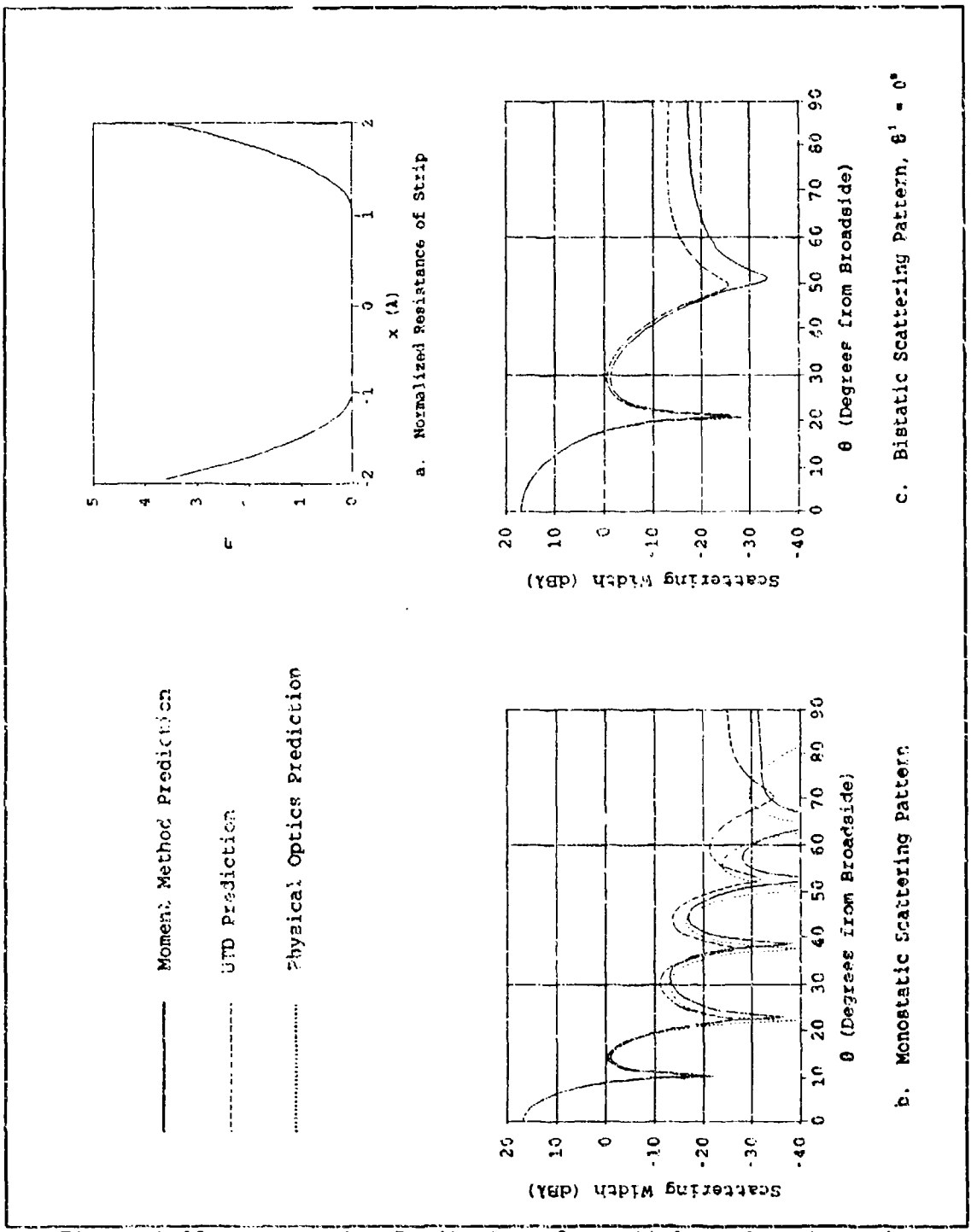

Figure 4.25. Scattering Predictions for a 4λ loaded strip with $\eta = 4x^2$ loads 1λ from the strip's edges, E-Polarization

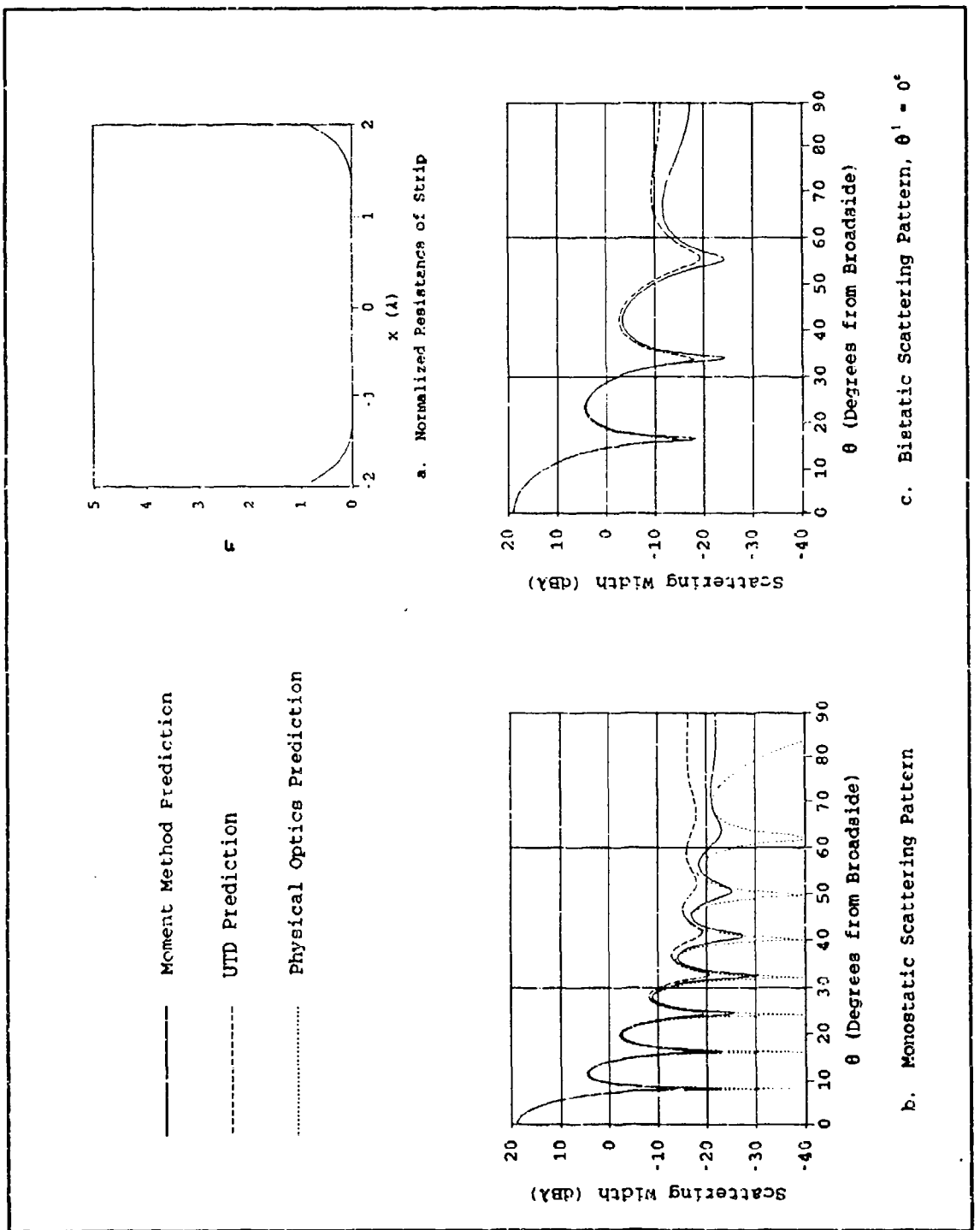

Figure 4.26. Scattering Predictions for a 4λ loaded strip with $\eta = x^4$ loads 1λ from the strip's edges, E-Polarization

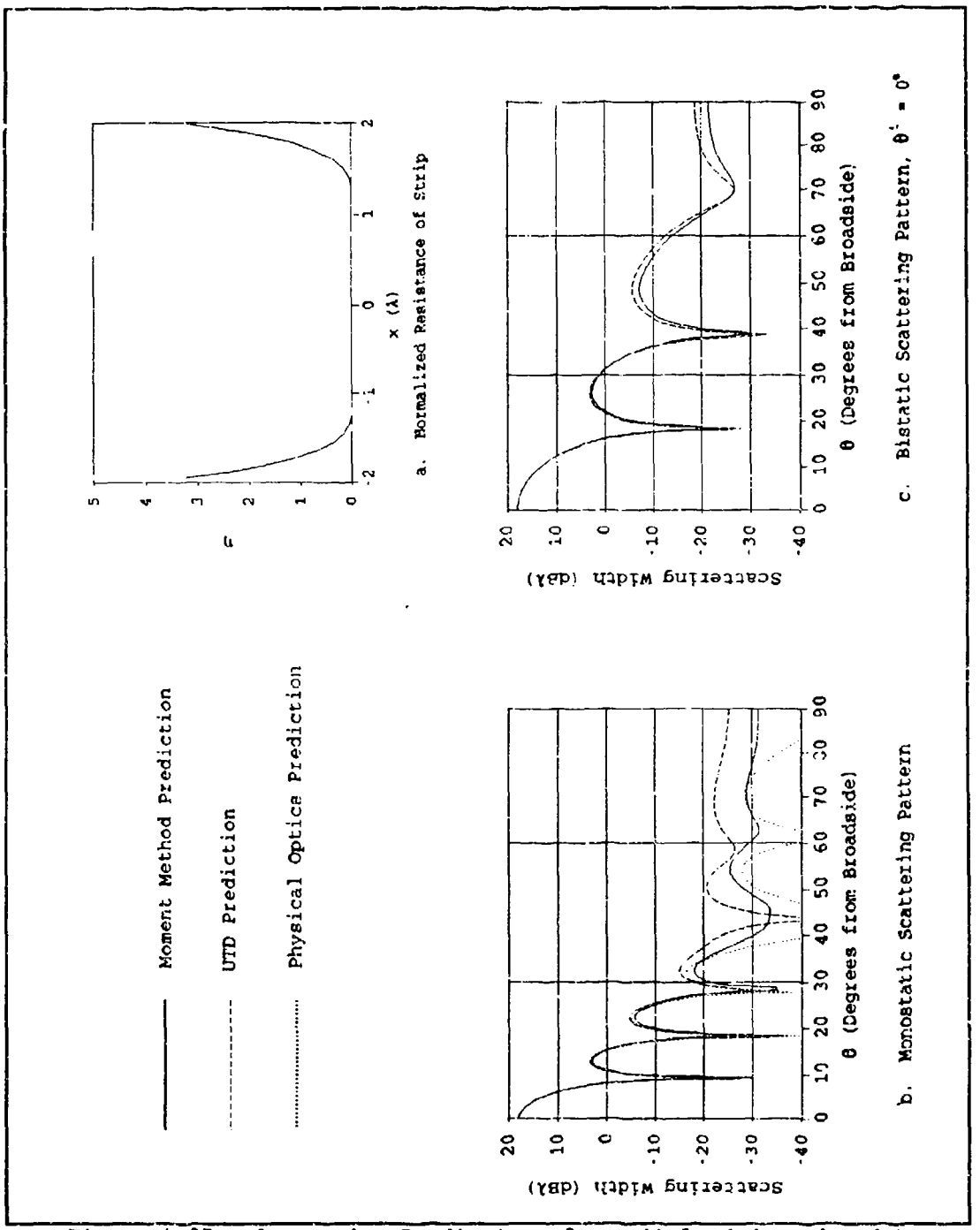

Figure 4.27. Scattering Predictions for a 4λ loaded strip with $\eta = 4x^4$ loads 1λ from the strip's edges, E-Polarization

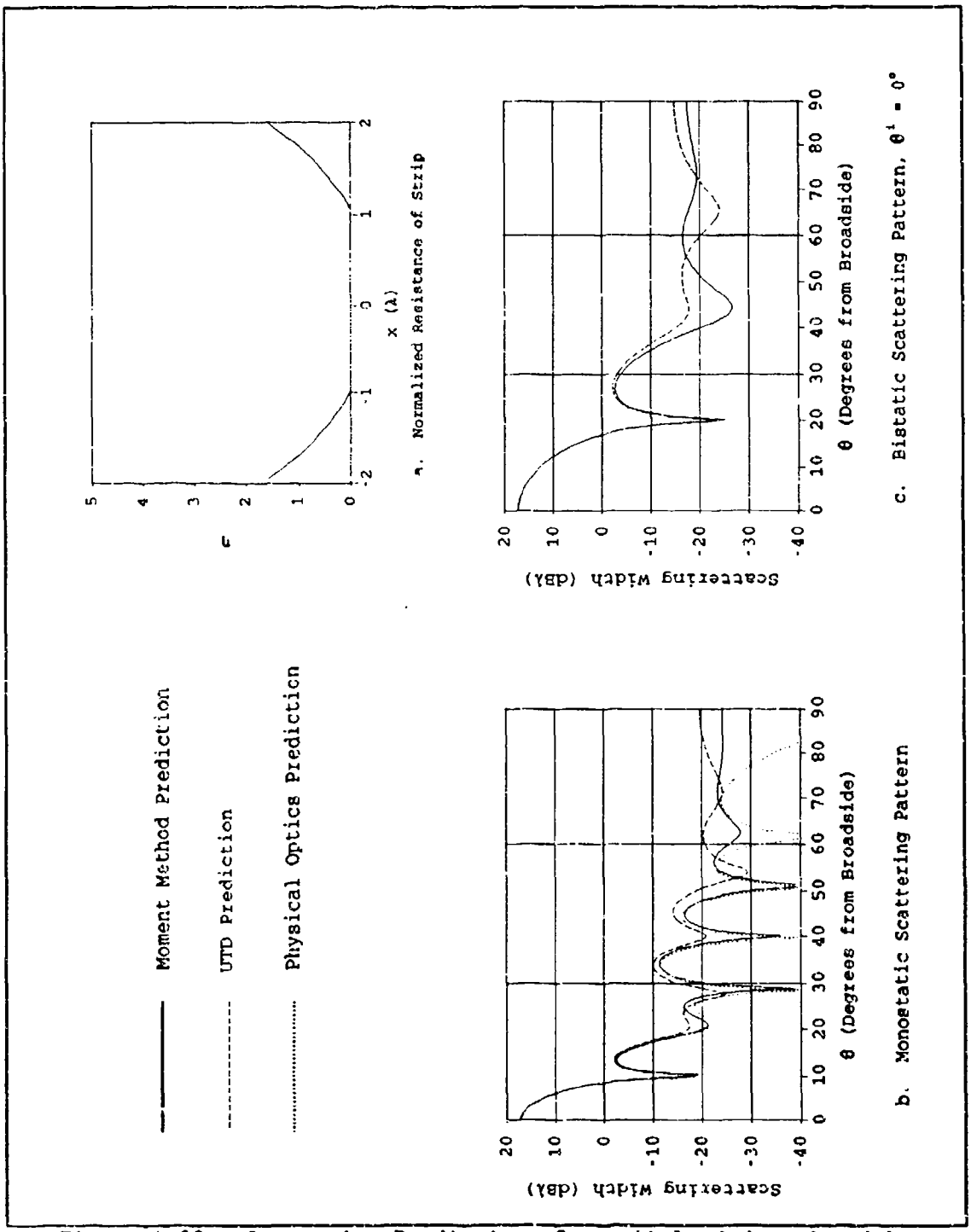

Figure 4.28. Scattering Predictions for a 4λ loaded strip with $\eta = e^x - 1$ loads 1λ from the strip's edges, E-Polarization

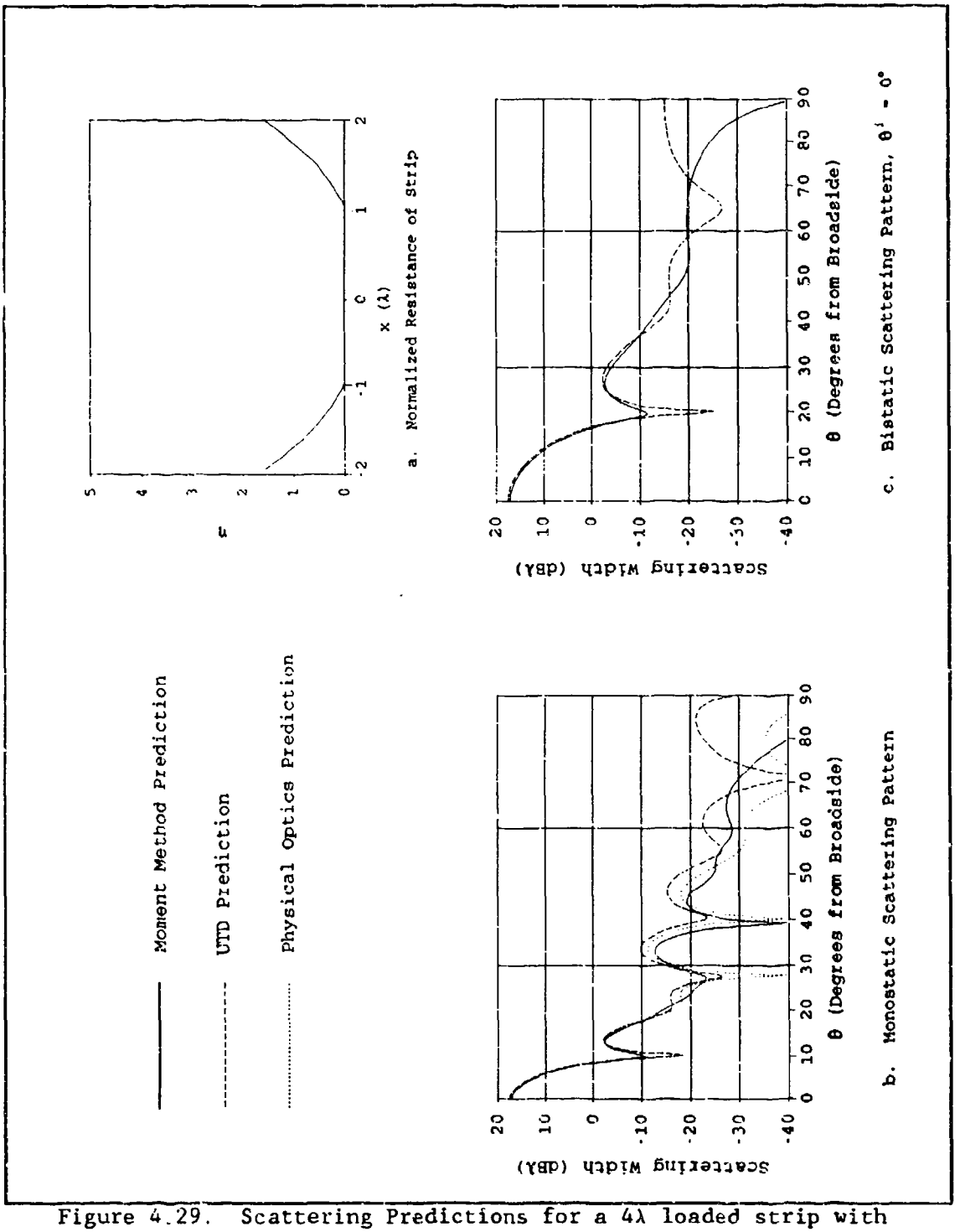

Figure 4.29. Scattering Predictions for a 4λ loaded strip with $\eta = e^{x} - 1$ loads 1λ from the strip's edges, H-Polarization

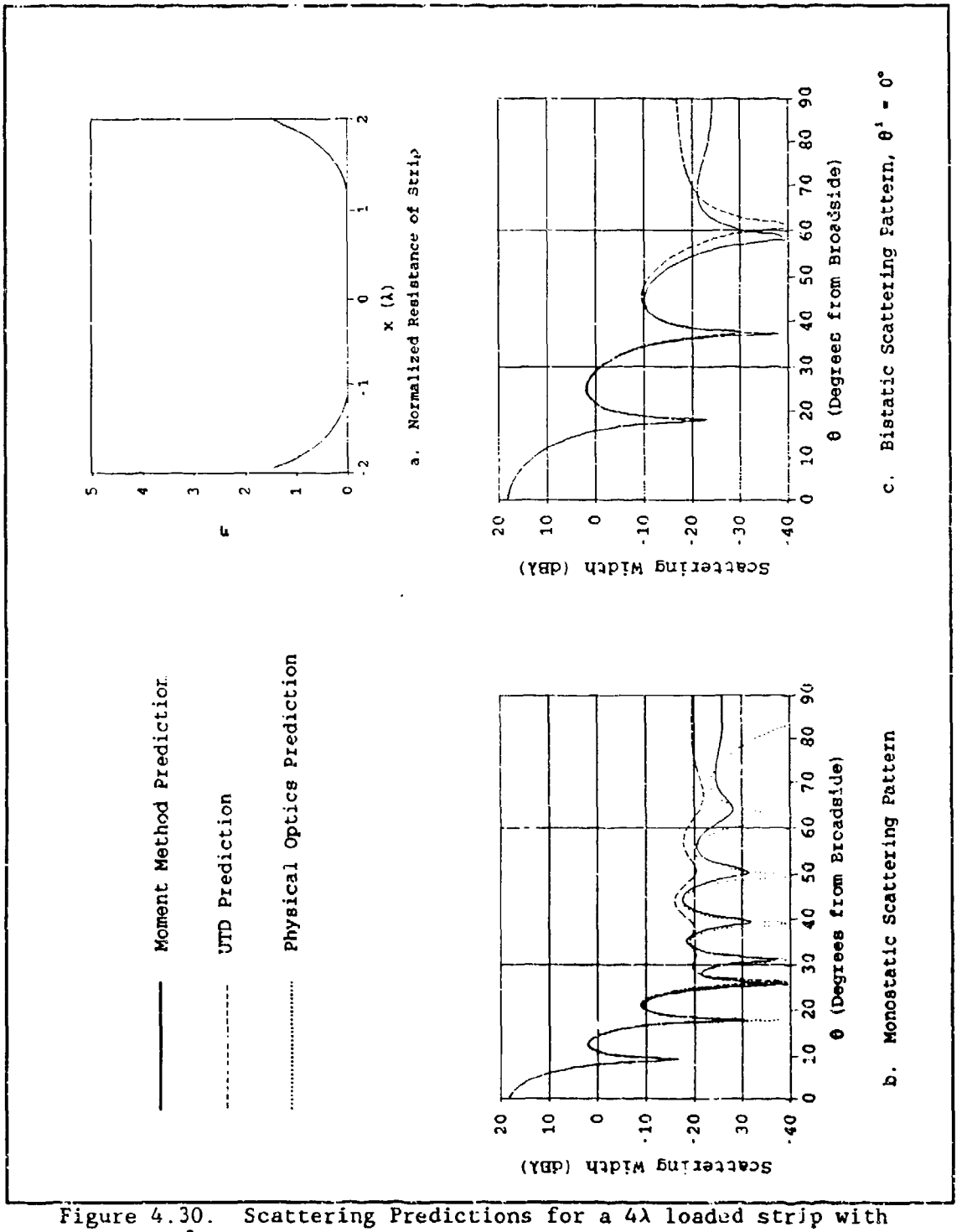

Figure 4.30. Scattering Predictions for a 4λ loaded strip with $\eta = \exp(x^2) - 1$ loads 1λ from the strip's edges, E-Polarization

exponential loads have less than half the resistive value of the $\eta = 4x^2$ loads, yet still yield similar scattering performance.

As with the constant impedance loaded strips the UTD predictions and moment method predictions match closely within 40° of broadside for monostatic scatter and within 60° of broadside for bistatic scatter. In many cases the UTD predictions closely match the moment method results for a much larger part of the scattering pattern. Within these regions the two methods yield peak levels that are not more than three dB apart, and by far most UTD sidelobe levels are less than one dB off of their moment method counterparts.

In general the UTD predictions come very close to the moment method predictions. The solution is especially close near broadside, which makes sense, since the UTD method was scaled to smooth the GO discontinuities which are present at $\theta = 0°$ for the cases presented herein. The UTD solution was also found to work better for impedance strips, both tapered and constant, than for the impedance-loaded conducting strips. This may be due to the sudden discontinuity at the conductor/load junction. The deletion of the non-equivalent term in the UTD junction diffraction coefficient was also found to be partly at fault.

A noticeable problem also exists for the bistatic H-Polarized scattering predictions in figures 4.9.c, 4.16.c, 4.18.c, and 4.29.c. It is observed that the UTD prediction does not go to zero when $\theta = 90°$, as does the moment method prediction. In the monostatic case the UTD prediction goes to zero because R_h and T_h go to zero and one, respectively, when $\theta = 90°$. These are the same reflection and

transmission coefficients as free space, so no diffractions occur. However, for the bistatic case θ is considered to be the average of the incident angle $\theta^i = 0°$, and the scattered angle $\theta^s = 90°$. This yields the value $\theta = 45°$ and R_h and T_h do not go to zero and one, but instead are given values between zero and one which depend on the material's impedance.

V. Scattering Measurements

The procedures involved in making RCS measurements of impedance strips and impedance loaded conducting strips, and the results obtained from these measurements are contained herein. First the targets and their preparation are discussed. Characteristics of the impedance materials are determined and different target configurations are considered. Finally, the experimental results are presented and compared with UTD and moment method predictions.

Targets

The scattering patterns of four different targets were measured. These consisted of two different impedance strips and two impedance loaded conducting strips. The impedance strips were four inches by six inches. The loaded strips were also four inches by six inches, with the loads one inch from the strips' edges. These geometries are shown in figure 5.1. Measurements were also made on a four inch by six inch conducting strip as a reference. All measurements were performed at 11.8 GHz, where one wavelength equals one inch.

Impedance Materials. Two impedance materials were used for the scattering measurements. Both were supplied by Emerson and Cuming. The first was Eccosorb VF 10, a conductive plastic film. The material's impedance was not specified by the manufacturer; waveguide measurements were made to determine it. The second material was Eccosorb SC 100, a graphite impregnated cloth. Although its impedance was stated to be

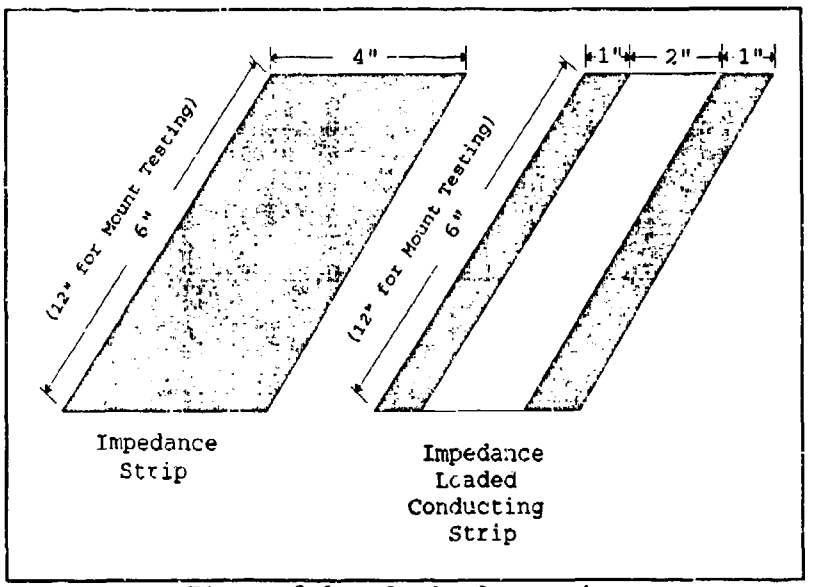

Figure 5.1. Strip Geometries

100Ω, RCS measurements indicated a different value at 11.8 GHz; thus waveguide measurements were made on it also.

The setup for the waveguide measurements is shown in figure 5.2. The impedance materials were measured at 11.8 GHz, the same as the RCS measurements. The equipment was calibrated using a sliding short and a waveguide termination. The sliding short was set to $\frac{1}{8}\lambda_g$ and $\frac{3}{8}\lambda_g$, and connected to the end of each of the waveguides to calibrate S_{11} and S_{22} for a short and open load. λ_g is the guide wavelength

$$\lambda_g = \frac{\lambda}{\sqrt{1 - \left(\frac{f_c}{f}\right)^2}} \qquad (5.1)$$

where λ is the free space wavelength and f_c is the cutoff frequency of the waveguide. For a rectangular waveguide of dimension a x b, f_c for the nm^{th} mode is given by

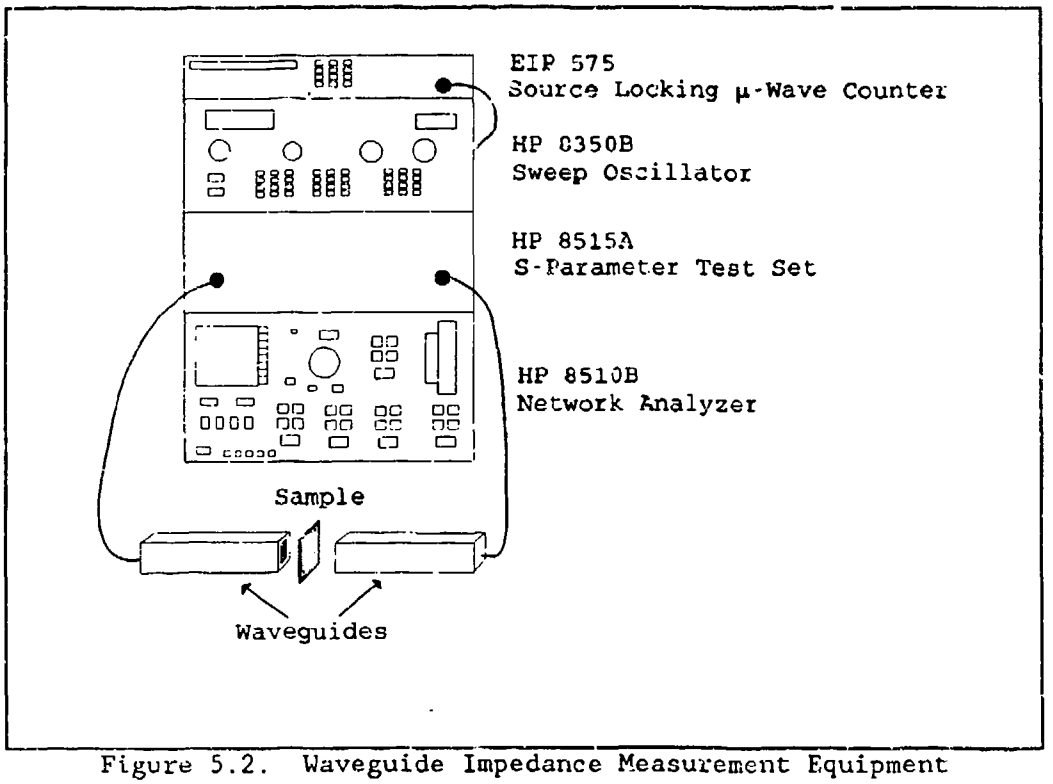

Figure 5.2. Waveguide Impedance Measurement Equipment

$$f_{c,nm} = \frac{c}{2\pi}\sqrt{\left(\frac{n\pi}{a}\right)^2 + \left(\frac{m\pi}{b}\right)^2} \qquad (5.2)$$

The waveguide termination was then attached to the end of each of the waveguides to calibrate for an infinite waveguide. Finally, two waveguides were connected to obtain S_{12} and S_{21} for the waveguides. A sample of the impedance material was then inserted between the two waveguides. The Smith Chart function of the HP 8510 was used to determine the impedance of the material normalized to the waveguide, Z_n. The HP 8510 determines the impedance using $Z_n = (1+R)/(1-R)$, where R is the reflection coefficient, either S_{11} or S_{22}, of the material.

To determine the actual impedance of the material the wave impedance must be determined. For the nm^{th} TE mode this is given by

$$Z_{TE,nm} = \frac{377\,\Omega}{\sqrt{1 - (f_c/f)^2}} \qquad (5.3)$$

where c is the free space speed of light and f is the operating frequency. For the waveguide used (a = 22.86mm, b = 10.16mm), only the TE_{10} mode (with cutoff frequency of 6.557 GHz) will propagate at an operating frequency of 11.8 GHZ. The wave impedance is then found to be $Z_{TE,10} = 454\Omega$. This is the ratio of E/H (transverse components only) at the operating frequency inside the waveguide, in contrast to 377Ω, which is the ratio of E/H in free space.

From the waveguide measurements the impedance of the VF 10, normalized to the waveguide, was 0.267 + j0.099Ω, and that of the SC 100 was 0.397 + j0.212Ω. This yields η = 0.320 + j0.120 for the VF 10, and η = 0.477 + j0.255Ω for the SC 100.

Preparing the Targets. The targets were mounted on a 5/8 inch thick sheet of styrofoam and held in place with Scotch tape. Four target/mounting configurations were investigated for the loaded strip and these are shown in figure 5 3. Results of the different mounting techniques which illustrate the problems with them are shown in figures 5.4 and 5.5. These were all measured using a 4" x 12" loaded strip conforming to the geometry given in figure 5.1. The first involved laying a 4" x 12" strip of the impedance material on the styrofoam mount. Then a 2" x 12" conducting strip was placed over the center of the impedance strip, taped at either end to the styrofoam, as shown in figure 5.3.a. This configuration was not used, however, because it was not an accurate model of the impedance loaded conducting strip, since the bare impedance material was visible behind the conductor. This

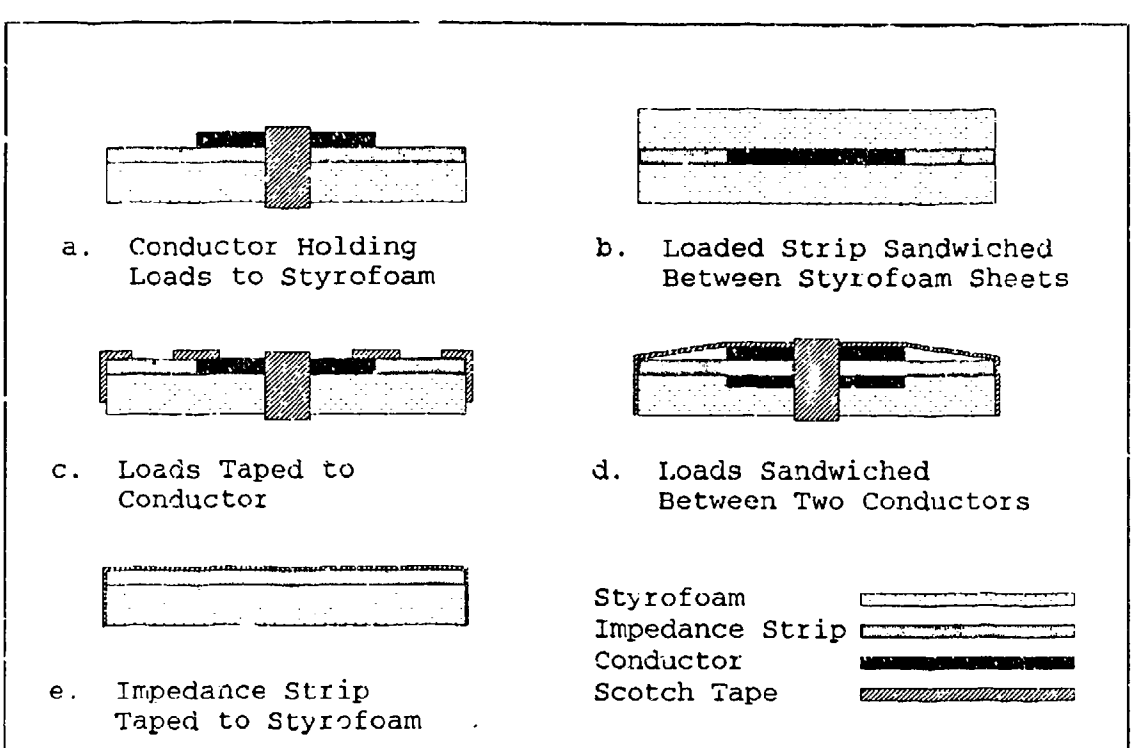

Figure 5.3. Target Mounting Configurations, End View

significantly altered the scattering pattern from that side, as seen in figure 5.4.a. In the center of the figure the conducting strip is seen through the impedance material. This shading of the conductor by the impedance strip clearly degrades the lobing structure of the scattering pattern.

Next, the conducting strip and the impedance loads were sandwiched between two sheets of styrofoam, as shown in figure 5.3.b. The sheets of styrofoam were held together by two styrofoam "clips". This method was not used because close contact between the impedance loads and the conducting strip could not be maintained; the styrofoam could not be held together tight enough to eliminate small gaps between the loads and

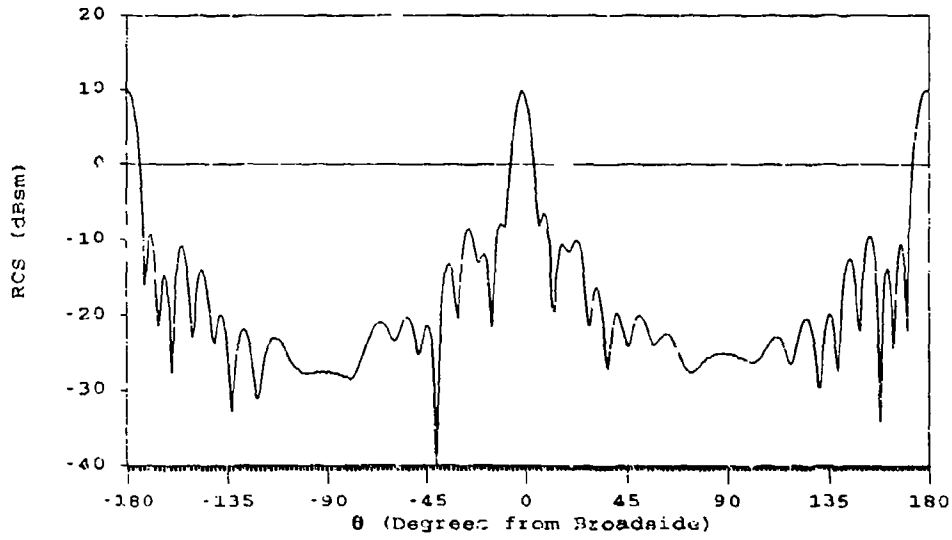

a. Impedance Material placed between conductor and styrofoam

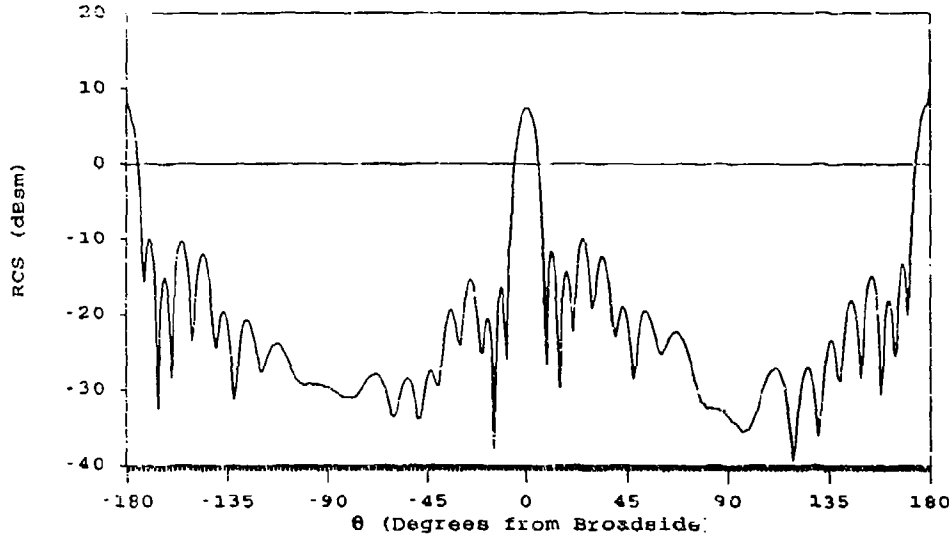

b. Loaded Strip Sandwiched between Two Styrofoam Sheets

Figure 5.4. Measurement Results of Mounting Techniques A and B

conductor. This problem was evidenced by extreme non-symmetry in the resultant scattering patterns, as seen in figure 5.4.b. There is as much as 6 dB difference between side lobes on opposite sides of the main lobe.

Another method investigated was to mount the strips using Scotch tape along the entire edge of the conducting strip/load junction, as shown in figure 5.3.c. This firmly held the conductor to the edge of the conducting strip. Tape was also used along the outer edges of the loads to hold them flat against the styrofoam. This configuration was not used, however, because RCS measurements showed that the tape significantly altered the scattering pattern. There was a large variation in the pattern between the side of the strip with the tape and the side without it, which is clearly seen in figure 5.5.a. In the center of the plot the tape is seen on top of the strips and it clearly affects the lobing structure near the center lobe. On the outer halves of the pattern the tape is mostly blocked by the conducting strip and it is not seen to cause a significant effect here.

The method finally used to mount the loaded strips was to sandwich a 4" x 12" impedance strip between two, 2" x 12" conducting strips, as shown in figure 5.3.d. This ensures good contact between the impedance loads and the conducting strip. It also eliminates the problem of the first case, where the bare impedance material was present along the back of the conducting strip. The loaded strip was then held to the styrofoam with two thin pieces of tape across the width of the strip. The result of this mounting technique is shown in figure 5.5.b. There is some minor asymmetry in this scattering pattern, mostly in the depth

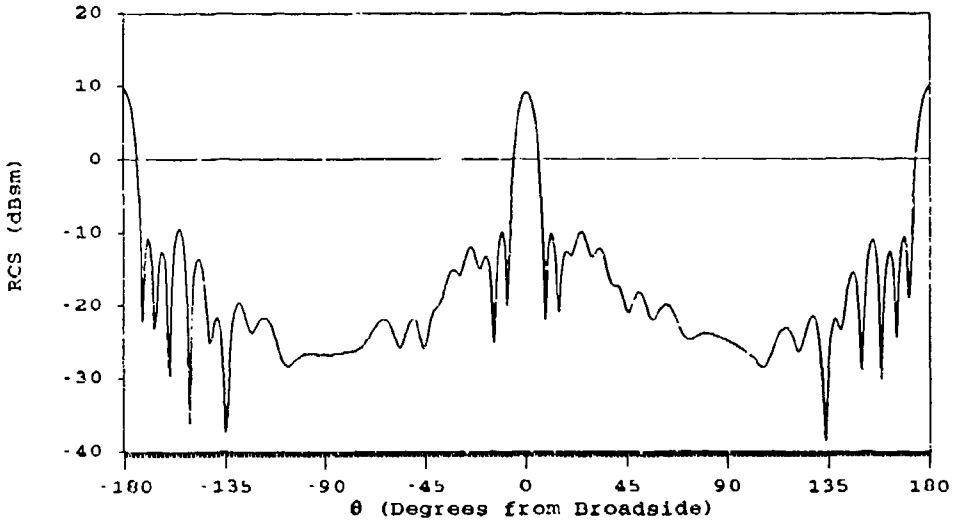

a. Impedance Loads Taped to Conductor

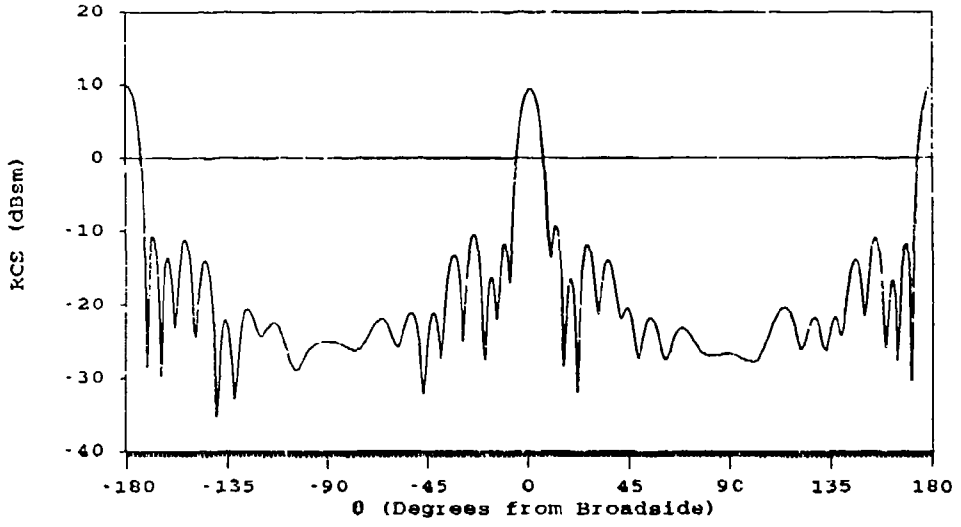

b Impedance Material Sandwiched Between Two Impedance Strips

Figure 5.5. Measurement Results of Mounting Techniques C and D

of the nulls. This is likely due to the styrofoam present on one side of the target only. In addition it was impossible to keep the loads perfectly flat. The SC 10C was rolled for shipment and the mild curvature that this introduced in the material could not be totally eliminated. The VF 10 was nearly flat but its edges could not be kept straight. To measure the impedance strips they were held flat against the styrofoam using thin strips of tape across their width, as shown in figure 5.3.e.

Measurements

All the measurements presented herein were taken at the AFIT School of Engineering's anechoic chamber. This is a far field measurement facility. It incorporates separate transmit and receive antennae, both of which are Flam & Russell 6414 horns with eight inch square apertures. The antennae are mounted one foot apart on a mount that can be rotated to allow both horizontal and vertical polarization measurements. The target is mounted on an ogive pedestal 27 feet from the antennae.

The chamber equipment is shown in figure 5.6. A frequency swept signal is generated by the synthesized sweeper. Part of this signal is bled off in the directional coupler to use as a reference for the received signal. The signal is then amplified by the microwave amplifier and transmitted from the TX antenna. The scattered signal is received by the RX antenna and fed to the frequency converter, where it is mixed down to IF along with the reference signal from the directional coupler. The two signals are then fed to the network analyzer and the received signal is compared to the reference signal. A software time

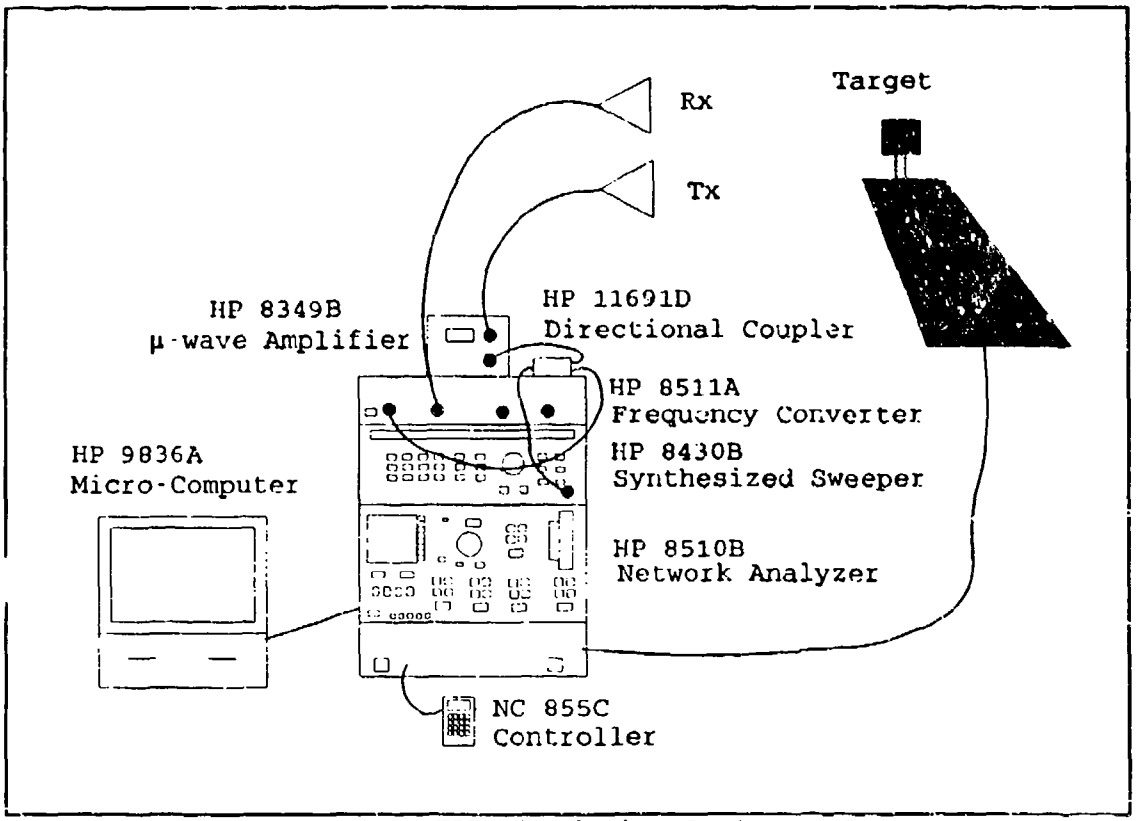

Figure 5.6. AFIT RCS Chamber Equipment Setup

gate and background subtraction are implemented in the calibration process. For the measurements presented herein the time gate was 3ns. As previously stated all measurements were made at 11.8 GHz.

Since the strips exhibit scattering symmetry over 90°, the scattering pattern results were averaged over the two 90° quadrants where the styrofoam was partially obscured behind the loaded or impedance strip. This was done to reduce any symmetry problems caused by the non-uniformity of the materials and to reduce the styrofoam's effect on the measurements. From hereon all measurements were made using a 6" x 4" strip. This was done because measurements of the 12" strips yielded slightly lower levels than expected. This is because the

12" strip has a narrow main lobe (in the vertical plane, not the horizontal plane that is measured); unless the target is aligned perfectly, the measurements will be slightly off to the side of the peak, resulting in a lower return. This reduction is nearly three dB when alignment is off by one degree, as compared to one-half dB for a 6" strip. The 6" strip has a wider main lobe so that alignment is not as critical.

Each of the measurements are plotted against both UTD and moment method predictions. The plotted measurements are scaled in order to be consistent with the predictions. The measurements are given in RCS, σ_{3D}(dBsm), but the predictions yield scattering width, σ_{2D}(dBλ). Two conversions are needed to obtain the scaling factor. First the measurement is converted from σ_{3D}(dBsm) to σ_{2D}(dBm) using (1:578):

$$\sigma_{2D} = \sigma_{3D} \frac{\lambda}{2l^2} \tag{5.4}$$

where l is the length of the target (6" (0.1524m)) and λ = 1" (0.0254m). This results in σ_{2D}(dBm) = σ_{3D}(dBsm) - 2.62dB. Next σ_{2D}(dBm) is converted to σ_{2d}(dBλ):

$$\sigma_{2D}(dB\lambda) = \sigma_{2D}(dBm) - 10LOG(\lambda) \tag{5.5}$$

where λ is in meters. This results in σ_{2D}(dBλ) = σ_{2D}(dBm) + 15.95dB. Therefore, a scaling factor of 13.33dB must be added to the measurements to convert them to σ_{2D}(dBλ); that is, σ_{2D}(dBλ) = σ_{3D}(dBsm) + 13.33.

Impedance Strips. Figures 5.7 and 5.8 contain the results of scattering pattern measurements for a 4λ conducting strip. The E-Polarization measurement and predictions in figure 5.7 match very well.

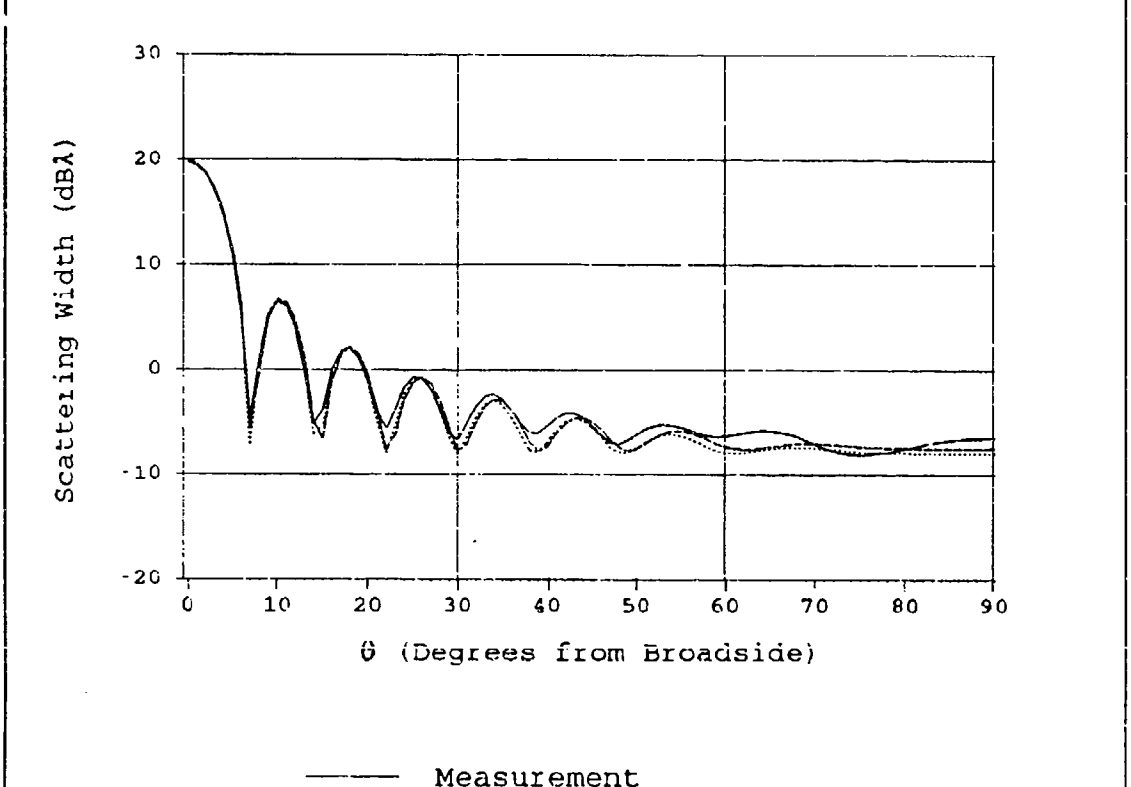

Figure 5.7. Comparison of Measured and Predicted Monostatic Scattering Pattern for a 4λ Wide Conducting Strip, E-Polarization

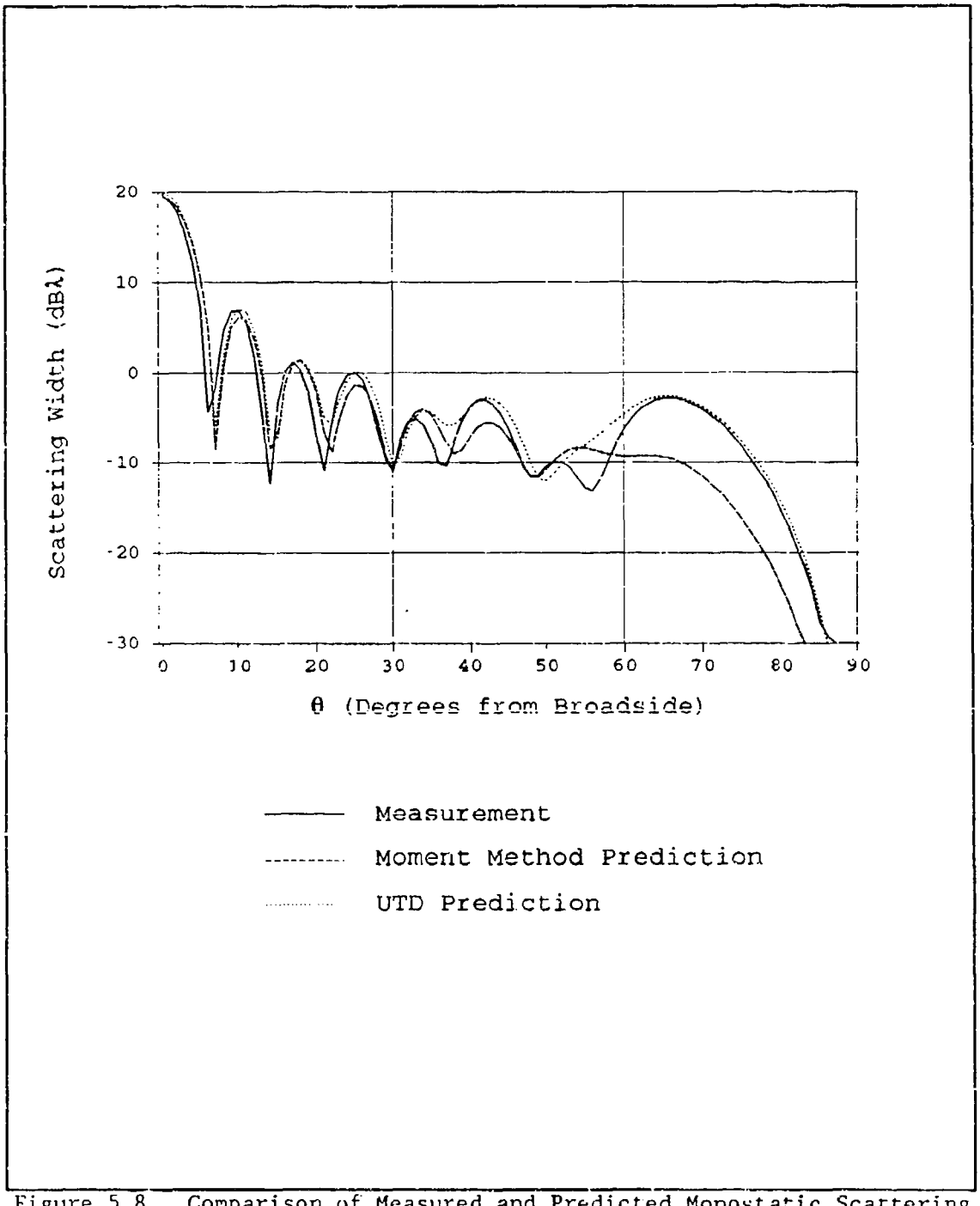

Figure 5.8. Comparison of Measured and Predicted Monostatic Scattering Pattern for a 4λ Wide Conducting Strip, H-Polarization

The measurement and the UTD prediction never differ by more than two dB and the difference is usually much closer than one dB. The H-Polarization UTD prediction also matches the measurement well, as seen in figure 5.8. The travelling wave is very accurately predicted by the UTD solution. The moment method solution fails to predict this accurately however, due to the problems discussed in chapter 4. There are some discrepancies in the lobing structure between the UTD solution and the measurement around θ = 35° and 55°. This may be caused by interactions with the mount and pedestal.

Scattering measurements of the impedance strips are contained in figures 5.9 through 5.12. The general effect of the finite impedance on the strips is a reduced scattering pattern. This was noted in chapter 4. The E-Polarization measurements in figures 5.9 and 5.10 show very good agreement between the UTD predictions and the measurements, especially figure 5.10. In both cases most sidelobes have a magnitude difference of less than one dB. The edge-on scattering level is off by five dB in figure 5.9, but only differs by two dB in figure 5.10.

The H-Polarization measurements in figures 5.11 and 5.12 do not show quite as good agreement between the UTD solution and the measured pattern. The UTD method predicts sidelobe levels within one dB of the measured levels within 30° of broadside, but the results are not as good nearer edge-on. The moment method solution appears to do a better job of predicting the travelling wave lobe for these measurements than it did for the conducting strip. The measurement in figure 5.11 is seen to rise slightly at edge-on instead of going to zero. This is likely due

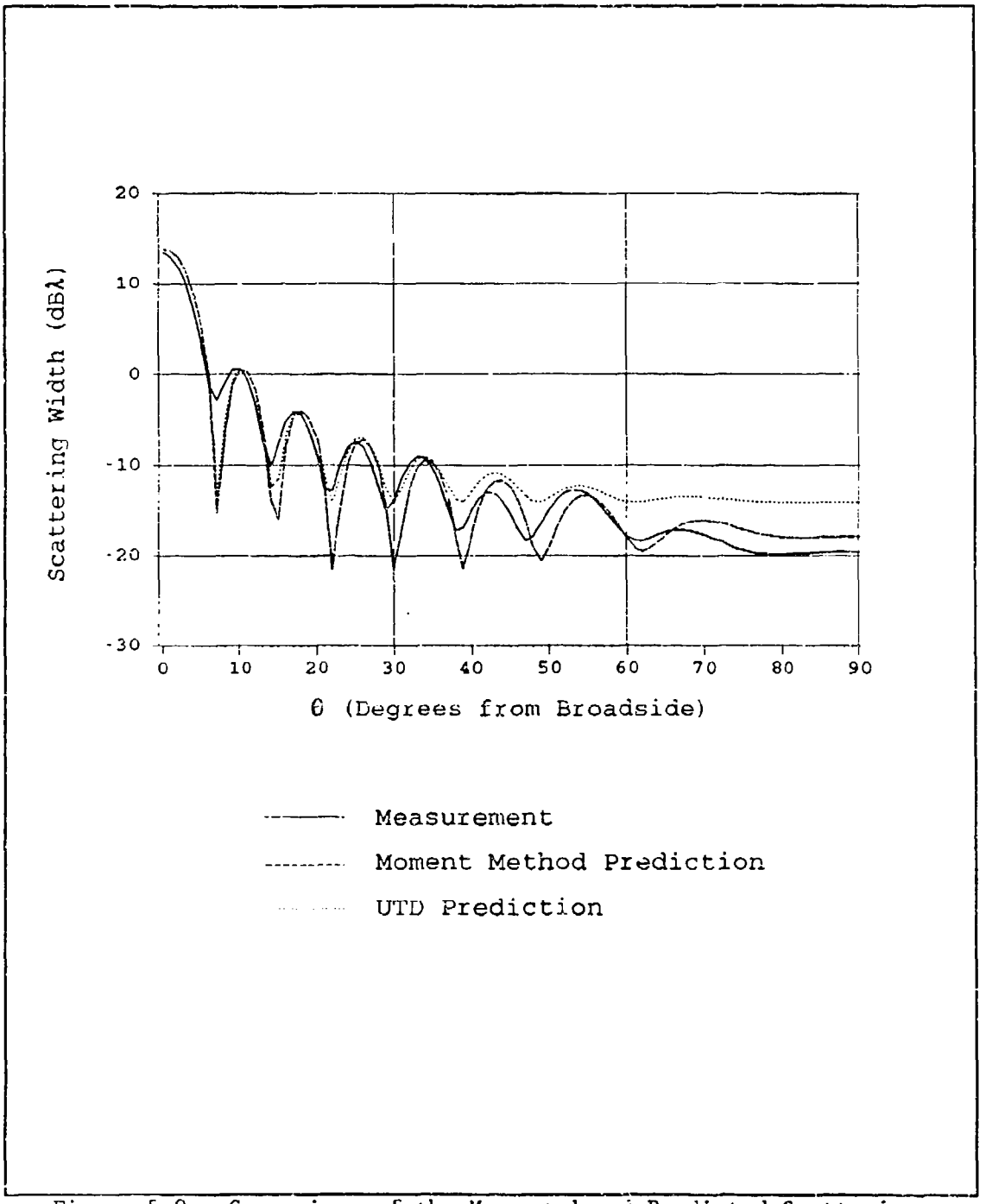

Figure 5.9. Comparison of the Measured and Predicted Scattering Pattern for a 4λ, $0.477 + j0.255\eta$ Strip, E-Polarization

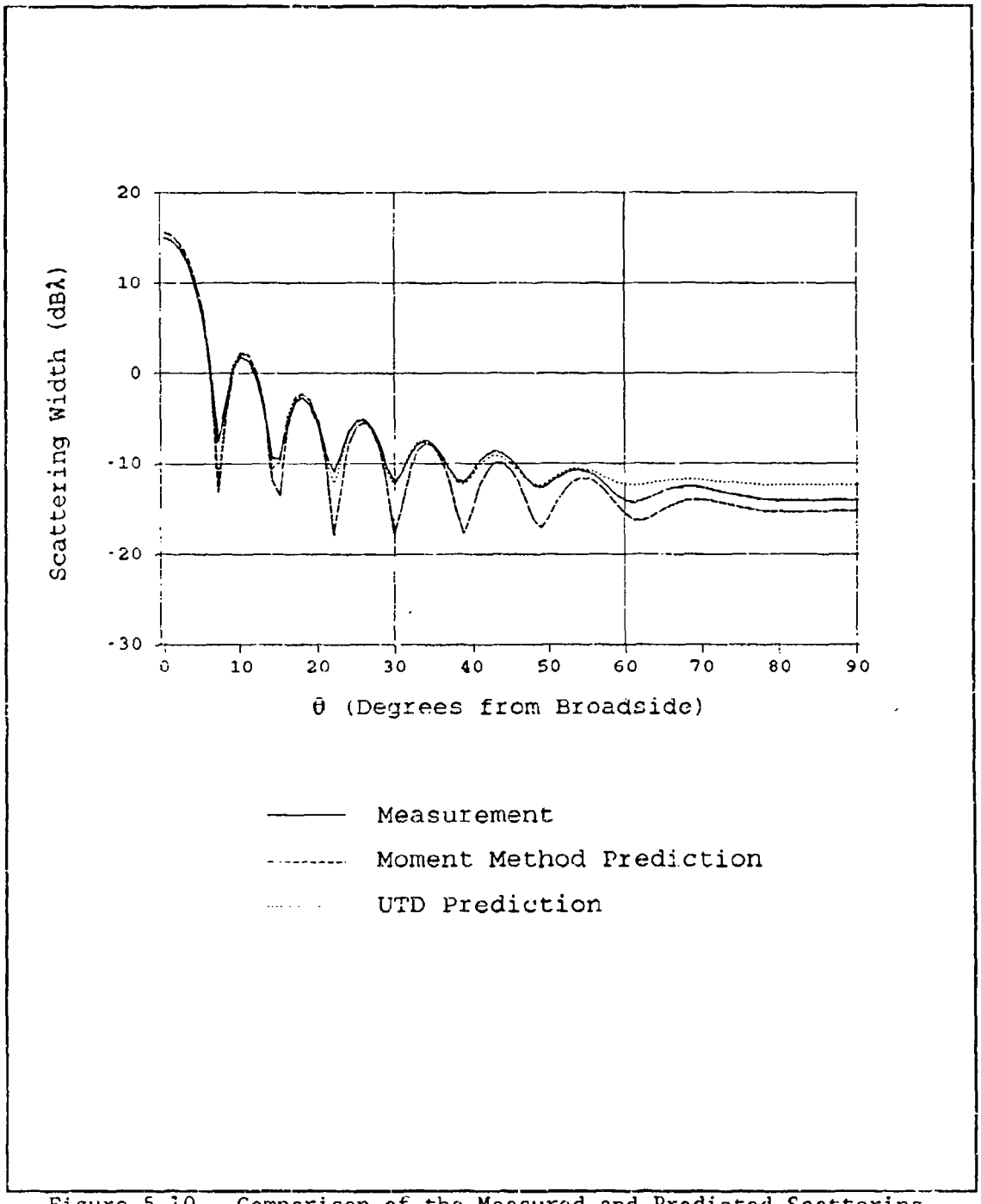

Figure 5.10. Comparison of the Measured and Predicted Scattering Pattern for a 4λ, $0.320 + j0.120\eta$ Strip, E-Polarization

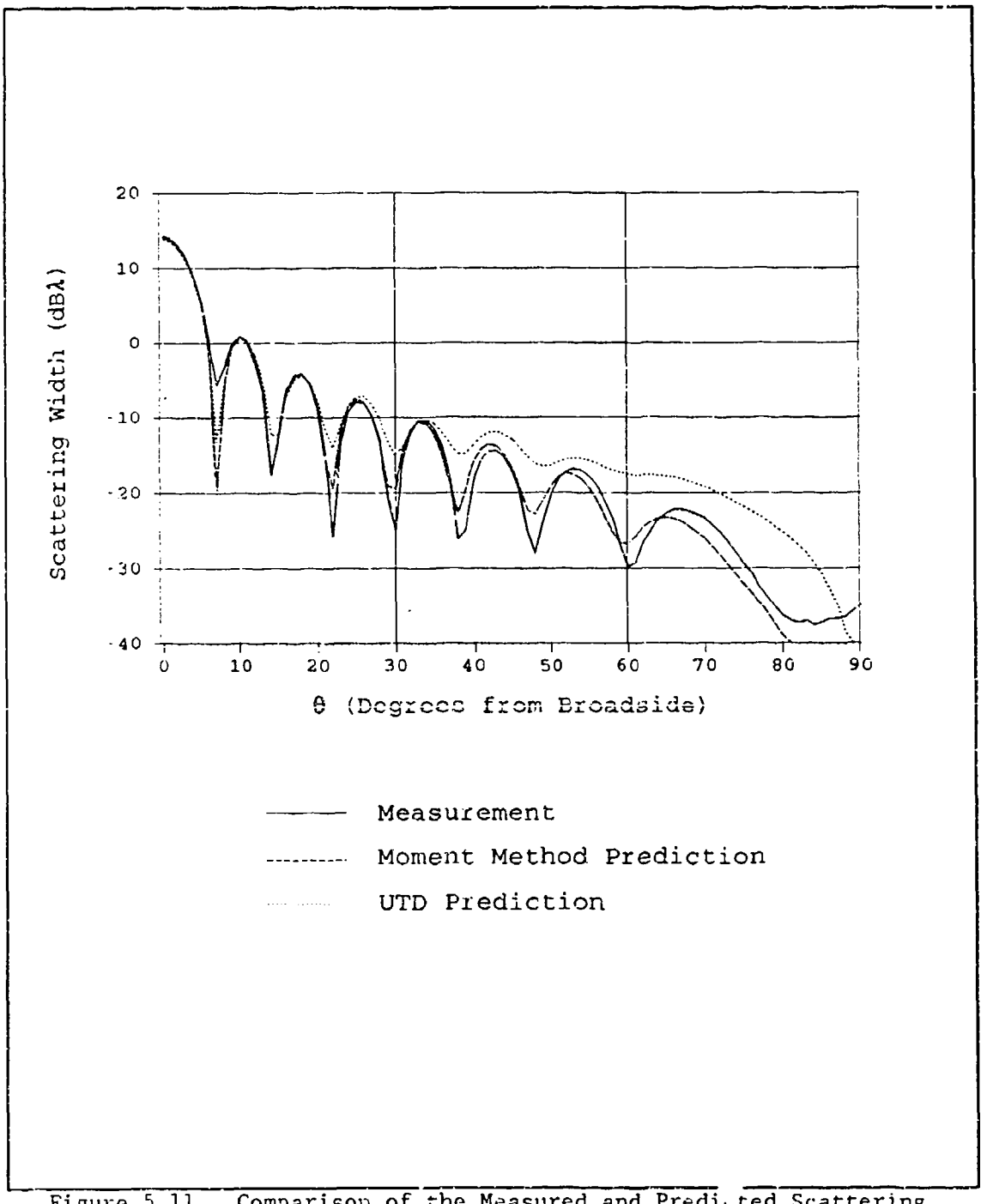

Figure 5.11. Comparison of the Measured and Predicted Scattering Pattern for a 4λ, 0.477 + j0.255η Strip, H-Polarization

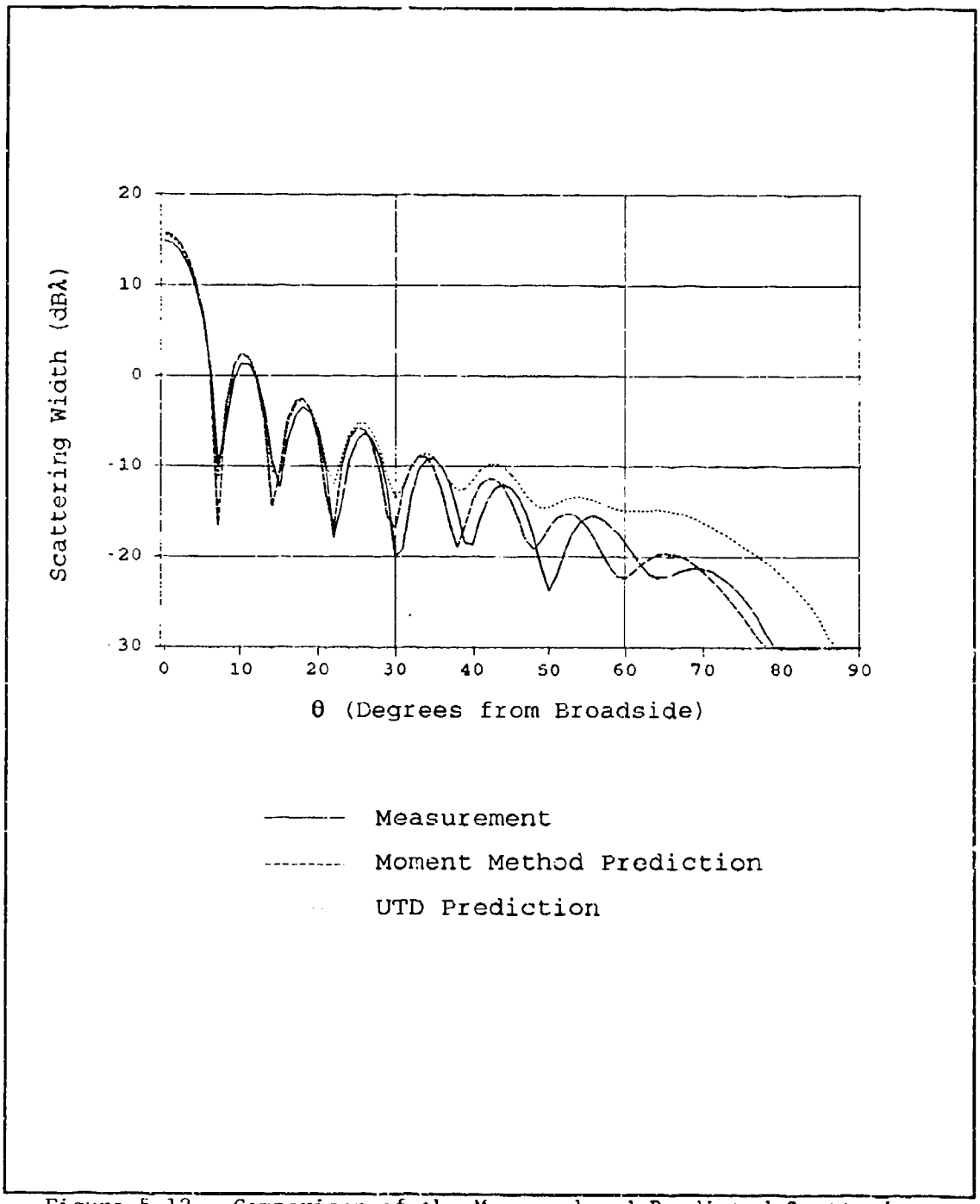

Figure 5.12. Comparison of the Measured and Predicted Scattering Pattern for a 4λ, 0.320 + j0.120η Strip, H-Polarization

to a minor curvature in the impedance material and the effects of the styrofoam mount.

Scattering measurements of the impedance loaded conducting strips are contained in figures 5.13 through 5.16. The impedance loads in both measurements broaden the main lobe and reduce the sidelobe levels relative to the main lobe. This was also seen in chapter 4. In addition, the edge-on scattering levels are reduced from -8 dBλ for the perfect conductor, to approximately -16 dBλ in figures 5.13 and 5.14. The UTD predictions match the measured pattern well within 40° of broadside; the sidelobe levels are within two dB. Beyond this the UTD method doesn't match the lobing structure of the measurement though. This is due in part to the elimination of the non-equivalent term in the junction diffraction coefficient, which was discussed in chapter 4. The UTD does a very good job of predicting the edge-on scattering levels for the two E-Polarization cases, however, being from one two three dB higher than the measurements.

The two H-Polarization measurements for the loaded strips are displayed in figures 5.15 and 5.16. The UTD predictions for these cases are only slightly worse than they were for the E-Polarization plots, but still have good accuracy near broadside. In addition, the UTD solution is much better at predicting the travelling wave lobe for these cases than it did for the impedance strips, and is also better than the moment method predictions. The measurements are observed to have a small lobe directly at edge-on, where they should be going to zero. The lobe is caused by the conducting strips that are placed on each side of the impedance strip. Since these strips are not infinitely thin, they

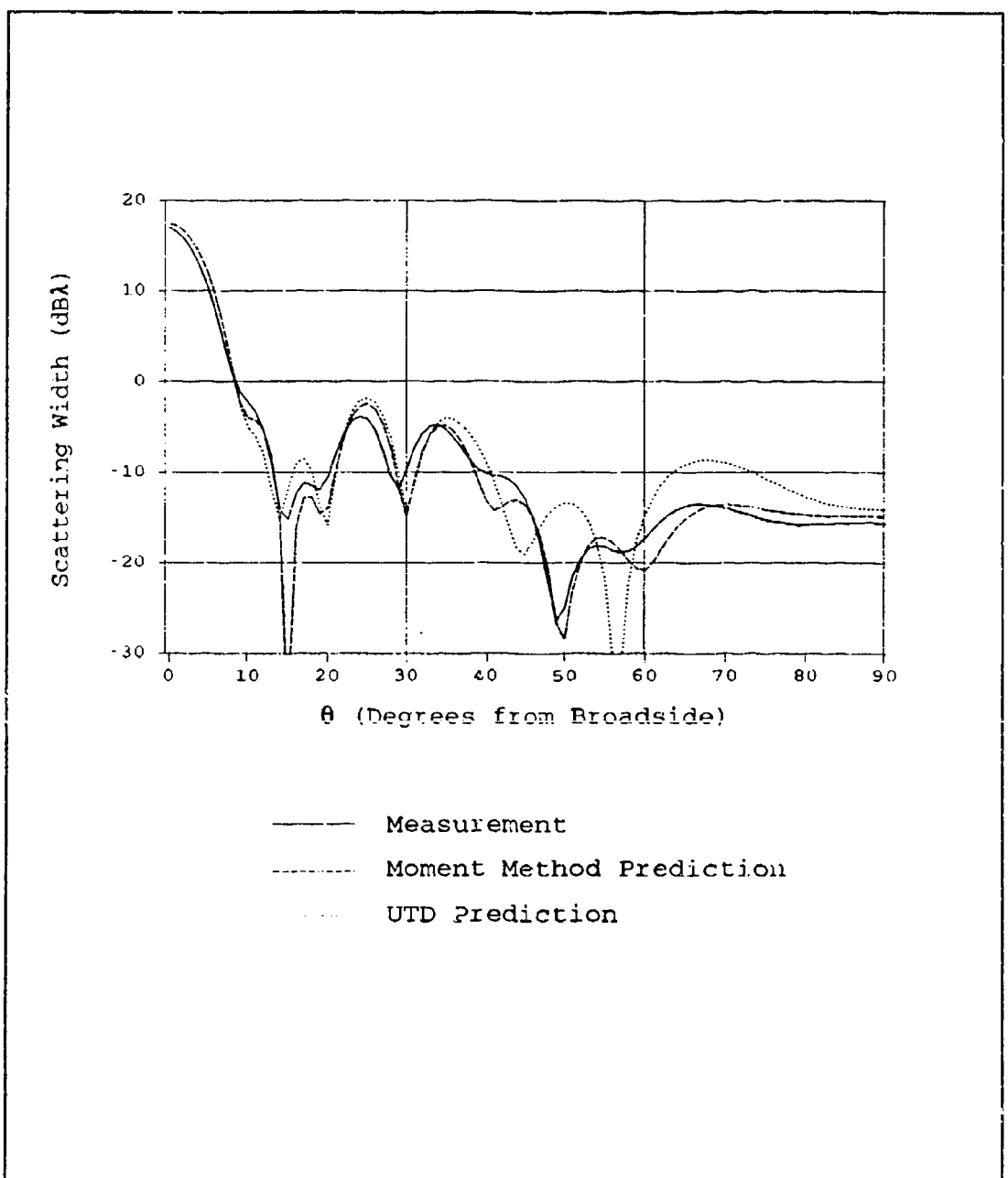

Figure 5.13. Comparison of the Measured and Predicted Scattering Pattern for a 4λ Strip with 0.477 + j0.255η Loads 1λ from the Edges, E-Polarization

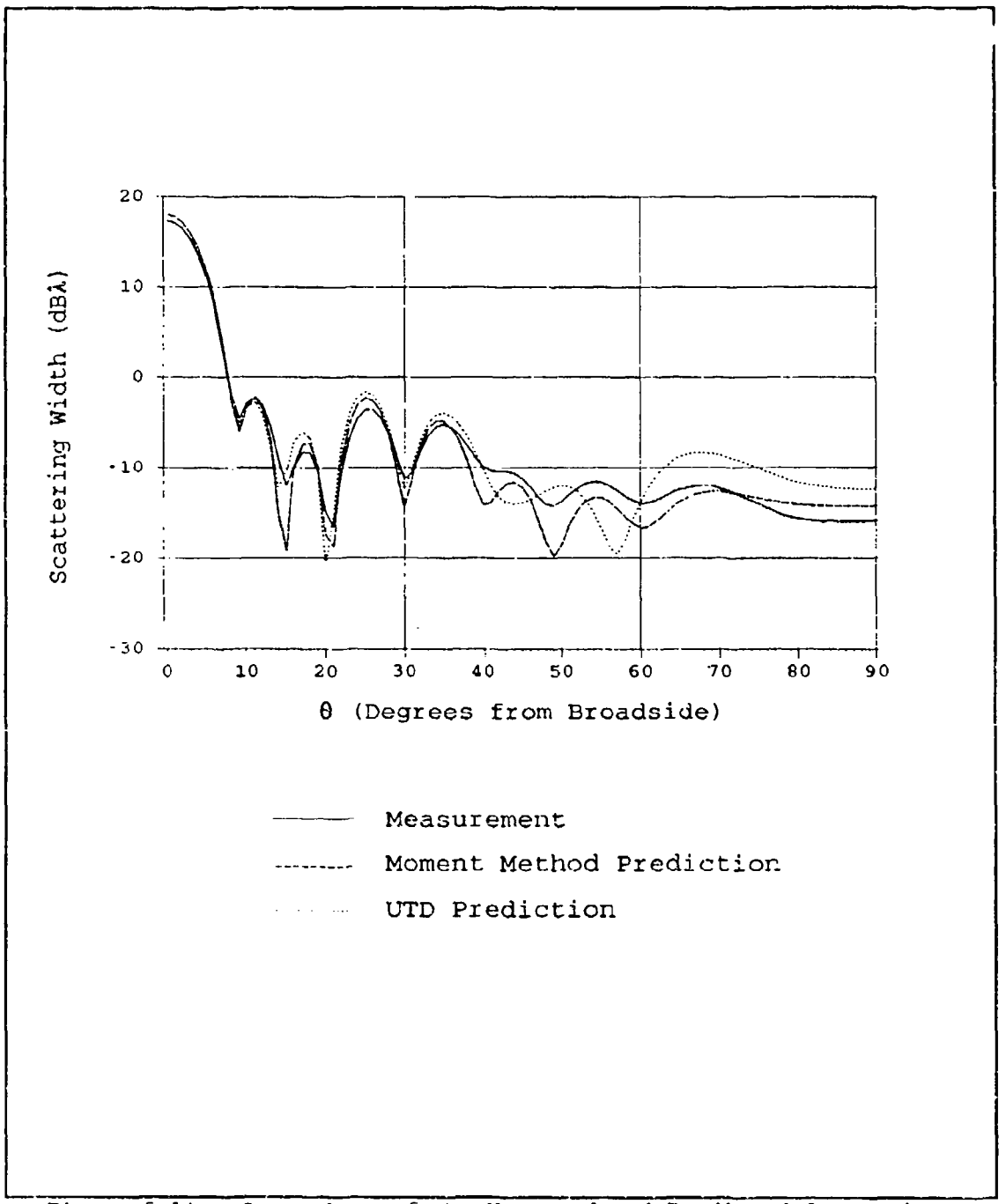

Figure 5.14. Comparison of the Measured and Predicted Scattering Pattern for a 4λ Strip with $0.320 + j0.120\eta$ Loads 1λ from the Edges, E-Polarization

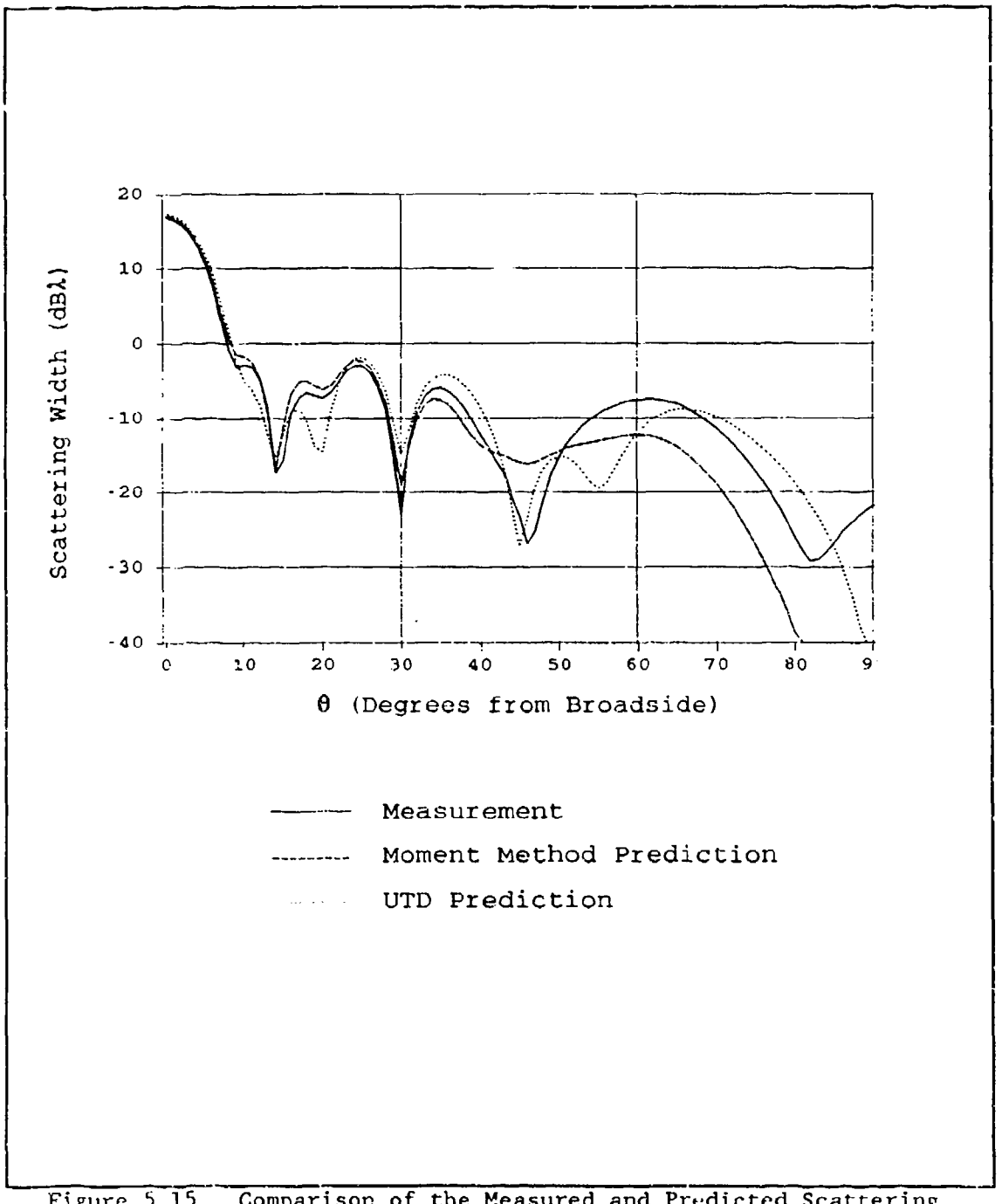

Figure 5.15. Comparison of the Measured and Predicted Scattering Pattern for a 4λ Strip with 0.477 + j0.255η Loads 1λ from the Edges, H-Polarization

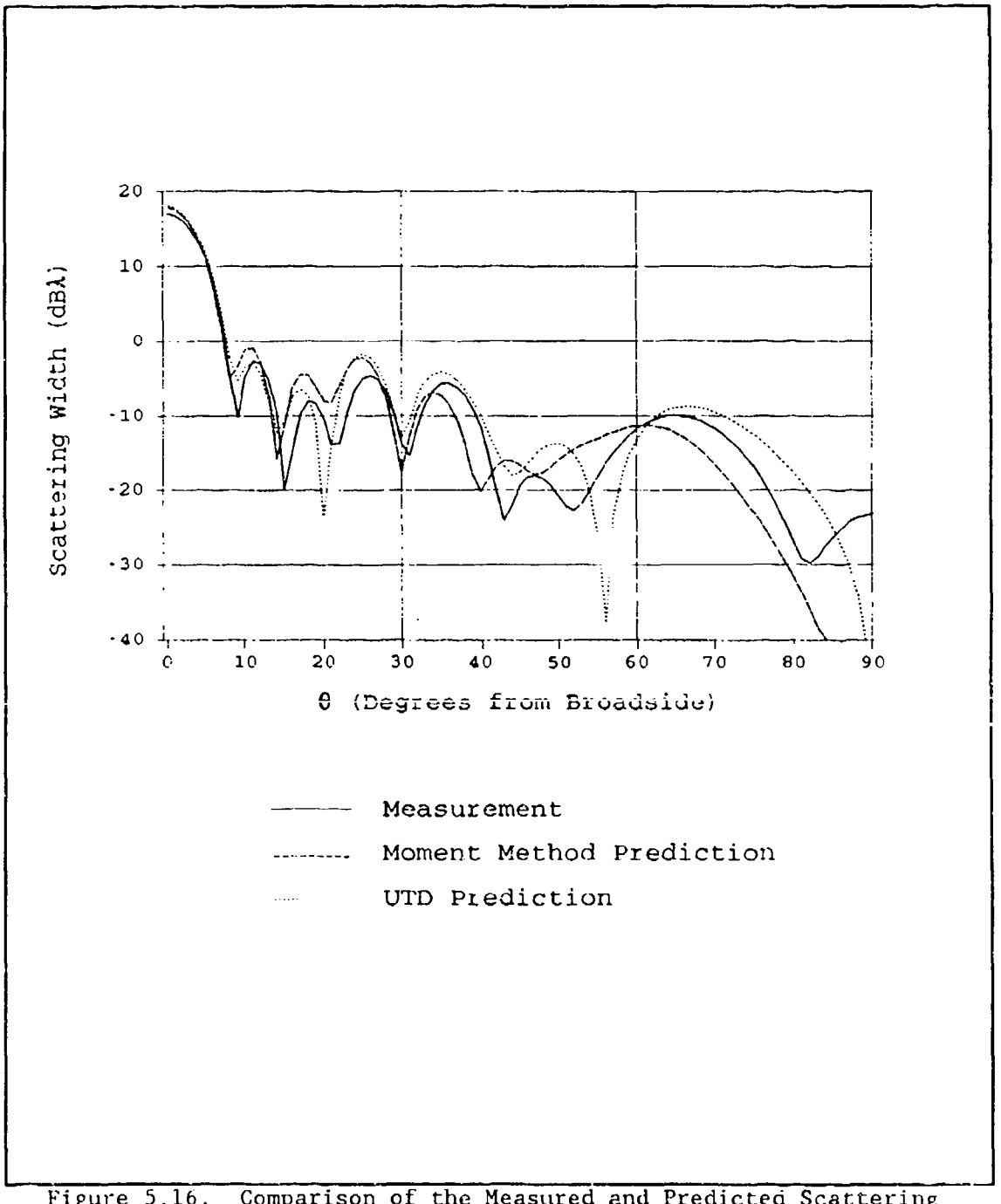

Figure 5.16. Comparison of the Measured and Predicted Scattering Pattern for a 4λ Strip with 0.320 + j0.120η Loads 1λ from the Edges, H-Polarization

produce diffractions from their leading and trailing edges. These diffractions add more coherently when the strip is viewed at edge-on than when viewed at a small grazing angle, resulting in the lobes.

VI. Conclusions

Summary

This thesis investigates scattering from impedance strips and impedance loaded conducting strips. First, UTD edge diffraction coefficients for a perfect conductor were heuristically modified to predict scattering from impedance edges and junctions. These modifications involved scaling the coefficients to account for changes in the GO field discontinuities. Multiple diffractions on the surface of a strip were also examined and composite multiple diffraction fields which include all of the multiple diffractions were developed.

The UTD formulae were then incorporated into Fortran programs that predict the scattering width of impedance strips and impedance loaded conducting strips. Both uniform and tapered strips and loads were considered. The UTD predictions were compared to moment method predictions and RCS measurements to determine the validity of the UTD formulae. The effects of different impedance values on the scattering patterns of the strips were also examined.

Scattering patterns of uniform impedance strips were similar to that of a conducting strip, but were basically scaled according to the strips' reflection coefficients. The nulls between the sidelobes and the edge on scattering levels, however, were lower than simple scaling would indicate. This effect was more prominant for higher impedance values. Tapering the strip's impedance was found to drastically lower the sidelobe levels relative to the main lobe. This effect was more prominant for strips with a higher taper.

Applying loads to a conducting strip also caused reduced sidelobe and edge-on scattering levels relative to the main lobe. However, if the load's impedance was too high, the resultant scattering was very similar to that of just the conducting strip alone. When the load was tapered the sidelobe and edge-on scattering levels were reduced drastically. As with the tapered strips the reduction was much greater when the tapers reached a higher impedance value.

In general the UTD predictions come very close to the moment method predictions and the measurement results. The UTD solution is especially close near broadside, which makes sense, since the UTD method was scaled to smooth the GO discontinuities which are present at $\theta = 0°$ for the cases presented herein. For the impedance strips, the UTD method accurately predicts monostatic sidelobe levels within 60° of broadside. The results for loaded strips were slightly worse, with close agreement limited to within 40° from broadside. In these regions the UTD method typically predicted sidelobe levels within one-half dB of the moment method predictions and measurement results, and was never more than two dB off. The bistatic predictions were accurate over a wider range than the monostatic predictions.

The UTD method did not accurately predict the level of the nulls or edge on scattering width, when compared to the moment method predictions, although it showed better agreement with the measurements. This effect was more pronounced for higher impedance values and near edge-on. The nulls were found to be much deeper in the moment method predictions than in the UTD predictions. These deeper nulls are caused by an increased level of destructive interference between the

diffraction sources, indicating that the diffractions from the two edges of the strip should be closer in magnitude than the diffractions from the two edges of a perfect conductor. Our solution could not predict this, however, because diffractions from both edges of the strip were scaled by the same amount, $R_{s,h}$. For E-Polarization the diffractions from the leading edges of the strip have a larger magnitude than those from the trailing edge. In order to produce the deeper nulls the leading edge diffraction should be scaled down relative to the trailing edge diffraction. The opposite is true for H-Polarization.

Recommendations

The application of impedance loads, in particular tapered impedance loads, was observed to significantly reduce the sidelobes and edge-on scattering from conducting strips. This displays the potential of edge loading for the reduction of RCS.

Further work could be done to make improvements to the formulae developed in this work. In addition, Rojas' solution for diffractions from impedance edges and junctions (13) could be implemented. Finally, the methods developed herein could be extended to make scattering predictions from 3-dimensional objects.

Bibliography

1. Balanis, Constantine A. Advanced Engineering Electromagnetics. New York: John Wiley & Sons, 1989.

2. Burnside, Walter D. and Ken W. Burgener. "High Frequency Scattering by a Thin Lossless Dielectric Slab," IEEE Transactions on Antennas and Propagation, 31: 104-110 (January 1983).

3. Fratamico, John J. Jr., Chief Engineer, Technology Research Group, Science Applications International Corporation, San Diego. "Radar Cross Section." Lecture to AFIT Students, Air Force Institute of Technology (AU), Wright-Patterson AFB OH, 4,5 October 1990.

4. Harrington, Roger F. and Joseph R. Mautz. "Control of Radar Scattering by Reactive Loading," IEEE Transactions on Antennas and Propagation, 20: 446-454 (July 1972).

5. Haupt, Randy L. and Valdis V. Liepa. Synthesis of Resistive Tapers to Control Scattering Patterns of Strips. PhD thesis. University of Michigan, Ann Arbor MI, 1988.

6. Haupt, Randy L., Capt, USAF. Personal Communication. U. S. Air Force Academy, Colorado Springs CO.

7. Joseph, Philip, Capt, USAF. Personal Communication. School of Engineering, Air Force Institute of Technology (AU), Wright-Patterson AFB OH.

8. Keller, J. B. "Geometrical Theory of Diffraction," Journal of the Optical Society of America, 52: 116-130 (February 1962).

9. Knott, Eugene F. and others. Radar Cross Section. Norwood MA: Artech House, 1985.

10. Kouyoumjian, Robert G. and Prabhakar H. Pathak. "A Uniform Geometrical Theory of Diffraction for an Edge in a Perfectly Conducting Surface," Proceedings of the IEEE, 62: 1448-1461 (November 1974).

11. Pathak, Prabhakar H. "Techniques for High-Frequency Problems," Radar Handbook, edited by Yuen T. Lo and Shung-Wu Lee. New York: Von Nostrand Reinhold Company, 1988.

12. Richmond, Jack H. "Scattering by Thin Dielectric Strips," IEEE Transactions on Antennas and Propogation, 33: 64-68 (January 1985).

13. Rojas, Roberto G. "Wiener-Hopf Analysis of the EM Diffraction by an Impedance Discontinuity in a Planar Surface and by an Impedance Half-Plane,: IEEE Transactions on Antennas and Propogation, 36: 71-83 (January 1988)

14. Schindler, J. K. and others. "The control of electromagnetic scattering by impedance loading," Proceedings of the IEEE, 53: 993-1004 (August 1965)

15. Senior, Thomas B. A. "Backscattering from Resistive Strips," IEEE Transactions on Antennas and Propogation, 27: 808-813 (November 1979).

16. Senior, Thomas B. A. and Valdis V. Liepa. "Backscattering from Tapered Resistive Strips," IEEE Transactions on Antennas and Propogation, 32: 747-751 (July 1984).

Vita

Lieutenant Mark C. Heaton was born on 14 October 1959 in West Covina California. He graduated from Simi Valley High School in Simi Valley, California in 1977. In 1978 he joined the U.S. Air Force and became a B-52 gunner at Ellsworth AFB, South Dakota. In 1983 he was accepted into the Airman Education and Commissioning Program and began attending California State University, Long Beach. He graduated wit. a Bachelor of Science in Electrical Engineering "With Great Distinction" in August 1986 and was commissioned an Air Force Second Lieutenant in December 1986, after attending Officer Training School. He was assigned to Space Systems Division at Los Angeles AFB, where he worked with the Global Positioning System until entering the School of Engineering, Air Force Institute of Technology, in May 1989.

REPORT DOCUMENTATION PAGE

Form Approved
OMB No. 0704-0188

1. AGENCY USE ONLY (Leave Blank)	2. REPORT DATE	3. REPORT TYPE AND DATES COVERED
	3 Dec 90	Master's Thesis

4. TITLE AND SUBTITLE
ELECTROMAGNETIC SCATTERING FROM IMPEDANCE STRIPS AND IMPEDANCE-LOADED CONDUCTING STRIPS

5. FUNDING NUMBERS

6. AUTHOR(S)
Mark C. Heaton, 1Lt, USAF

7. PERFORMING ORGANIZATION NAME(S) AND ADDRESS(ES)
Air Force Institute of Technology, WPAFB OH 45433-6583

8. PERFORMING ORGANIZATION REPORT NUMBER
AFIT/GE/ENG/90D-26

9. SPONSORING/MONITORING AGENCY NAME(S) AND ADDRESS(ES)

10. SPONSORING/MONITORING AGENCY REPORT NUMBER

11. SUPPLEMENTARY NOTES

12a. DISTRIBUTION/AVAILABILITY STATEMENT
Approved for public release; distribution unlimited

12b. DISTRIBUTION CODE

13. ABSTRACT *(Maximum 200 words)*

This paper investigates the scattering from impedance strips and impedance-loaded conducting strips. The UTD diffraction coefficient for an edge in a conductor is heuristically modified for impedance edges and junctions. Essentially, this is done by scaling the UTD diffraction coefficients according to changes in the geometrical optics field. The new diffraction coefficients are then used to investigate the scattering from impedance strips and impedance-loaded conducting strips. Both uniform and tapered impedances are considered. Results are compared to moment method and physical optics predictions and to measured data. The scattering pattern of a uniform impedance strip was seen to behave as that for a conducting strip, but at a lower level. However, tapering the impedance was seen to significantly decrease the sidelobe levels relative to the main lobe. Also, applying an impedance load to a conducting strip reduced the sidelobe levels. This was most pronounced for loads of tapered impedance. The modified UTD approach accurately predicted the sidelobe levels and locations for the simple impedance strips, and worked fairly well for the impedance-loaded conducting strips. The predictions for all geometries were better near broadside incidence than near edge-on. Keywords:

14. SUBJECT TERMS	15. NUMBER OF PAGES
Electromagnetic Scattering, Strip Scattering, Impedance Loading, Uniform Theory of Diffraction (UTD), Multiple Diffractions, (THT) Theses,	125
	16. PRICE CODE

17. SECURITY CLASSIFICATION OF REPORT	18. SECURITY CLASSIFICATION OF THIS PAGE	19. SECURITY CLASSIFICATION OF ABSTRACT	20. LIMITATION OF ABSTRACT
Unclassified	Unclassified	Unclassified	UL

GENERAL INSTRUCTIONS FOR COMPLETING SF 298

The Report Documentation Page (RDP) is used in announcing and cataloging reports. It is important that this information be consistent with the rest of the report, particularly the cover and title page. Instructions for filling in each block of the form follow. It is important to ***stay within the lines*** to meet ***optical scanning requirements***.

Block 1. Agency Use Only *(Leave blank)*.

Block 2. Report Date. Full publication date including day, month, and year, if available (e.g. 1 Jan 88). Must cite at least the year.

Block 3. Type of Report and Dates Covered. State whether report is interim, final, etc. If applicable, enter inclusive report dates (e.g. 10 Jun 87 - 30 Jun 88).

Block 4. Title and Subtitle. A title is taken from the part of the report that provides the most meaningful and complete information. When a report is prepared in more than one volume, repeat the primary title, add volume number, and include subtitle for the specific volume. On classified documents enter the title classification in parentheses.

Block 5. Funding Numbers. To include contract and grant numbers; may include program element number(s), project number(s), task number(s), and work unit number(s). Use the following labels:

C	- Contract	**PR**	- Project
G	- Grant	**TA**	- Task
PE	- Program Element	**WU**	- Work Unit Accession No.

Block 6. Author(s). Name(s) of person(s) responsible for writing the report, performing the research, or credited with the content of the report. If editor or compiler, this should follow the name(s).

Block 7. Performing Organization Name(s) and Address(es). Self-explanatory.

Block 8. Performing Organization Report Number. Enter the unique alphanumeric report number(s) assigned by the organization performing the report.

Block 9. Sponsoring/Monitoring Agency Name(s) and Address(es). Self-explanatory.

Block 10. Sponsoring/Monitoring Agency Report Number. *(If known)*

Block 11. Supplementary Notes. Enter information not included elsewhere such as: Prepared in cooperation with...; Trans. of...; To be published in.... When a report is revised, include a statement whether the new report supersedes or supplements the older report.

Block 12a. Distribution/Availability Statement. Denotes public availability or limitations. Cite any availability to the public. Enter additional limitations or special markings in all capitals (e.g. NOFORN, REL, ITAR).

- **DOD** - See DoDD 5230.24, "Distribution Statements on Technical Documents."
- **DOE** - See authorities.
- **NASA** - See Handbook NHB 2200.2.
- **NTIS** - Leave blank.

Block 12b. Distribution Code.

- **DOD** - Leave blank.
- **DOE** - Enter DOE distribution categories from the Standard Distribution for Unclassified Scientific and Technical Reports.
- **NASA** - Leave blank.
- **NTIS** - Leave blank.

Block 13. Abstract. Include a brief *(Maximum 200 words)* factual summary of the most significant information contained in the report.

Block 14. Subject Terms. Keywords or phrases identifying major subjects in the report.

Block 15. Number of Pages. Enter the total number of pages.

Block 16. Price Code. Enter appropriate price code *(NTIS only)*.

Blocks 17. - 19. Security Classifications. Self-explanatory. Enter U.S. Security Classification in accordance with U.S. Security Regulations (i.e., UNCLASSIFIED). If form contains classified information, stamp classification on the top and bottom of the page.

Block 20. Limitation of Abstract. This block must be completed to assign a limitation to the abstract. Enter either UL (unlimited) or SAR (same as report). An entry in this block is necessary if the abstract is to be limited. If blank, the abstract is assumed to be unlimited.